JRC-10-90

ARCTIC ACOUSTICS ULTRASONIC MODELING STUDIES

by

Jacques R. Chamuel

March 1990

Sonoquest/Advanced Ultrasonics Research
P. O. Box 153, Wellesley Hills, Massachusetts 02181, USA

REPORT DOCUMENTATION PAGE

March 1990 | Final Report Mar 87-Feb 90

Arctic Acoustics Ultrasonic Modelling Studies | 61153N

Jacques R. Chamuel

Sonoquest/Advanced Ultrasonic Research
P.O. Box 153
Wellesley Hills, MA 02181

JRC-10-90

ONR POC - Robert Obrochta 696-4118

Approved for Public Release | Distribution Unlimited

A unique collection of laboratory ultrasonice modeling results are presented revealing and characterizing hidden pulsed seismoacoustic wave phenomena from 3-D range dependent liquid/solid boundaries. The research succeeded in isolating and identifying low-frequency (10-500 Hz) transmission loss mechanisms and provided physical insight into Arctic acoustic problems generally beyond the state-of-the-art of theoretical and numerical analysis. Results from the collaboration of J. R. Chamuel (experimental ultransonic modeling/Sonoquest Advanced Ultrasonics Research, U.S.A.) and G. H. Brooke (numerical modeling/Defence Research Establishment Pacific, Canada) obtained under the joint sponsorship of DREP and ONR are included. The ultrasonic modeling studies dealtwith controversial issues and existing discrepancies on seismo-acoustic waves at water/ice interface, sea-ice thickness determination, low-frequency transmission loss,and bottom leaky Rayleigh waves.

Acoustics Scattering From Ice Rayleigh Waves
Sckolte Waves | 136

Unclassified | Unclassified | Unclassified

ABSTRACT

A unique collection of laboratory ultrasonic modeling results are presented revealing and characterizing hidden pulsed seismo-acoustic wave phenomena from 3-D range dependent liquid/solid boundaries. The research succeeded in isolating and identifying low-frequency (10-500 Hz) transmission loss mechanisms and provided physical insight into Arctic acoustic problems generally beyond the state-of-the-art of theoretical and numerical analysis. Results from the collaboration of J. R. Chamuel (experimental ultrasonic modeling / Sonoquest Advanced Ultrasonics Research, U.S.A.) and G. H. Brooke (numerical modeling / Defence Research Establishment Pacific, Canada) obtained under the joint sponsorship of DREP and ONR are included.

The ultrasonic modeling studies dealt with controversial issues and existing discrepancies on seismo-acoustic waves at water/ice interface, sea-ice thickness determination, low-frequency transmission loss, and bottom leaky Rayleigh waves. The areas investigated include leaky Rayleigh waves at water/ice interface, leaky flexural waves in floating ice plates, effects of dry/wet cracks in sea-ice on plate waves and near-grazing acoustic waves, edge waves in floating plates, low-frequency backscatter from ice keel-width resonances, conversion of underwater acoustic waves into plate waves by keels, nondispersive flexural wave along apex of small-angle solid wedge, Scholte and leaky Rayleigh waves along apex of immersed 90° ice wedge, backscatter from trailing edge of floes, floating plate resonances associated with near-grazing underwater acoustic waves, acoustic coupling between adjacent floes, and multiple bottom leaky Rayleigh wave components in water layer over solid bottom. A wide range of relative liquid/solid elastic properties and densities were studied. Most of the findings were presented at the Acoustical Society of America meetings between 1986 and 1989.

ACKNOWLEDGEMENTS

The work reported here was jointly sponsored by the Defence Research Establishment Pacific, Canada (contract No. 10SB.W7708-6-7789 and partially under contract No. 01SB.97708-5-6753), and the U. S. Office of Naval Research Code 1125AR (contract No. N00014-86-C-0206). The author gratefully acknowledges the contributions of G. H. Brooke / DREP which include Arctic field data and numerical results. The enlightening discussions with R. F. Obrochta / ONR were invaluable. The author would like to thank D. Chimenti / AFWAL Materials Laboratory, Wright-Patterson Air Force Base for providing calculations for two liquid/solid models. Thanks to G. H. Brooke, R. F. Obrochta, and T. B. Curtin for making this study possible.

TABLE OF CONTENTS

(136 pages, 4 tables and 105 figures)

1. INTRODUCTION

Major gaps exist in the understanding of key seismo-acoustic wave phenomena on the interaction of underwater acoustic waves with the ice cover and/or ocean bottom affecting long-range propagation characteristics and interpretation of short-range shallow water Arctic field data. Similar fundamental seismo-acoustic phenomena at different frequency ranges play a major role in the fields of seismology, ultrasonic nondestructive testing, geophysics, microwave surface acoustic wave devices, acoustic microscopy, and noise control of fluid-loaded structures. The mathematical approach to solving problems involving the interaction of guided underwater acoustic waves with rough penetrable solids having 3-D boundary discontinuities is exceedingly difficult especially when the dimensions of the features are comparable to the wavelength. Additional complexities arise when the shear wave velocity of the solid approaches the liquid compressional velocity, and also when the liquid density is greater than the density of the solid, which is the case for the water/ice interface. Arctic field experiments are too costly and provide data from variable uncontrolled environmental conditions.

Figure 1.1 shows dispersion curves [1] of the lowest modes of elastic wave propagation in sea-ice from D. L. Anderson's 1961 unpublished mathematical work [2]. In the Arctic acoustics literature, the two dispersion curves marked with the large black arrows in figure 1.1 are not fully described [3-5]. The bottom arrow corresponds to the a leaky flexural wave and the top arrow to a leaky Rayleigh wave at the water/ice interface. Low-frequency underwater acoustic waves penetrate sea-ice and interact with cracks, keels, and plate edges. Upward refraction in Arctic water increases the interaction of acoustic waves with the ice cover and also increases the percentage of energy intercepted by each scatterer in the waveguide because the acoustic waves become confined to a shallower water layer as the strength of upward refraction is increased. Near-field and leaky modes which have usually been ignored for long-range propagation become significant in the problem of low-frequency scattering from ice discontinuities and bottom topography. It is important to develop a complete understanding of three basic generic models: a) liquid half-space on solid half-space, b) solid plate on liquid half-space, and c) liquid layer on solid half-space before introducing the complexities of 3-D range dependent liquid/solid boundaries. Controversial issues exist on the leaky Rayleigh wave at a water/ice interface [6-10, 95]. Discrepancies have been observed between measured and calculated sea-ice thickness from the flexural wave dispersion characteristics [4] and between measured and

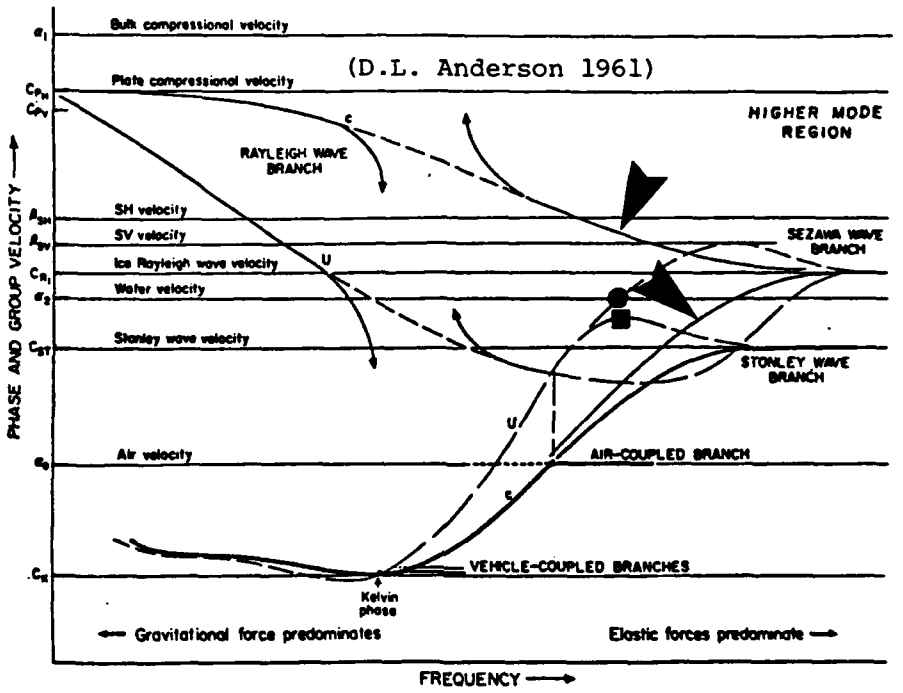

FIG. 1.1. Dispersion curves of the lowest modes of elastic waves propagating in sea-ice (D. L. Anderson 1961 unpublished mathematical theory, copied from reference 1, page 65). The top black arrow corresponds to the Rayleigh wave, and the bottom arrow to the leaky flexural wave. Geophone data from sea-ice are misinterpreted due to interference of the leaky flexural wave component (black dot) and the Scholte flexural wave branch (black square on Stoneley wave branch) as described in Section 3.

predicted low-frequency transmission loss in the Arctic [11-14]. There are conflicting views on the existence of the leaky Rayleigh wave in a water layer over a rock bottom analogous to the liquid-filled borehole problem [14-17].

In order to obtain a quick global view of realistic Arctic seismo-acoustic phenomena and complement both the Arctic theoretical and field efforts, laboratory ultrasonic modeling techniques have been used in this study to isolate and identify different transient seismo-acoustic wave phenomena to investigate problems generally beyond the state-of-the-art of theoretical and numerical analysis. Prior to the start of this research, the effect of cracks in sea-ice were ignored regarding low-frequency propagation and there were no published Arctic field data or numerical results on acoustic waves interacting with crack in a floating plate. Section 5 demonstrates that cracks in sea-ice decrease the flexural wave velocity and create ice thickness determination discrepancies. Section 5.4 focuses on the attenuation of near-grazing low-frequency underwater acoustic waves by cracks in floating plates. Section 3 shows the existence of a leaky flexural wave in a floating ice plate and its effect on interpretation of ice geophone data, and conversion of underwater acoustic waves. Section 4 deals with the controversial leaky Rayleigh wave at a water/ice interface. It also includes the results of a temperature controlled experiment varying the relative elastic properties of a liquid/solid interface to cross a critical limiting temperature on the existence of the leaky Rayleigh wave. Section 6 isolates the trapped edge flexural wave and the edge leaky Rayleigh wave (horizontal particle motion) propagating along the edges and cracks of floating ice plates. Section 7 examines the large backscatter obtained from the trailing edge of floating plates and their associated water-coupled waves. Section 8 presents ultrasonic modeling results on the conversion of underwater acoustic waves into plate waves by ice keels, and the role of ice keel-width resonances on the transmission loss of low-frequency underwater acoustic waves. Section 9 investigates edge waves propagating along apex of immersed solid wedges, and also includes interesting results on the nondispersive edge flexural wave. Section 10 isolates multiple pulsed supersonic leaky Rayleigh wave components generated in a liquid layer over a solid half-space. The research investigated a broad range of hidden seismo-acoustic phenomena, and provided physical insight critical to the understanding and interpretation of Arctic field data.

Most of the ultrasonic modeling findings discussed in this report were presented at the Acoustical Society of America meetings [6,18-23] between 1986 and 1989, and at the ONR 1989 Arctic Acoustic Workshop at MIT [24].

2. EXPERIMENTAL SETUP

The basic experimental setup used in the ultrasonic modeling studies was previously described in references 25 and 26. In all of the experiments, generation and detection of the ultrasonic signals were accomplished using broadband ultrasonic transducers (Sonoquest, 1.5 - 4 mm in diameter). Nominally, a 1.5 - 3.0 μs single broadband pulse was applied to the source transducer. Figure 2.1 shows typical transducers' response obtained in water. Useful signals were available from about 30 kHz to 900 kHz. This report covers a wide range of experiments and models which will be described in each corresponding section of the report as needed.

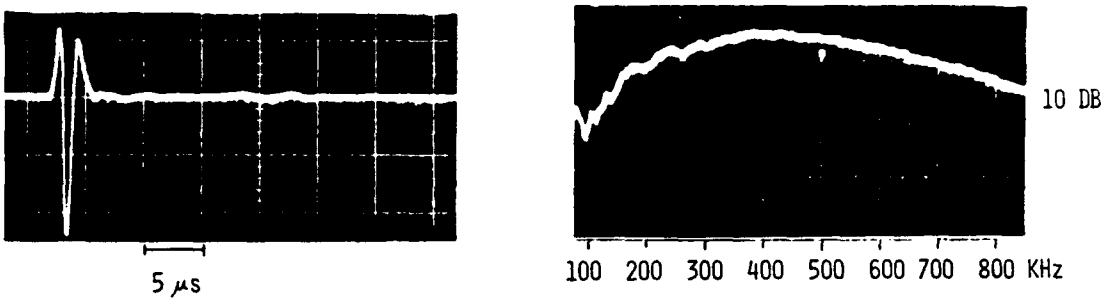

FIG. 2.1. Typical transducers' response. Waveshape and spectrum of acoustic waves in water.

3. LEAKY FLEXURAL WAVE IN FLOATING ICE PLATE

Flexural waves in a free solid plate follow a single dispersion curve that asymptotically reaches the Rayleigh wave velocity at high frequencies. When the plate is bounded on one side by air and the other side by water, additional flexural wave branches appear [1,5,27]. The complexity of the fluid-loaded thick plate problem was described by Pierucci and Graham's [72]. In the Arctic acoustics literature, the focus has been on the subsonic water-coupled flexural wave branch (Scholte wave branch) shown in figure 3.1, and b) the air-coupled flexural wave branch [54]. Little work has been devoted to the coexisting leaky flexural wave branch in floating ice plates. Anderson's unpublished mathematical results [2] showed a family of dispersion curves for the lowest modes of elastic waves propagating in sea-ice (FIG. 1.1, copied from reference 1) which includes a "Sezawa" wave branch without discussions. Stein [3], for example, treated the Rayleigh wave originating from the air/water interface, which has a real Rayleigh wave pole at high frequencies and a complex pole at low frequencies; and did not specifically discuss the leaky flexural wave branch that asymptotically reaches the leaky Rayleigh wave velocity (complex pole from water/ice interface) at high frequencies. Detailed theoretical studies are needed to characterize the branching of the flexural waves for floating ice plates.

We are interested in the leaky flexural wave because: 1) Unlike the subsonic flexural wave, it can be generated by incident underwater acoustic waves causing an increase in low-frequency transmission loss, 2) it can contribute to ambient noise by radiating to the water thermal cracking noise components, 3) it can be locally excited by the conversion of underwater acoustic waves at discontinuities such as cracks, ridges, and leads affecting transmission loss prediction and ambient noise characteristics, and 4) It obscures the determination of sea-ice shear wave properties by interfering with the onset of the Scholte flexural wave component as described below.

Two sets of experiments were conducted on the leaky flexural waves. The first utilized a stable repeatable setup based on floating glass plates, and the second used floating ice plates.

FLOATING GLASS PLATE ON WATER

In this section, plates with a high shear wave velocity and a large acoustic impedance relative to the water ("hard" plates) were investigated.

The effect of fluid loading on the vibration of an immersed

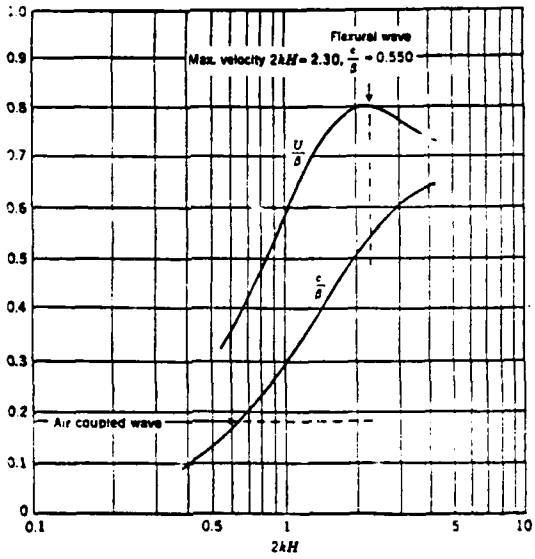

FIG. 6-7. Theoretical phase- and group-velocity curves for a floating ice sheet; α = 12,400 ft/sec, β = 6,040 ft/sec, σ = 0.345 for ice, a = 4,800 ft/sec for water (*After Crary.*)

FIG. 3.1. Theoretical phase and group velocity curves for flexural wave in floating ice sheet. (After Crary, from Ewing, Jardetsky, and Press, 1957, p. 298). The leaky flexural wave is not plotted.

plate increases as the fluid density is increased. Plate waves traveling with a velocity greater than the fluid compressional wave velocity are severely attenuated by radiation to the fluid. Figure 3.2 shows the effect of water loading on the flexural wave in a floating aluminum plate (0.78 mm thick). The water compressional wave velocity C_w was 1480 m/s. The flexural wave was detected with a receiver transducer located on the top surface of the plate at a range of 15 cm. The waveshape of the flexural wave from the free plate (FIG. 3.2(a)) was compared to the wave from the floating plate (FIG. 3.2(b)). The water attenuated the first-arriving high frequency components and decreased the velocity of the low-frequency waves.

Figure 3.3 shows a theoretical flexural wave group velocity dispersion curve provided by G. H. Brooke for a 5.8 mm thick glass plate on water. The group velocity maximum for the floating glass plate is 2017 m/s. The theoretical group velocity maximum for the flexural wave is independent of the plate thickness for a given set

of elastic properties. Figures 3.4 and 3.5 display waveforms measured at different ranges along the top surface of an infinite floating glass plate. The plate thickness was 5.65 mm in figure 3.4 and 3.06 mm in figure 3.5. One notices that the apparent time of arrival of the flexural wave onset is earlier than predicted based on the maximum group velocity and range. At short range, a dispersed component "leaky flexural wave" appeared between the first-arriving compressional plate wave and the flexural wave. This wave component decayed rapidly with range and also merged with the flexural wave. A plot of the measured group velocity for the flexural waves from the ultrasonic measurements is shown in figure 3.6. In addition to the commonly known flexural wave dispersion curve (Scholte wave branch), a second higher dispersed branch "leaky flexural wave" was obtained from the experimental data.

The high-frequency onset of the leaky flexural wave decays rapidly with range leaving late-arriving low-frequency components merging with the onset of the nonradiating flexural wave (Scholte wave branch , FIG. 3.5). This gives the impression of observing early arrival of the common flexural wave. Interference of these two wave components makes it difficult to obtain experimental points on the two group velocity dispersion curves near the bifurcation. If one tries to increase the range to separate the leaky from the nonradiating flexural wave, the amplitude of the leaky flexural wave becomes greatly attenuated. In figure 3.6 few experimental points are also plotted regarding the phase velocity at the onset of the flexural wave.

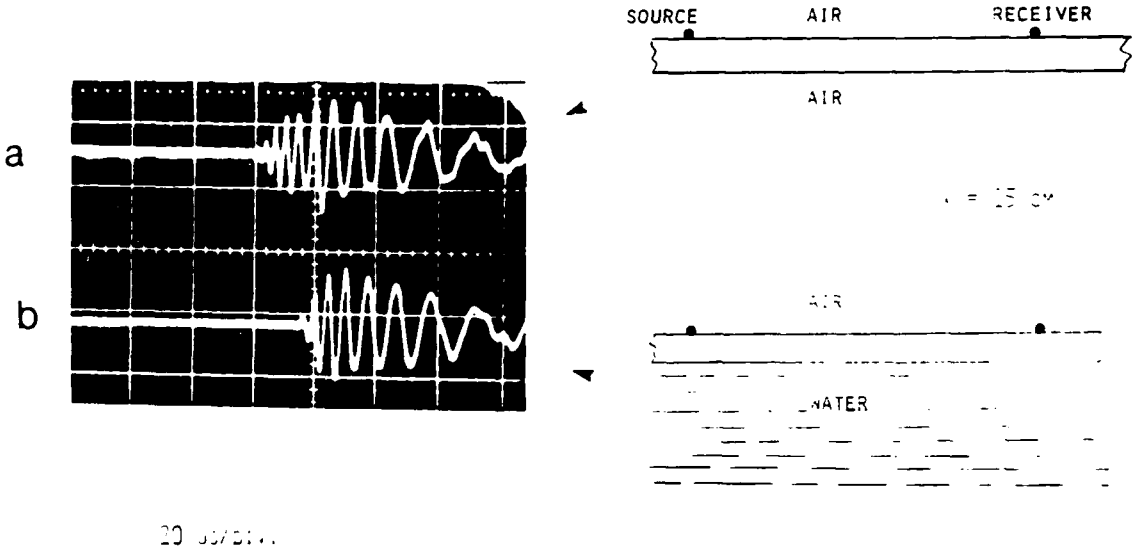

FIG. 3.2. Effect of water loading on flexural wave in "hard" floating plate. (Aluminum plate 0.78 mm thick)

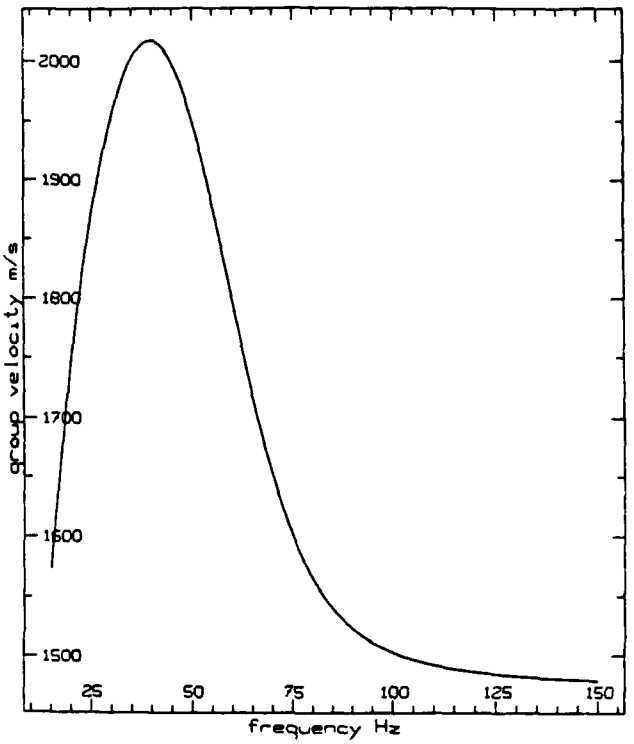

FIG. 3.3. Theoretical flexural wave group velocity for floating glass plate 5.8 mm thick on water. (G. H. Brooke/DREP 1988).

The apparent group velocity of the resulting wavetrain at the onset of the flexural wave is function of range. At close range, one obtains an effective high group velocity maximum for the flexural wave component near, and at large distances the group velocity approaches the maximum group velocity of the Scholte wave branch as the leaky flexural wave is attenuated. This effect can be observed from the results of figure 3.6 around fh = 230 Hhz-m, where the points are scattered. These data points were accurately measured and were obtained from waveforms corresponding to different ranges.

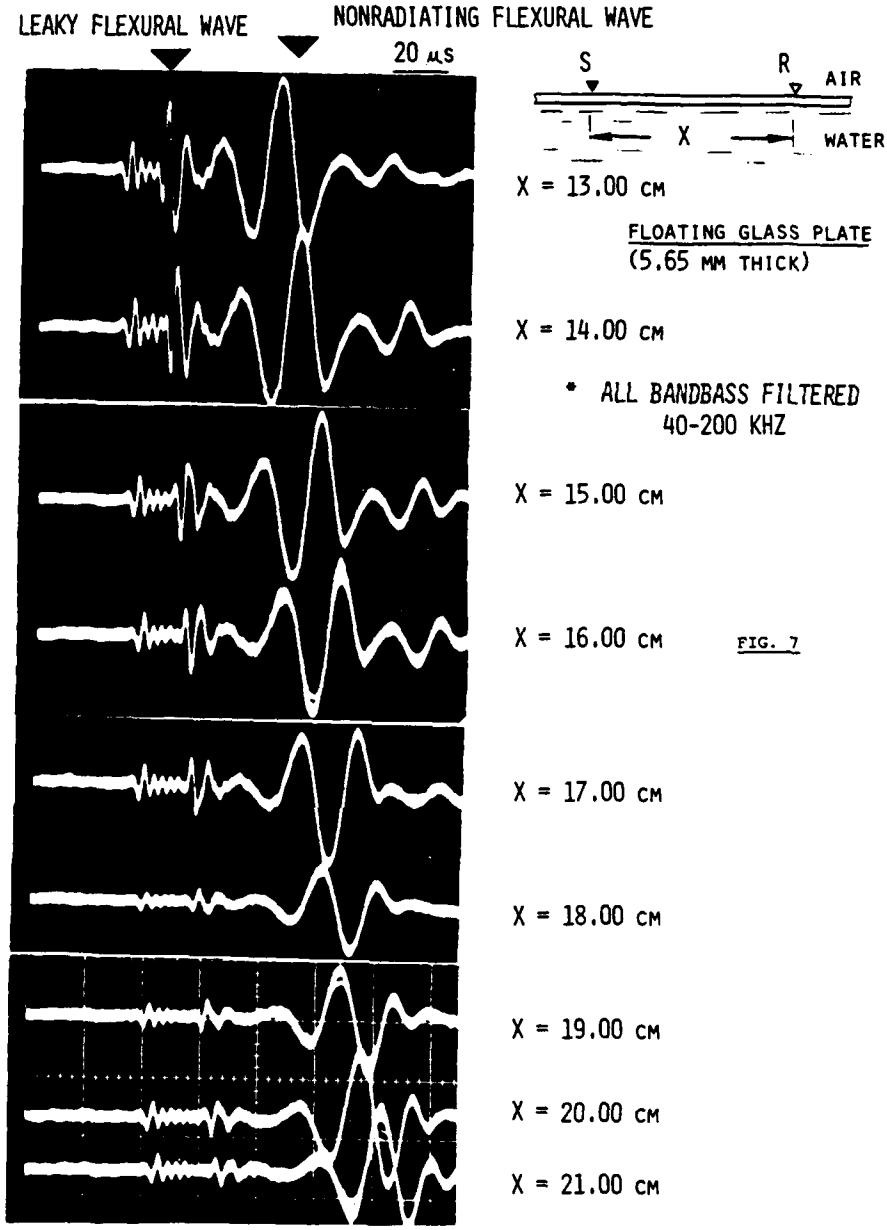

FIG.3.4. Experimental observation of coexistence of leaky flexural wave and Scholte wave branch flexural wave in floating plate with shear wave velocity greater than water compressional velocity. Notice tail of leaky flexural wave mixes with onset of nonradiating flexural wave causing misinterpretation of arrival time of Scholte wave branch flexural wave.

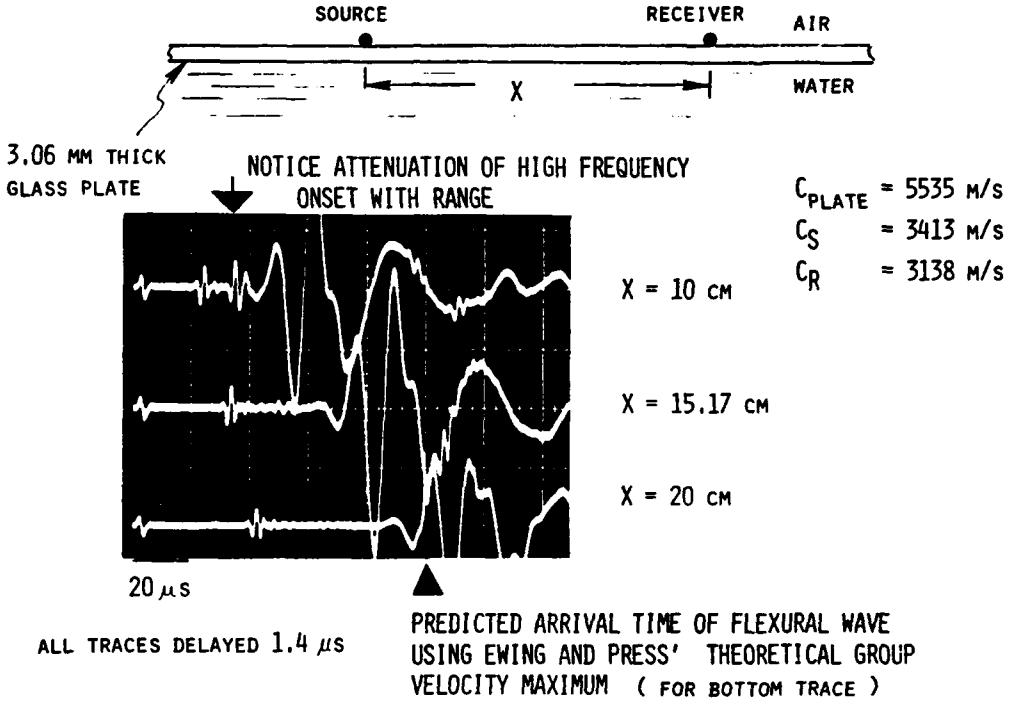

FIG.3.5. In thinner floating plates, if one is not aware of the existence of the leaky flexural wave, the onset of observed flexural waves appears faster than predicted by the theoretical group velocity maximum of the Scholte wave branch of the antisymmetric mode. Notice wave portion to the left of the marker in bottom trace.

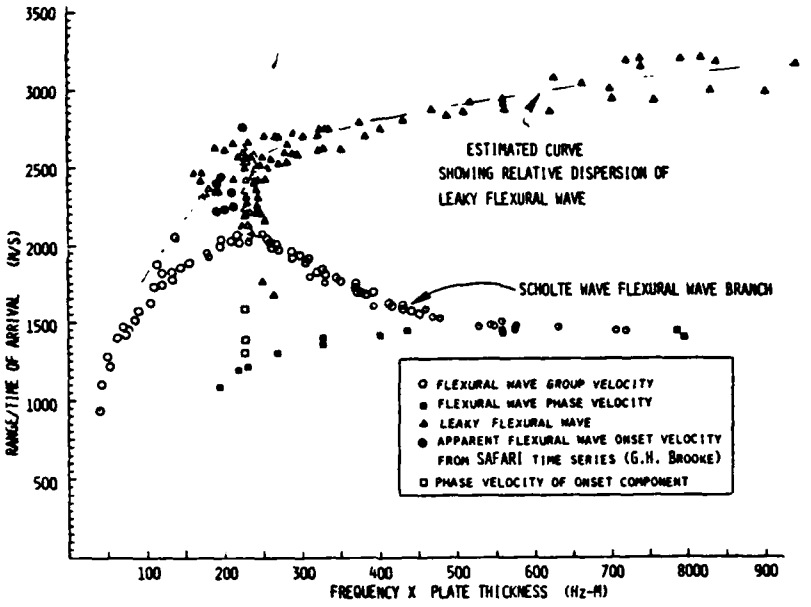

FIG. 3.6. Experimental ultrasonic results demonstrating existence of two flexural wave branches for floating glass plate. The top branch is the leaky flexural wave.

ICE/WATER

A controlled ultrasonic experiment was conducted on floating ice plates demonstrating the existence of a leaky flexural wave in addition to the subsonic flexural wave (FIG. 3.7 and 3.8). Source and receiver transducers were placed at the air/ice interface of a floating ice plate of thickness H. With a large plate thickness representing a free solid half-space "H = ∞" , the Rayleigh wave was recorded at a 3 cm range. A reference time marker was obtained by removing the ice and allowing the transducers to contact the water directly (H = 0). This is indicated in figure 3.7 by $T = X/C_w = t_w$, where C_w is the compressional wave velocity in water. The time of arrival of the flexural wave was compared to the Rayleigh wave as the ice thickness was varied. Figure 3.7 shows photographs of the received waveshapes for different ice plate thicknesses "H". The white arrow at the top of each photograph is set to indicate t_w. The onset of the leaky flexural wave from the different ice plates appeared substantially to the left of the white arrow. Figure 3.8 superimposes: a) the waveshapes from the H = 0 and H = 1.5 mm models, and b) the waveshapes from the H = ∞ and H=1.5 mm models.

The leaky flexural wave decays very rapidly with range due to the severe water loading on the ice. Stein [3] noted that the group velocity of the Scholte wave branch is slightly above the Arctic water wave velocity while its phase velocity is subsonic. Here we are focusing on the leaky flexural wave which has both phase and group velocities greater than C_w. In the Arctic, upward refraction in the water forces underwater acoustic waves to bend upward and

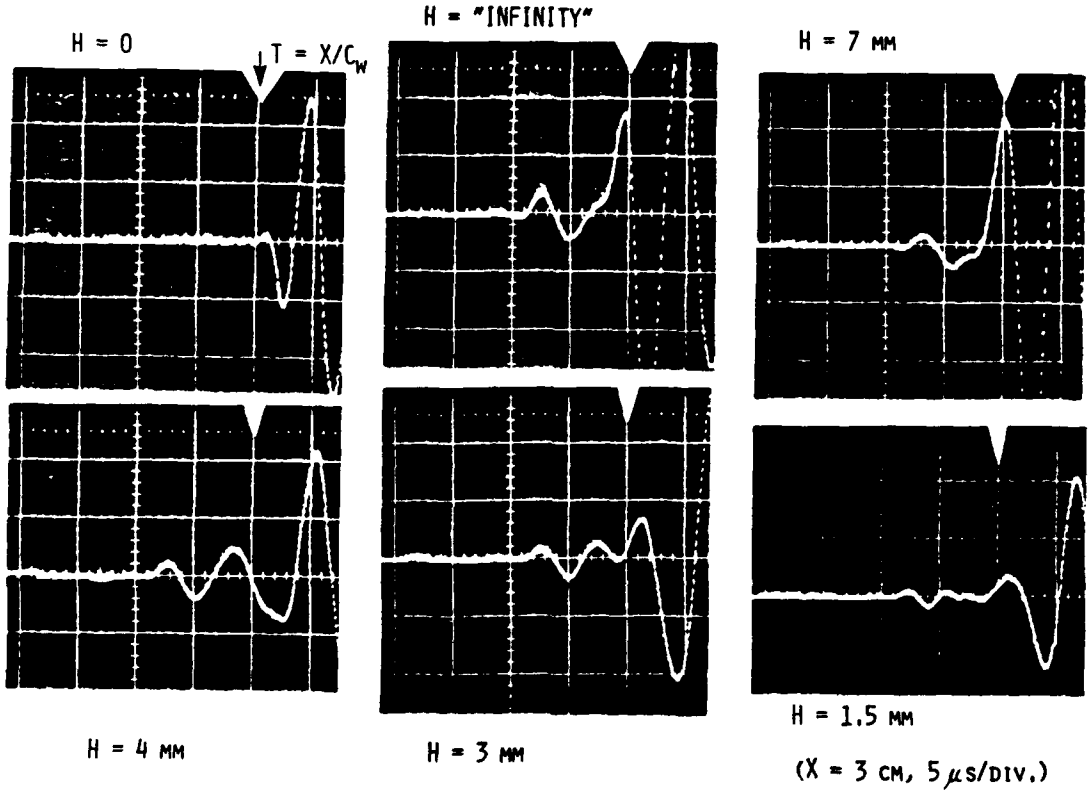

FIG.3.7. Experimental results demonstrating existence of leaky flexural wave in floating ice sheet of thickness "H" . Source and receiver located at air/ice interface at a fixed range x = 3 cm. Top left signal obtained with H = 0 (no ice plate) as a time marker determined by direct water wave arrival. Top middle trace was obtained with $H = \infty$ corresponding to a free ice half-sapce to capture the Rayleigh wave. Bottom right trace shows the leaky flexural wave starting to the left of the white arrow from a 1.5 mm thick floating ice plate.

interact several times with the ice cover generating leaky flexural waves and satisfying Snell's law. The results of figures 3.7 and 3.8 are the first laboratory experimental data demonstrating the existence of leaky flexural waves in floating ice plates.

Numerical synthetic time series plots obtained by Brooke using the SAFARI program [28] also demonstrated the early arrival of the onset of the flexural wave (Fig. 3.9). Similar to the laboratory results, the apparent group velocity of the onset of the flexural wave decreases with range. For a given low frequency wave component near fh = 230 Hz-m, the apparent group velocity was about 2770 m/s at x = 200 m, and 2250 m/s at x = 1000 m. Brooke observed the same early-arriving flexural wave components in his Arctic field data from 2.3 m thick sea-ice at a range of 200 m (FIG. 3.10).

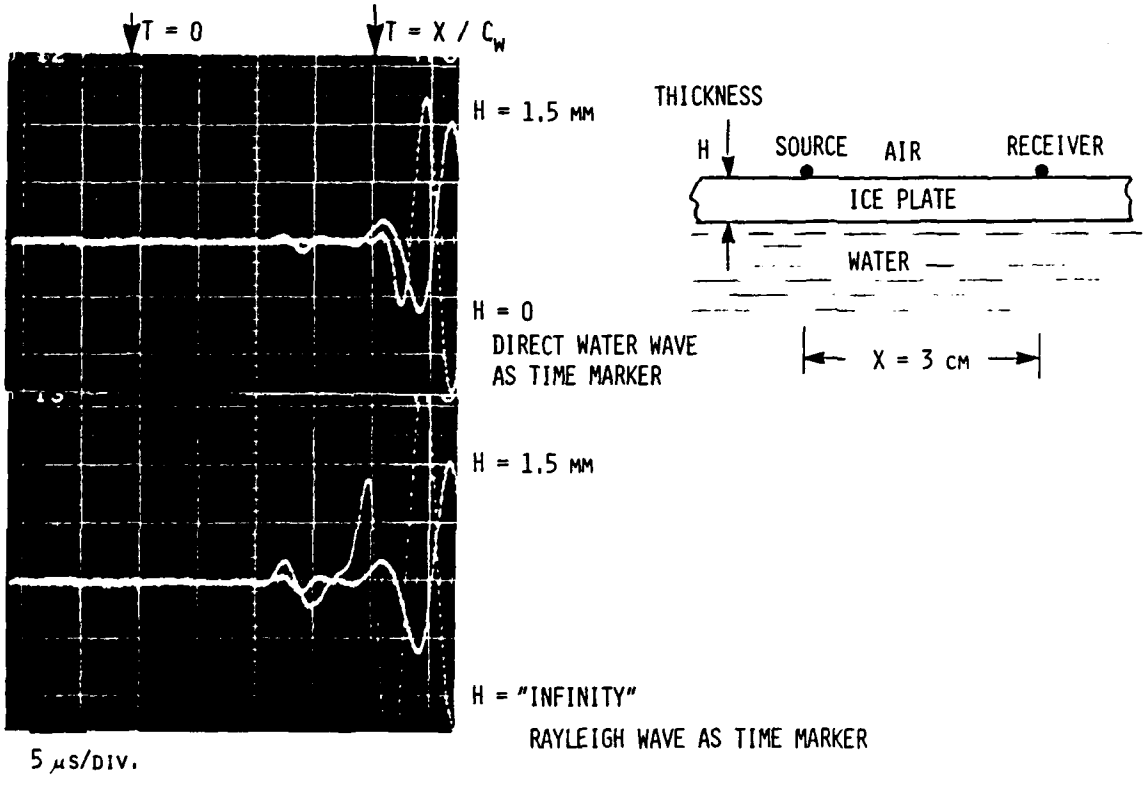

FIG. 3.8. Existence of supersonic flexural wave in floating ice plate. A time marker is obtained with the ice plate removed (H = 0). The Rayleigh wave from a free ice half-space (H = ∞) is compared with the flexural wave from a 1.5 mm thick floating ice plate. The onset of the leaky flexural wave is before the direct water wave.

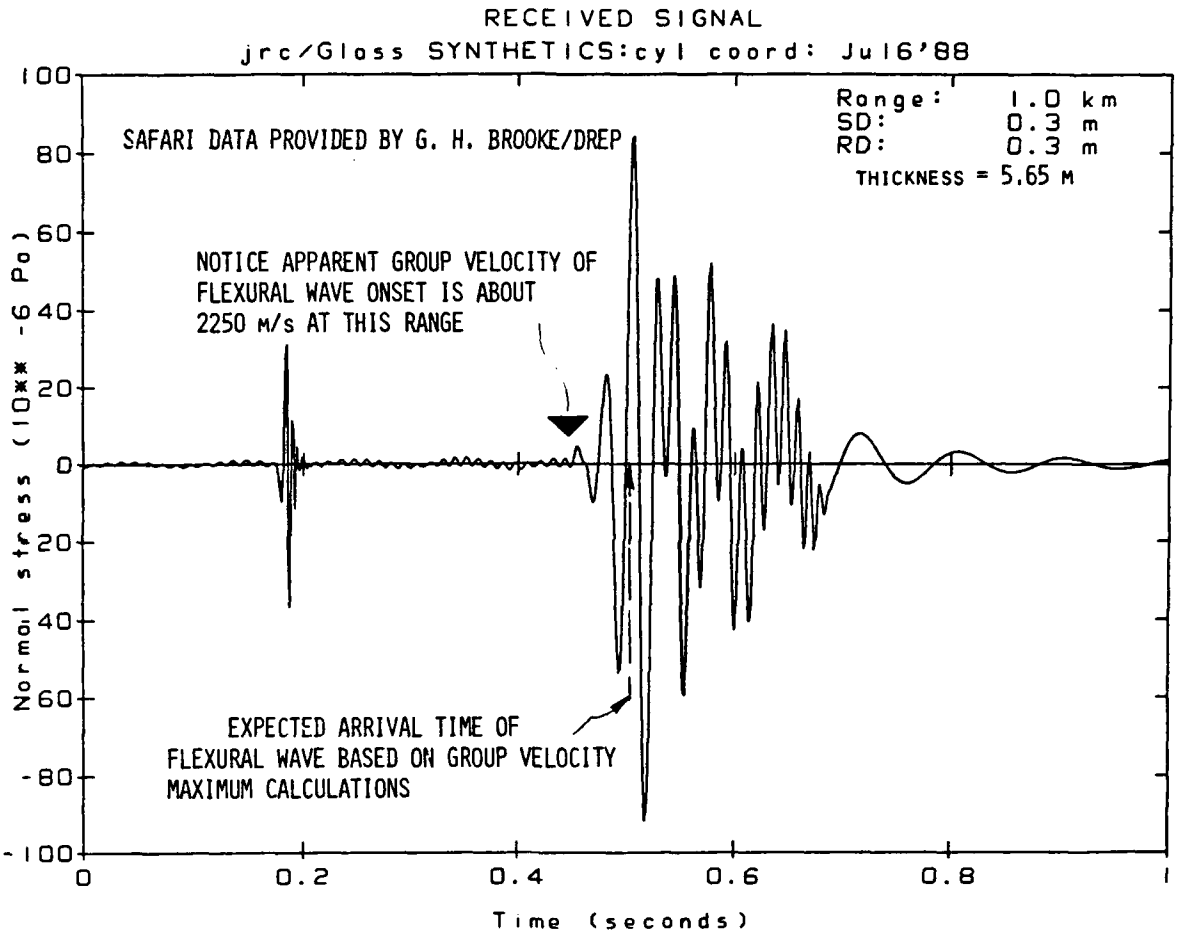

FIG.3.9. Synthetic time series using SAFARI for floating "hard" plate. Similar to the ultrasonic experimental results, the onset of the flexural wave arrives earlier than predicted by the group velocity maximum of the Scholte wave branch of the antisymmetric mode. Glass plate on water.

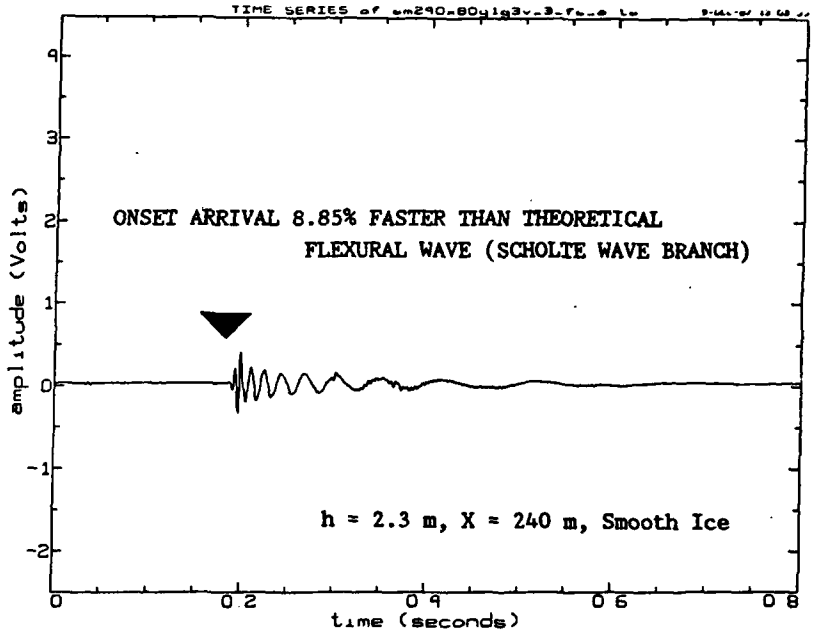

FIG.3.10. Arctic field data obtained by G. H. Brooke/DREP indicating arrival of wave componen ahead of flexural wave (Scholte branch) observed at close range.

4. LEAKY RAYLEIGH WAVE AT WATER/ICE INTERFACE

In an infinite elastic solid, only compressional and shear waves can exist, however, at the free surface of a solid half-space the compressional and shear waves combine to satisfy the boundary conditions creating a slow guided surface wave known as the Rayleigh wave [29]. The Rayleigh wave is confined to propagate near the free surface of the solid and has its amplitude decrease exponentially with depth. The addition of a liquid half-space to the solid half-space modifies the boundary conditions and results in new interface waves that depend on the relative elastic properties of the liquid and the solid. When the Rayleigh wave velocity C_R is faster than the liquid compressional wave velocity C , the Rayleigh wave radiates its energy to the liquid and becomes rapidly attenuated with range. This damped Rayleigh wave is referred to in the literature as the leaky Rayleigh wave or pseudo-Rayleigh wave. The leaky Rayleigh wave has been studied by several authors [5,6,8-10,15-17,22,23,30-44] and has been extensively used in seismology and in the nondestructive testing fields. Detailed theoretical analysis of the leaky Rayleigh wave is described in references 31, 34, 8, and 32.

In addition to the leaky Rayleigh wave, there is another unattenuated interface wave "Scholte wave" which travels with a velocity C_{Sch} that is slower than C. The Scholte wave always exists at a liquid/solid interface, however, there are restrictions on the existence of the leaky Rayleigh wave [8-9]. Brower et al. obtained limits on the ratios of C/C_p , C/C_s, and ρ/ρ_s restricting the existence of the leaky Rayleigh wave (FIG. 4.1) using numerical analysis, where C_p, C_s, ρ, and ρ_s are the solid compressional velocity, the shear wave velocity, the liquid density, and the solid density respectively. When C_s is almost equal to C, the leaky Rayleigh wave ceases to exist. Having $C_s > C$ is a necessary but not a sufficient condition to guarantee the existence of the leaky Rayleigh wave. The water/ice case does not satisfy Brower's restrictions, therefore one is not expected to detect a leaky Rayleigh wave at the water/ice interface.

The theoretical background for the leaky Rayleigh wave is briefly described followed by experimental results on pulsed leaky Rayleigh waves at water/limestone, water/ice, freon 113/ice, and freon 113/acrylic. Laboratory experimental results obtained from water/ice models [6,22,23] demonstrated the existence of a leaky Rayleigh wave contradicting the current theoretical predictions as described below.

TABLE II

Examples of Liquid/Elastic Solid Combinations which Fail the Existence Condition

Liquid/Elastic Solid	V_L/V_D	V_L/V_S	ρ_L/ρ_S
Hg/Al	0.226	0.477	5.0
CCl_4/Lucite	0.366	0.862	1.35
Hg/Pt	0.265	0.485	1.53
Hg/Fused Silica	0.243	0.385	6.14
H_2O/Ice[4]	0.429	0.968	1.11

TABLE I

Maximum Acceptable ρ_L/ρ_S as a Function of V_L/V_D (Horizontal Heading) and V_L/V_S (Vertical Heading)

	0.05	0.10	0.15	0.20	0.25	0.30	0.35	0.40	0.45	0.50	0.55
0.10	7.14										
0.15	4.87	5.26									
0.20	3.68	3.76									
0.25	2.83	2.89	3.05								
0.30	2.20	2.26	2.43	2.58							
0.35	1.93	1.96	2.01	2.09							
0.40	1.65	1.66	1.70	1.75	1.83						
0.45	1.52	1.43	1.46	1.49	1.55	1.60					
0.50	1.26	1.25	1.26	1.29	1.32	1.37					
0.55	1.05	1.09	1.10	1.12	1.16	1.18	1.21				
0.60	0.95	0.95	0.96	0.97	0.97	1.03	1.05	1.06			
0.65	0.83	0.83	0.84	0.85	0.86	0.88	0.90	0.92			
0.70	0.77	0.72	0.73	0.73	0.76	0.75	0.77	0.79	0.80		
0.75	0.62	0.62	0.62	0.63	0.63	0.64	0.66	0.67	0.69	0.70	
0.80	0.52	0.52	0.53	0.53	0.53	0.54	0.55	0.56	0.57	0.59	
0.85	0.43	0.43	0.44	0.44	0.44	0.45	0.45	0.46	0.47	0.48	0.50
0.90	0.30	0.30	0.30	0.31	0.31	0.32	0.32	0.33	0.33	0.34	0.35
0.95	0.22	0.22	0.23	0.23	0.24	0.24	0.25	0.26	0.27	0.27	0.29

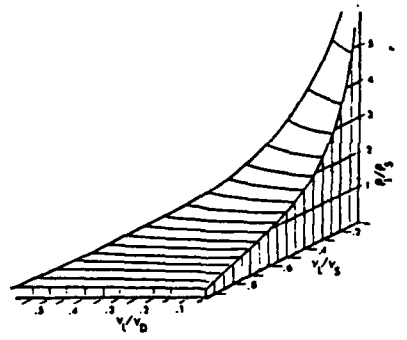

Fig. 1. Combinations of V_L/V_S, V_L/V_D, and ρ_L/ρ_S which allow propagation of a leaky Rayleigh wave. Points must be within the volume shown for wave to exist.

FIG. 4.1. Restrictions on the existence of the leaky Rayleigh wave. (Brower et al., IEEE Trans. Sonics Ultrasonics SU 26(4), 306-308, 1979).

4.1 THEORETICAL BACKGROUND

The theoretical background for the leaky Rayleigh wave at a liquid/solid interface has been described by Strick [31] , Viktorov [32] , Brekhovskikh [33] , Phinney [34] , and many others. In summary, a surface wave solution to the equations of motion for an isotropic elastic solid half-space in contact with a liquid half-space is obtained satisfying the interface boundary conditions and an exponential decay of the particle displacement in the solid normal to the interface. A characteristic equation is obtained having one real root corresponding to the Scholte wave, and a complex root associated with the leaky Rayleigh wave. The characteristic equation may be written as:

$$4[1-(V/C_p)^2]^{0.5}\,[1-(V/C_\varepsilon)^2]^{0.5} - [2-(V/C_s)^2]^2 = \frac{i\rho V^4[1-(V/C_p)^2]^{0.5}}{\rho_s C_s^4\,[(V/C)^2-1]^{0.5}}\ ; \quad (4.1)$$

where V is the velocity of the surface wave.

The leaky Rayleigh wave originates from a pole which lies on a lower Riemann sheet in the complex plane and not from a pole on the real axis [31] . It looks like an interface wave with respect to the solid, however, it has many properties of critically refracted ray in the fluid [34]. The loading effect of the liquid on the solid half-space increases the surface wave velocity [32]. The increase is more pronounced the greater is the ratio ρ/ρ_s [31,34]. Strick showed that the Rayleigh wave velocity and the leaky Rayleigh wave velocity are always the same for a delta-function excitation and that for harmonic waves the leaky Rayleigh wave does not travel with the free Rayleigh wave velocity. Controversial issues seem to exist regarding the characteristics of the leaky Rayleigh wave. Strick mentioned that the real part of the pole gives approximately the leaky Rayleigh wave velocity since the actual velocity is precisely that of the true Rayleigh wave. Press and Ewing [44] followed Osborne and Hart's method [38] to approximate the phase velocity of the leaky Rayleigh wave for the water/ice interface case. Their theoretical result was adequate to represent the attenuation coefficient of the leaky Rayleigh wave, however, it did not demonstrate the characteristics of the Rayleigh wave velocity for the water/ice problem. The amplitude of a pulsed leaky Rayleigh wave increases as the receiver is moved away from the solid surface, but this increase ends as soon as the time of arrival of the theoretically refracted shear wave becomes smaller than the travel time of the direct water wave [31]. From Snell's law, the leaky Rayleigh wave radiates to the liquid at an angle θ from the normal to the interface satisfying the relation $\sin\theta = C / C_{RL}$, where CRL is the leaky Rayleigh wave velocity. Strick demonstrated theoretically that the point of zero amplitude in the pressure response travels precisely with the Rayleigh wave velocity independent of the existence of the liquid.

Van der Hijden [8] presented a quantitative description of the characteristics of the leaky Rayleigh wave and came up with a condition limiting the range of existence of the leaky Rayleigh wave. According to Van der Hijden, the leaky Rayleigh wave does not exist if the $F < 1$, where

$$F = \frac{\rho_s C_p [C_s^2 - C^2]^{\frac{1}{2}}}{\rho C [C_p^2 - C_s^2]^{\frac{1}{2}}} \quad ; \quad (4.2)$$

and that it is not proper to associate with the complex root a leaky Rayleigh wave speed because it has no wavefront associated with it, however, one can define the speed of the amplitude peak of the leaky Rayleigh wave pulse. Based on a liquid/solid model with $C_p = 4C$ and

C_s = 2C, Van der Hijden showed that the leaky Rayleigh wave velocity coincides with the shear wave velocity if the calculated value of F = 1 and decreases to the Rayleigh wave velocity if F $\rightarrow \infty$. He also mentioned that for an ice/water interface with C = 1500 m/s, C_p = 3695 m/s, C_s =1820 m/s, ρ = 1020 kg/m^3, and ρ_s = 917 kg/m^3, the leaky Rayleigh wave may not exit since F is 0.71 (less than one).

For a water/ice model with the following parameters: C_p = 3488 m/s, C_s = 1940 m/s, ρ_s = 0.906 kg/m^3, and C = 1403 m/s, the calculated leaky Rayleigh wave root is

$$C_{RL} = 2055.7 - 267.38i$$

and F = 1.041. Although F is greater than 1 (meaning that the leaky Rayleigh wave can exist), the real part of the leaky Rayleigh wave root exceeds the shear wave velocity. Van der Hijden's factor F, which was derived for the condition that the leaky Rayleigh wave velocity < C_s, is now supporting the existence of a leaky Rayleigh wave having a velocity greater than C_s. Figure 4.2 shows a plot of the migration of the complex leaky Rayleigh wave root as the shear wave velocity is varied between 1700 m/s - 2400 m/s, while the other parameters are fixed. It is interesting to note that the real part of the leaky Rayleigh wave root would exceed the shear wave velocity if C_s is below 2238 m/s, and that van der Hijden's factor F becomes > 1 if C_s is increased beyond 1909.84 m/s. With F = 1 at C_s 1909.84 m/s, the ratio of $Re[C_{RL}]/C_s$ is 1.06726. Chamuel's calculations raise questions regarding the validity of the existence factor F > 1 for the water/ice case since $Re[C_{RL}] > C_s$. Gordon [10] also reported that the calculated leaky Rayleigh wave velocity for water/ice exceeds C_s.

The pulsed ultrasonic modeling results [6,22,23] obtained so far indicate that: 1) a leaky Rayleigh wave exists at a water/ice interface contradicting the theoretical predictions, 2) the leaky Rayleigh wave is faster than the Rayleigh wave, 3) the zero amplitude travels with a velocity faster than the Rayleigh wave not in agreement with the theoretical calculations [31,34,8] , and 4) the velocity of the leaky Rayleigh wave at the water/ice interface does not exceed the shear wave velocity inspite of having the real part of C_RL greater than C_s. Further theoretical and experimental investigations are needed to fully resolve this issue.

4.2 EXPERIMENTAL PROCEDURE

Broadband piezoelectric ultrasonic transducers (Sonoquest 1.5 mm and 2.3 mm diameter) were used to generate and detect ultrasonic waves in the frequency range 70 kHz - 700 kHz on a flat surface of a large block of commercial fresh-water ice. The dimensions of each ice block under study were large enough to delay all reflections of

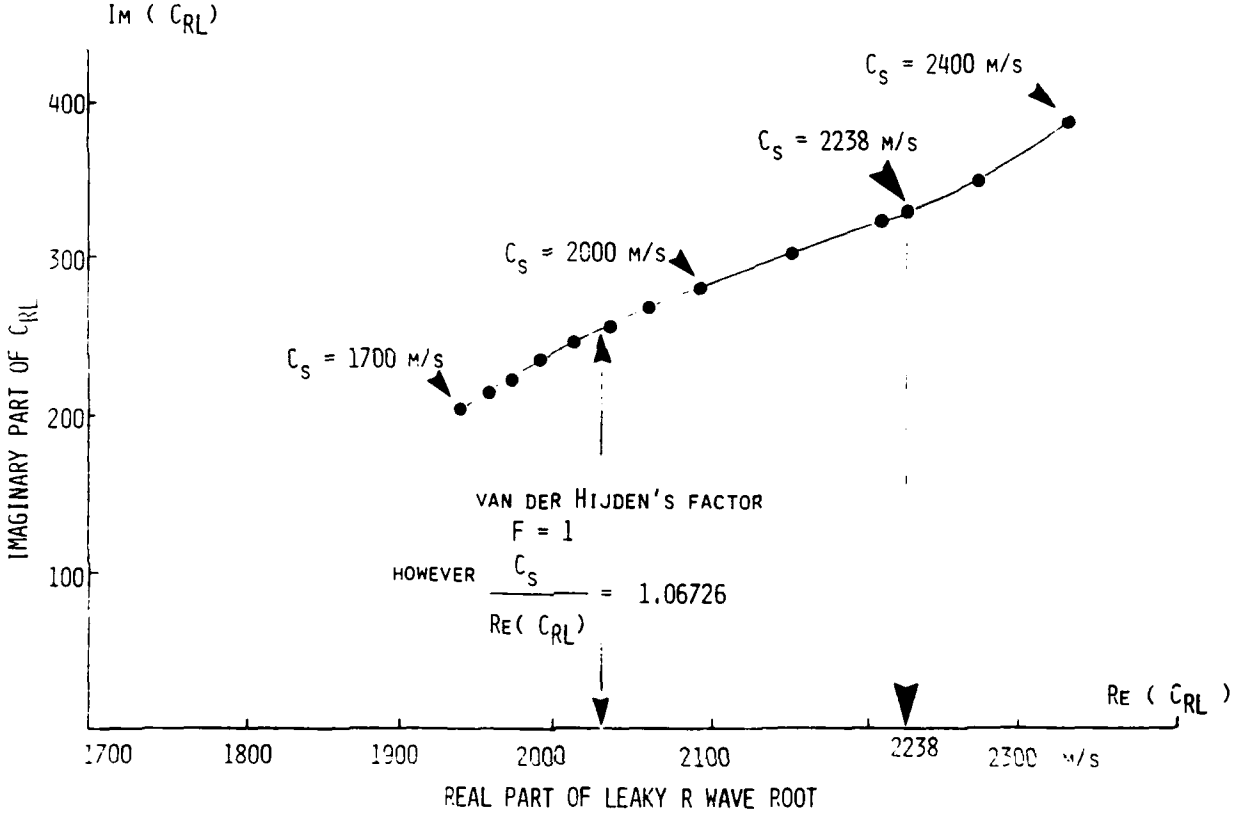

FIG. 4.2. Migration of th eaky Rayleigh wave complex root of the characteristi uation as the shear wave speed is varied from 1700-2' m/s for a water/ice interface. The real part of the complex root corresponds to the phase velocity of the leaky Rayleigh wave. Van derHijden's leaky Rayleigh wave existence factor F = 1 when C_s = 1909.84 m/s , however, the real part of the leaky Rayleigh wave root is greater than C_s seemingly in conflict with the definition of F. The leaky Rayleigh wave can exist if F is greater than one. The solid curve joins the discrete calculated dots (Chamuel).

the elastic waves from the ice boundaries by at least 80 μs. The source transducer was pulsed with a 2.5 μs pulse and the receiver was connected to an amplifier, a bandpass filter (70 kHz -700 kHz), and an oscilloscope. The filtering improved the signal to noise ratio without distorting the received signal. When tested in a large water tank, a single pulse excitation produced a single pulse at the receiver followed by a region free of pulses for about 150 μs. Placing the transducers on the free flat surface of the ice block resulted in the waveform displayed in figure 4.3(a).
The compressional, shear, and Rayleigh wave velocities were determined from the travel time and source/receiver range. In the text, C_R is used to denote the Rayleigh wave velocity at the air/ice interface and C_{RL} for the corresponding leaky Rayleigh wave at the water/ice interface. The received signal was recorded photographically from the oscilloscope. After characterizing a block of ice, a fresh water half-space at near freezing temperature was added to study the leaky Rayleigh wave.

In order to facilitate the experiments, the block of ice was held down at the bottom of the water tank to prevent it from floating and conduct the measurements on its top surface. The experiments were repeated over several selected ice blocks to obtain unbiased results unaffected by the characteristics of a specific block. The transducers produced a sharp well defined pulse without ringing which allowed us to separate in time and space the different seismo-acoustic wave components. The Rayleigh wave recorded from the air/ice interface was used as a reference signal in the study. The oscilloscope traces were shifted vertically to compare the time of arrival of different waves recorded from the air/ice and water/ice models. In some experiments, both source and receiver were placed normal to the interface and in other experiments the receiver was tilted from the vertical direction to increase the coupling to the leaky Rayleigh wave. The source was always on the interface touching the ice. The distance between the receiver and the interface varied depending on the experiment. The figures presented in this section display the water on top of the ice which is opposite to the normal configuration in the Arctic where sea-ice is on top of the water.

4.3 EXPERIMENTAL RESULTS

A reference Rayleigh wave signal was obtained from the flat air/ice interface with the 1.5 mm diameter transducers and with the receiver placed normal to the interface (FIG. 4.3(a)). The results are similar to the classic free solid half-space problem analyzed by Lamb [45] . The distance between source and receiver was x = 6.7 cm. Without disturbing the setup, a fresh-water half-space at near freezing temperature was added on the ice block (clamped down). The received signal from the water/ice model is shown in figure 4.3(b). The original Rayleigh wave disappeared and two new waves resulted. The first wave was small and its onset arrived slightly before the

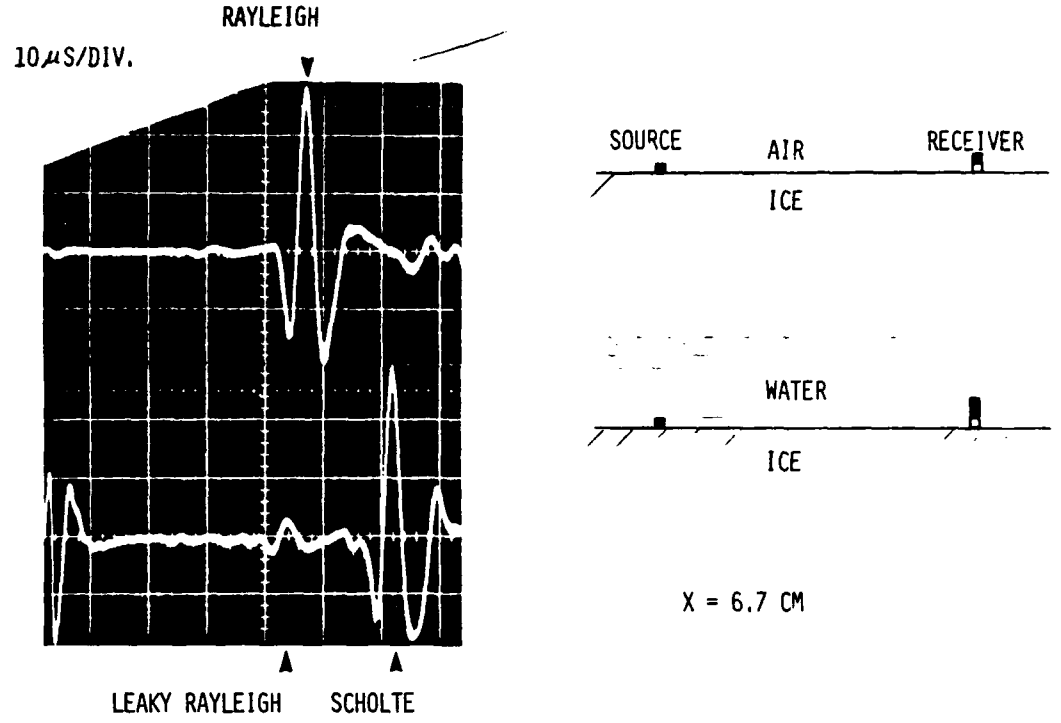

FIG. 1.

FIG. 4.3. Leaky Rayleigh wave and Scholte wave at a water/ice interface.

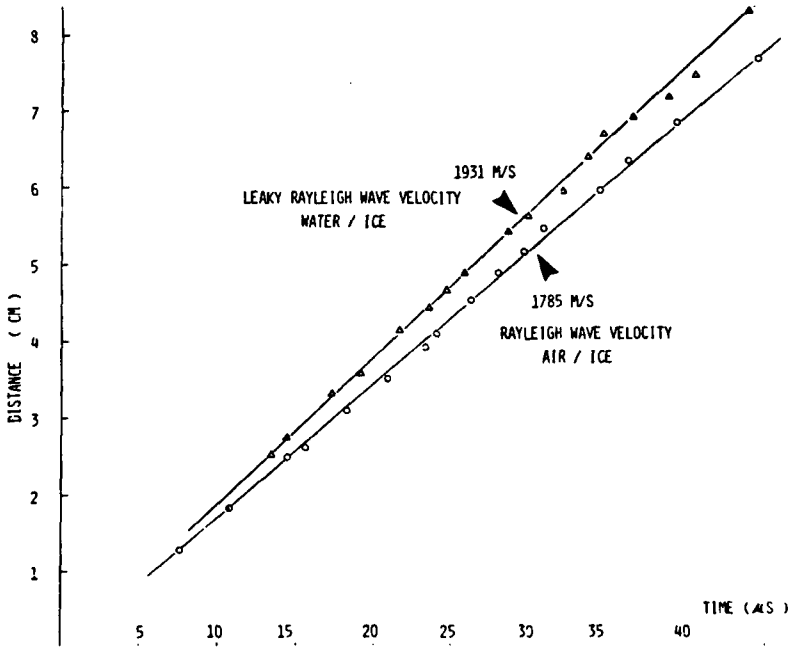

FIG. 4.4. Laboratory measurement of velocity of Rayleigh wave and leaky Rayleigh wave along a water/ice interface. The shear wave velocity was 1945 m/s along the same path.

corresponding time of arrival of the Rayleigh wave. The second wave was large and arrived later than the corresponding direct acoustic wave in the water. These two waves were identified as the shear-leaky Rayleigh wave and the Scholte wave, respectively, as shown below.

The time of arrival of the Rayleigh wave and the leaky Rayleigh wave was plotted as function of range (FIG. 4.4). Along the wave propagation path the measured velocities were C_p = 3556 m/s, C_s = 1944 m/s, C_R = 1785 m/s, C_{RL} = 1931 m/s, C_{Sch} = 1243 m/s initially and dropped to 1233 m/s, and C_w = 1428 m/s away from the interface and 1403 m/s close to the ice. The leaky Rayleigh wave velocity was about 8 % greater than C_R. The effect of anisotropy of the ice block was of secondary importance to our immediate problem of determining the relative time of arrival of the different wave components along a fixed path along the interface. Table 1 shows the range of velocities obtained from different ice blocks.

The leaky Rayleigh wave decays rapidly with range (FIG.4.5). In this experiment, the 2.3 mm diameter transducers were used and the receiver was tilted to increase the coupling to the leaky Rayleigh wave. The received signal was recorded at different ranges x = 2.4, 2.7, 3.2, and 4.5 cm. A leaky compressional wave, a leaky Rayleigh wave, a small direct water wave, and a Scholte wave were detected.

The effect of lifting the receiver transducer away from the interface is demonstrated in figure 4.6. The top waveform was obtained with the receiver at the interface (z = 0), where z is the vertical distance between the receiver and the ice surface. The distance between source and receiver was 3.6 cm. A distinct Scholte wave much greater than the leaky Rayleigh wave was observed. As the receiver was lifted slightly above the interface (z = 4 mm), the amplitude of the leaky Rayleigh wave increased while the Scholte wave amplitude decreased drastically. Brekhovskikh [33] and Strick [31] gave a good description of the field in the liquid indicating that the amplitude of a pulsed leaky Rayleigh wave should increase as the receiver is lifted from the interface but the increase ends as soon as the time of arrival of the theoretical refracted shear wave becomes smaller than the travel time of the direct water wave.

4.4 LEAKY R WAVE OR REFRACTED SHEAR WAVE

Broadband single pulse excitation was utilized to separate in space and time the different wave components along the liquid/solid interface. Strick [31] and van der Hijden [8] showed that the velocity of the leaky Rayleigh wave increases from the Rayleigh wave velocity to the shear wave velocity as the liquid density is increased. The time separation between a shear wave pulse and a leaky Rayleigh wave would therefore decrease as $C_{RL} \rightarrow C_s$. The ultrasonic experiments yielded C_s = 1944 m/s and CRL = 1931 in the above water/ice model. At a range of 4 cm, the difference in time of arrival of the shear wave and the leaky Rayleigh wave is only 0.14 μs

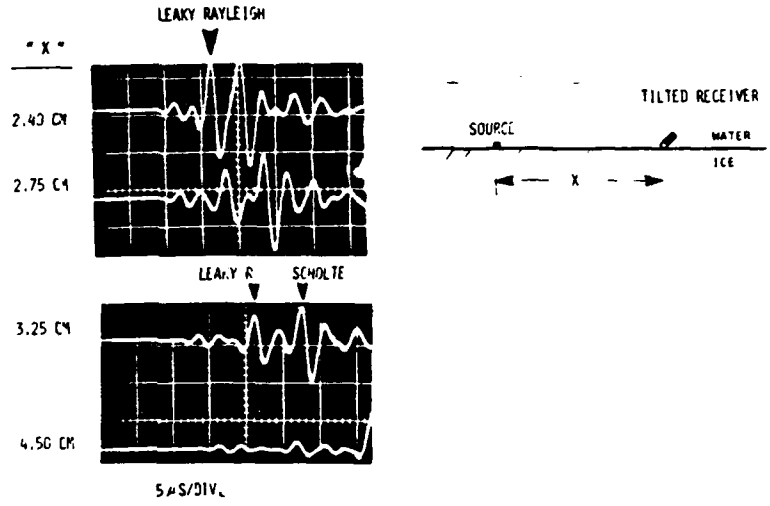

FIG. 4.5. Attenuation of leaky Rayleigh wave at water/ice interface with range.

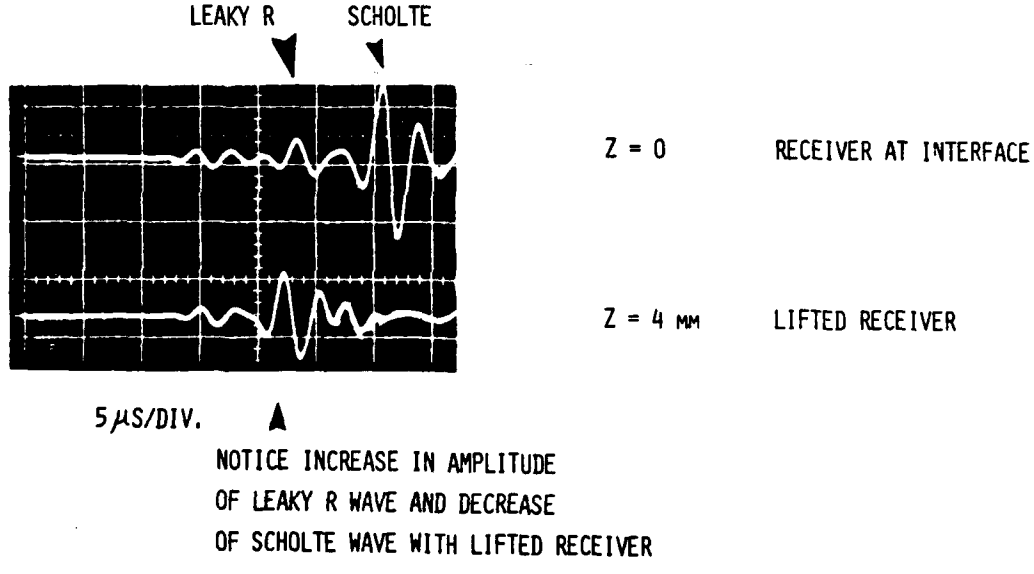

FIG. 4.6. Effect of lifting receiver transducer away from ice/water interface. Notice increase of leaky Rayleigh wave amplitude and decrease of Scholte wave with lifting the receiver.

which is about 1/18 th of the leaky Rayleigh wavelength. It is not practical to try to increase the pulse frequency or range to separate in time RL and S because RL decays rapidly with range at a fixed rate per wavelength. Could a refracted shear wave have been interpreted as the leaky R wave ?

The leaky Rayleigh wave has most of its energy in a thin layer near the surface of the solid which decays exponentially with depth. The shear wave however, is a body wave with most of its energy located deep into the solid forming a shear window around 45° for a small circular disc source on a solid half-space [96]. The presence of a shallow crack at the solid surface would have a much greater effect on the surface leaky R wave than on the body shear wave. A baseline experiment was conducted with a large limestone block to first demonstrate the effect of a shallow crack on the Rayleigh wave. The parameters of the limestone block were c_p = 3656 m/s, C_s = 2249 m/s, CR = 2076. Figure 4.7(a) shows the configuration with compressional vertical source and receiver transducers on the free surface of the limestone block separated by 6.1 cm. The received signal consisted of a small compressional wave, a large Rayleigh wave, and a negligible shear wave. Notice that the compressional receiver detects the vertical motion of the solid which would couple to an adjacent liquid half-space. After recording the received signal, the transducers were then replaced with transversely oriented shear wave transducers and the new received signal was recorded (FIG.4.7(c)). The signal was dominated by a shear wave. An "infinitely " long shallow groove (1.6 mm wide x 5 mm deep) was machined on the surface of the limestone block interrupting the wave path between source and receiver as shown in figure 4.7. The previous measurements were repeated with the groove present. The shallow groove severely attenuated the Rayleigh wave and had a small effect on the compressional wave (FIG.4.7(b)) and on the shear wave (Fig.4.7(d)). In this experiment, the groove was empty and not filled with water.

The second experiment extended the shallow crack measurements to the water/ice model (FIG. 4.8). A long shallow groove (about one wavelength deep) was made on the flat surface of an ice block submerged in water. Compressional source and receiver transducers were placed on the ice surface with x = 4.4 cm. The receiver was located before the groove as shown. A distinct pulse was received at the time corresponding to the transit time of a leaky R wave (this time also closely coincided with the time of arrival of the shear wave). The receiver was then moved to x = 5.5 cm after the crack. The received signal preserved the first arriving leaky compressional wave, however, the leaky Rayleigh wave almost disappeared, while the Scholte wave was partially attenuated.

The third experiment examined the vertical and radial particle motion at the water/ice interface. Figure 4.9 shows expanded

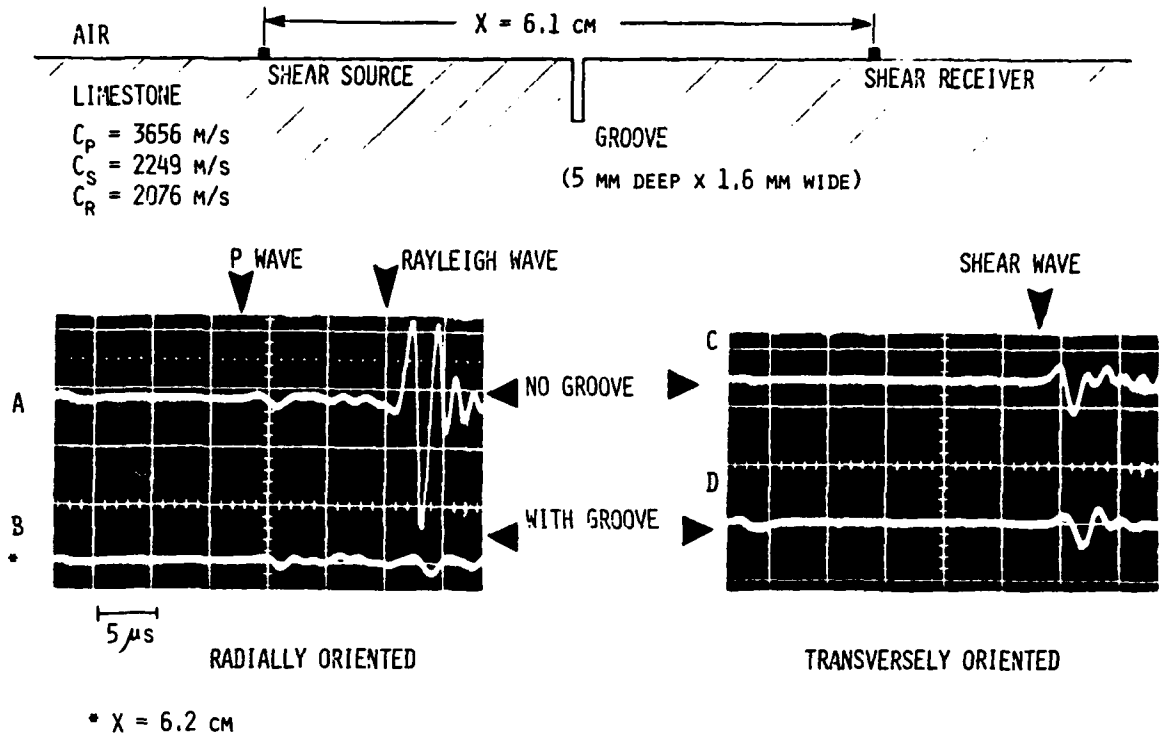

FIG.4.7. Effect of shallow groove in solid half-space on transmission of compressional, shear, and Rayleigh waves.

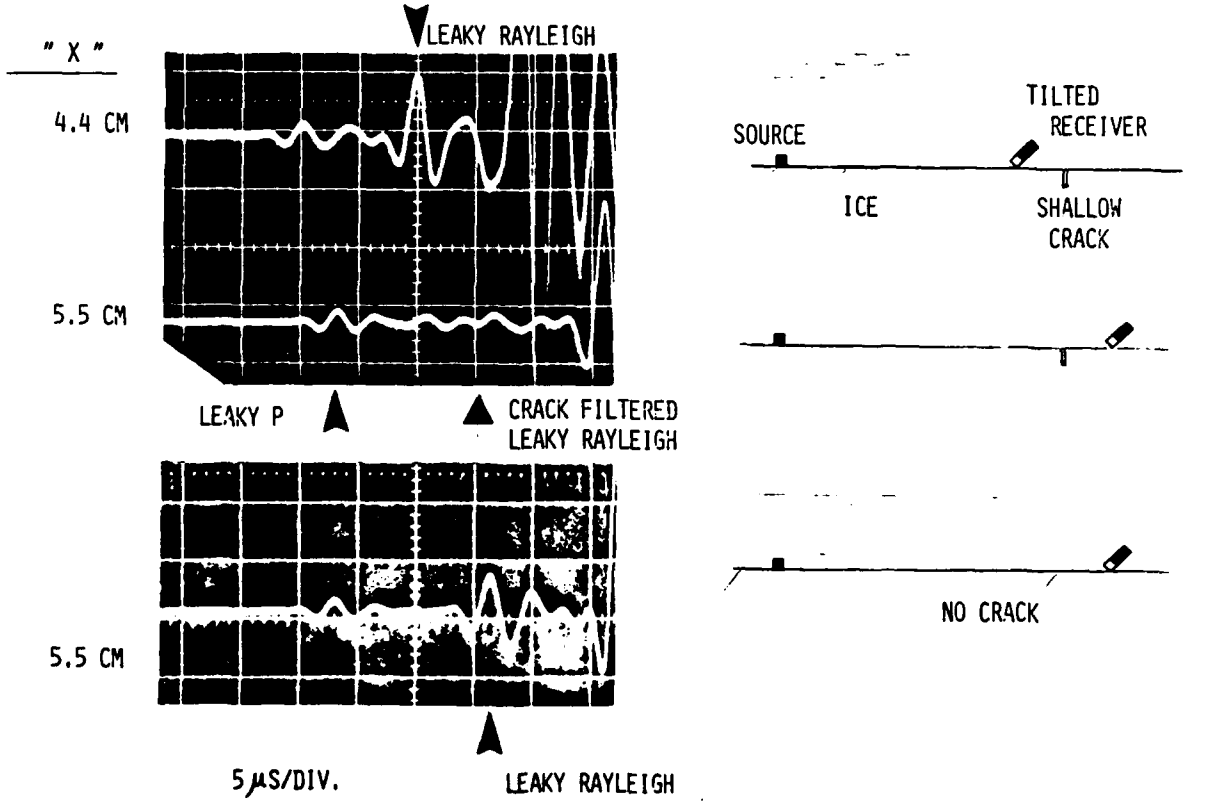

FIG.4.8. Effect of shallow crack on interrupting the leaky Rayleigh wave at a water/ice interface.

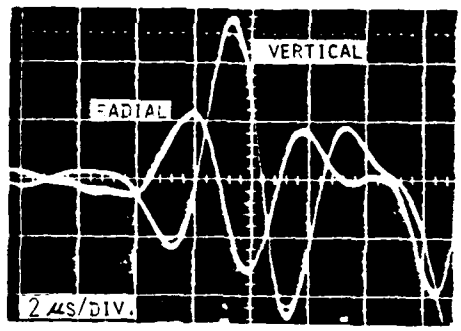

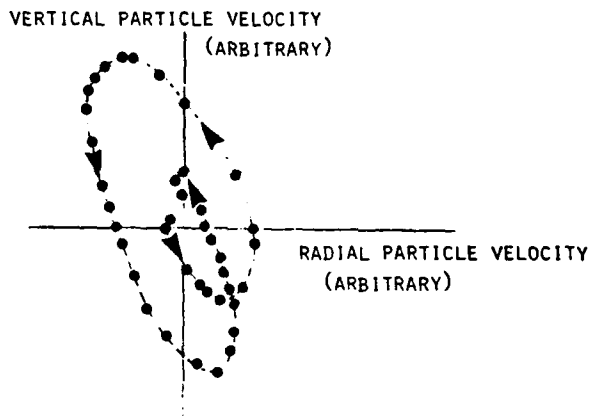

Figure 7.

FIG.4.9. Vertical and radial particle velocity of leaky Rayleigh wave at water/ice interface with corresponding hodograph.

TABLE 1. MEASURED WAVE VELOCITIES AT WATER/ICE INTERFACE

	WAVE TYPE	RANGE OF VELOCITIES FROM DIFFERENT MODELS	MEASURED VELOCITIES (ONE DIRECTION & ONE MODEL)
FRESH WATER ICE	COMPRESSIONAL	3100 - 3775 m/s	3556 m/s
	SHEAR	1844 - 1980 m/s	1944 m/s
	RAYLEIGH	1690 - 1829 m/s	1785 m/s
WATER	COMPRESSIONAL VELOCITY	1428 m/s **	1428 m/s AT 5°C
WATER / ICE	SCHOLTE	1224 - 1275 m/s	1243 m/s
	LEAKY RAYLEIGH	1766 - 1950 m/s	1931 m/s

** 1403 at 0°C and a corresponding Scholte wave of 1233 m/s.

TABLE 2. VELOCITY AND DENSITY RATIOS FOR WATER/ICE INTERFACE COMPARED TO BROWER'S MAXIMUM ALLOWABLE DENSITY RATIO RESTRICTING THE EXISTENCE OF THE LEAKY RAYLEIGH WAVE

		MAXIMUM ALLOWABLE DENSITY RATIO
WATER/SEA-ICE	$C_W / C_P = 0.429$ $C_W / C_S = 0.968$ $\rho_W / \rho_{ICE} = 1.11$ ----------	$\rho_W / \rho_{ICE} < 0.27$
FRESH WATER/ICE	$C_W / C_P = 0.416$ $C_W / C_S = 0.740$ $\rho_W / \rho_{ICE} = 1.087$ ----------	$\rho_W / \rho_{ICE} < 0.75$

oscilloscope traces of vertical and radial particle velocity components of a pulsed leaky R wave at a water/ice interface measured at x = 5.4 cm. The corresponding hodograph formed retrograde elliptical paths providing an additional proof that the detected pulse is a leaky R wave and not a refracted shear wave.

In order to provide additional insight into the propagation of a leaky Rayleigh wave at a water/ice interface, a comparison was made between the Rayleigh wave from the air/ice interface and the leaky Rayleigh wave detected by a buried receiver near the ice surface. Figure 4.10(a) shows the free surface Rayleigh wave and figure 4.10(b) shows the water/ice leaky Rayleigh wave. The receiver was located 2.5 mm below the interface (1/10th of a wavelength) at a range of 7.1 cm. The onset of the leaky Rayleigh wave was mixed with a small high frequency shear wave component. The Scholte wave was also detected by the buried receiver.

In table 2 , the velocity and density ratios for the water/ice interface are compared to Brower's maximum allowable density ratio restricting the existence of the leaky R wave. For the sea-ice case, the water to ice density ratio is 1.11 while the maximum allowable density ratio is less than 0.27. The fresh-water ice model has a density ratio of 1.087 and a maximum allowable density ratio less than 0.75.

FREON 113/ICE INTERFACE

Strick [31] and Phinney [34] theoretically demonstrated the effect of increasing the ratio of liquid to solid density on the velocity of the leaky R wave. An experiment was carried out to examine the leaky R wave at the interface of a dense low-velocity liquid in contact with ice. Freon 113 was chosen in the experiment because its density is greater than water 1.565 kg/m^3, and its compressional velocity is much lower than the shear wave velocity of ice. The measured compressional wave velocity was 671 m/s at 0°C of this first Freon 113 sample. The ice block was fixed at the bottom of the tank. The measured parameters of this ice block were : C_p = 3350 m/s and C_s = 1901 m/s along the wave propagation path. The velocity of the leaky R wave was first obtained from the Freon 113/ice model, then the Freon was replaced with water and the measurement was repeated. The measured leaky R wave velocity was 1821 m/s from the Freon/ice model and 1852 m/s from this water/ice model. The accuracy of the velocity measurement was about 0.5 %. The results indicated that although Freon 113 was heavier than water, its corresponding leaky R wave velocity was lower than the water/ice case. A typical waveshape of the received signal from the Freon 113/ice interface is shown in figure 4.11. Both the leaky compressional and leaky Rayleigh waves are very well defined.

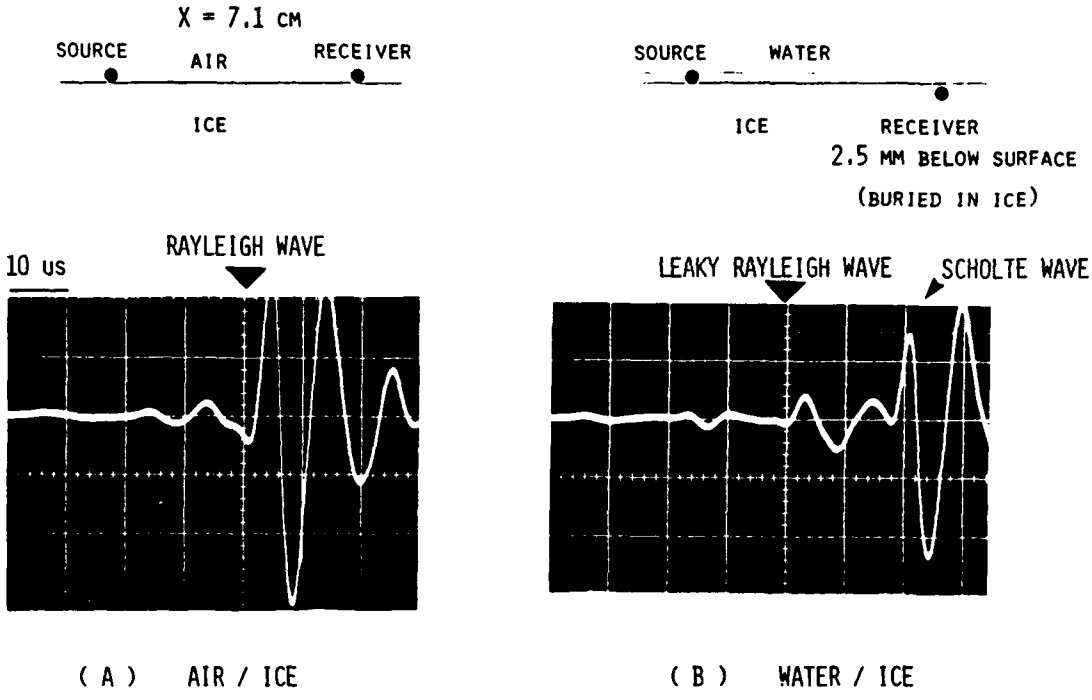

FIG. 4.10. Comparison of the Rayleigh wave at an air/ice interface to the leaky Rayleigh wave at a water/ice interface detected with a receiver buried in the ice at a depth of $\lambda / 10$. The onset of the leaky Rayleigh wave is mixed with a small shear wave component at higher frequencies. The Scholte wave was also detected by the buried receiver.

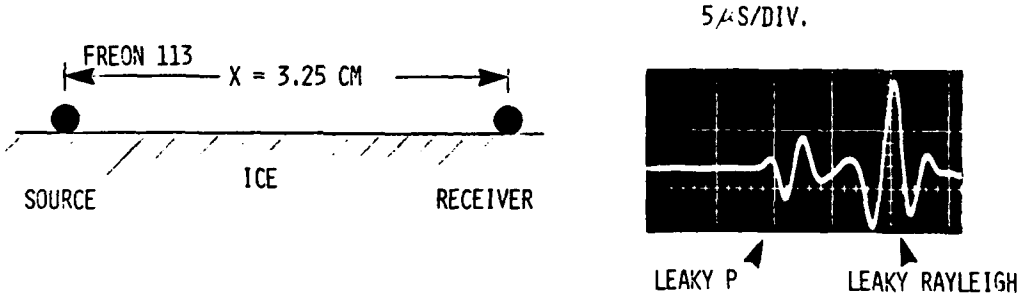

$$C_{FREON} = 671 \text{ M/S}$$

$$\frac{\rho_{FREON}}{\rho_{ICE}} = 1.7$$

FIG. 4.11. Leaky Rayleigh wave at Freon 113/ice interface demonstrating the effect of a dense liquid.

4.5.EXPERIMENT CONTROLLING RELATIVE ELASTIC PROPERTIES OF LIQUID/SOLID INTERFACE CROSSING THEORETICAL LIMIT ON EXISTENCE OF LEAKY RAYLEIGH WAVE

The relative elastic properties of Freon 113 and acrylic were varied by controlling their temperature to provide a unique opportunity to examine the changes in the leaky Rayleigh wave as the theoretical limit on its existence was crossed. The Freon 113 batch used in this experiment had a higher compressional wave velocity than the first sample used in figure 4.11. Figure 4.12 presents the results of the experiment and the measured model parameters at 3 different temperatures 4°C, 9.2°C, and 15.4°C. Using these model parameters, the theoretical leaky Rayleigh wave roots of the characteristic equation were calculated for the three different temperatures. According to the theoretical results, the real part of the leaky Rayleigh wave root equals the shear wave velocity of the acrylic at 9.2°C. Above this temperature the leaky Rayleigh wave can exist, and below this temperature it violates the theoretical existence condition by exceeding the shear wave velocity. Figure 4.12(b) shows the leaky compressional wave and the leaky Rayleigh wave obtained at 15.4°C. At this temperature, the shear wave velocity was 1359 m/s and the calculated leaky Rayleigh wave root was 1352 - 155i. The middle trace in figure 4.12 corresponds to the critical temperature results where the leaky Rayleigh wave root equaled 1370 - 162i, and the shear wave velocity was 1370 m/s. The top trace obtained at 4°C shows the leaky P wave and the leaky Rayleigh wave in the domain where the theoretical existence condition was violated. At this temperature, the real part of the leaky Rayleigh wave root (1397 -167i) exceeded the shear wave velocity (1382 m/s). The waveshape of the received signal at the three different temperatures is practically the same. The onset of the Scholte wave can also be seen from the photographs. The greatest effect of the temperature change was on the compressional wave velocity of the Freon. This drastically increased the Scholte wave velocity as the temperature dropped from 15.4°C to 4°C (notice the Scholte wave in top trace is more to the left than that of the bottom trace). The ultrasonic modeling results did not find evidence that the leaky Rayleigh wave can have a phase velocity greater than C_s.

For comparison purposes, figure 4.13 shows the measured Rayleigh wave at the free surface of a limestone half-space compared to the leaky Rayleigh wave at the water/limestone interface. The measured velocities were C_R = 1989 m/s and C_{RL} = 2103 m/s. The waveshape of the leaky Rayleigh wave was similar to the water/ice case consisting of a distorted pulse with a high-frequency onset and a low-frequency tail. The leaky Rayleigh wave from the freon/ice model (FIG. 4.11) did not exhibit this waveshape characteristic.

Further theoretical and experimental investigations are needed on the water/ice leaky Rayleigh wave.

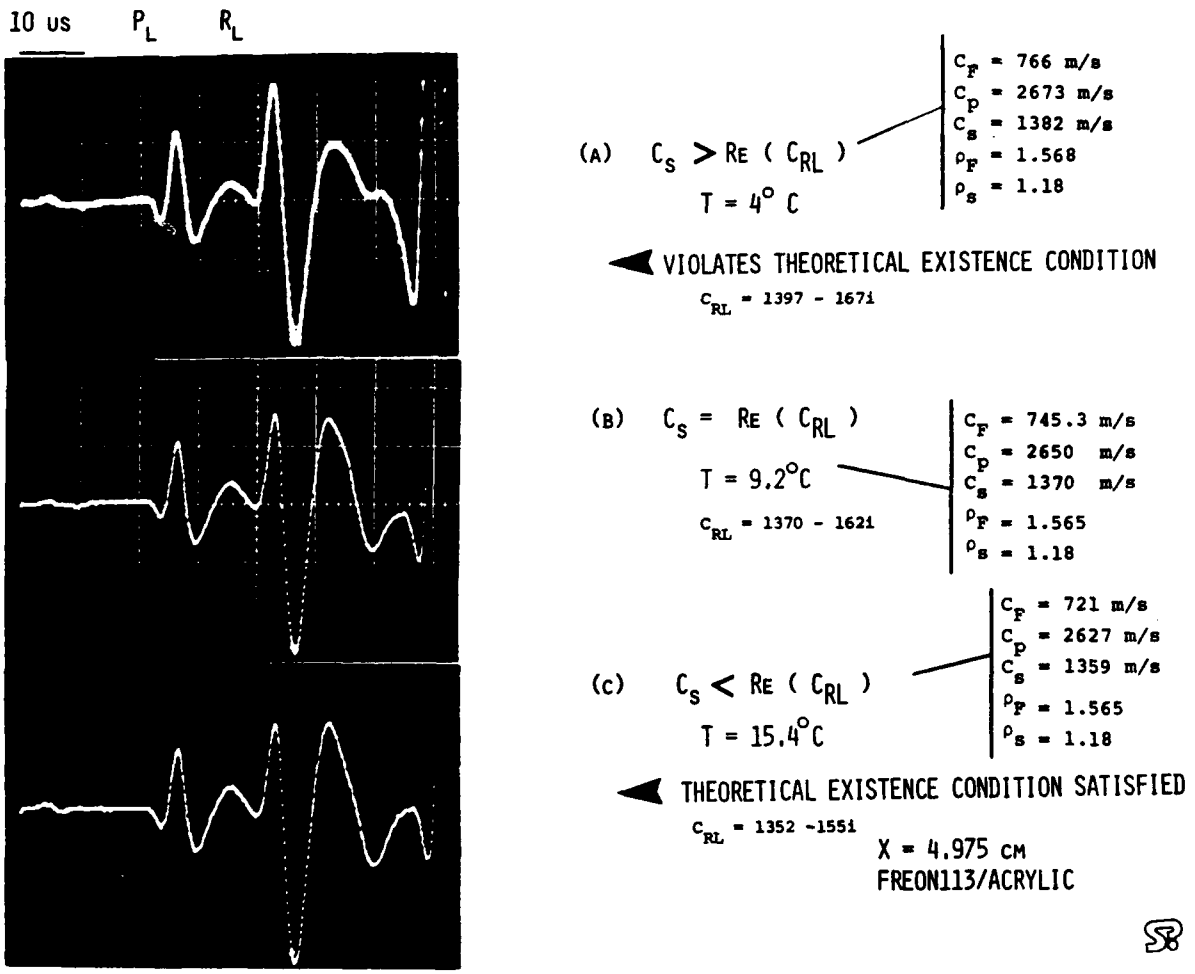

FIG.4.12. Relative elastic properties of liquid/solid controlled by changing the temperature to demonstrate the effect of crossing the theoretical limit on the existence of the leaky Rayleigh wave. The density of the liquid is greater than the density of the solid similar to the water/ice case. The dominant effect of varying the temperature is on the Freon 113 compressional velocity. The leaky Rayleigh wave velocity increases as the fluid loading effect increases. The ultrasonic modeling results do not indicate that the leaky Rayleigh wave can propagate with a velocity greater than the shear wave velocity contradicting the theoretical predictions.

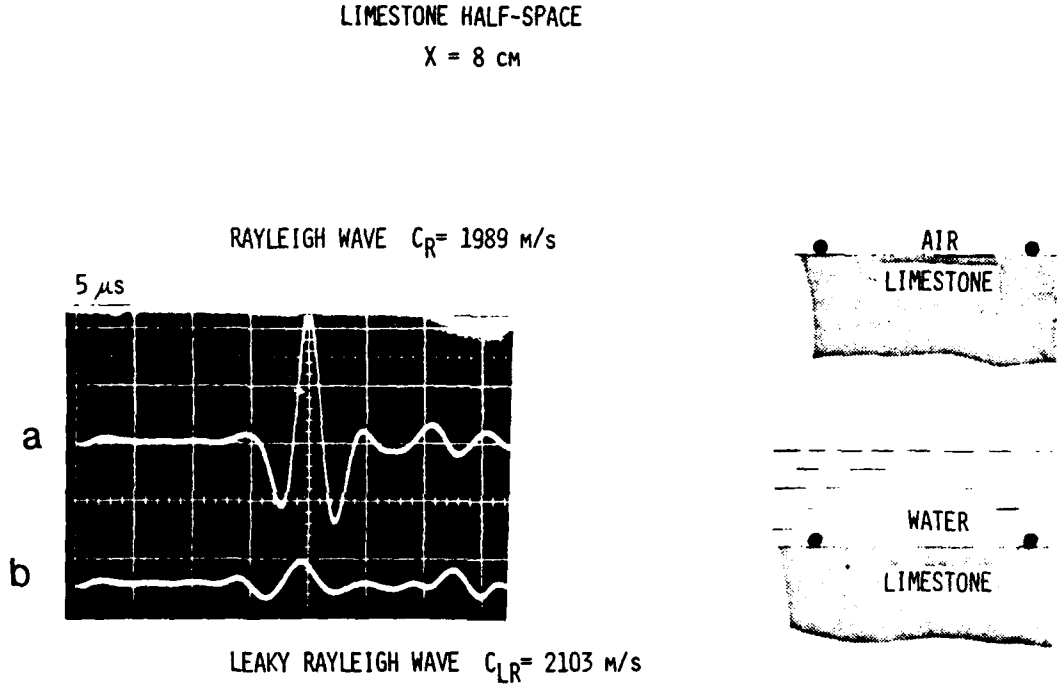

FIG. 4.13. Comparison of Rayleigh wave at air/limestone interface and leaky Rayleigh wave at water/limestone interface.

5. CRACKS IN ARCTIC ICE COVER

Understanding elastic wave propagation phenomena in floating ice sheets is important to the interpretation of Arctic field data and characterization of the ice cover. A great deal of work has been done on thermal cracking noise and on the effect of surface roughness on scattering of underwater acoustic waves. Little is known about the effects of near-closed dry surface cracks in a floating plate on the coupled liquid/solid elastic waves. The characteristic equation for elastic waves in a floating isotropic elastic plate was derived by Press and Ewing [49] assuming a Poisson's ratio of 0.25. Hunkins [4] studied seismic waves in sea-ice and used Press and Ewing's theoretical results to determine the thickness of the ice plates from the flexural wave dispersion curve. Hunkins observed that the plate thickness determined from the theoretical dispersion curve and from the air-coupled flexural waves is generally lower than the actual thickness found by direct measurement. Stein [3] derived theoretical solutions for the floating ice sheet for arbitrary Poisson's ratio and including the effects of absorption. Recently, Tolstoy [50] calculated the effect of mass loading created by added scatterers to a smooth plate on reducing the flexural wave velocity, where the spacing between scatterers is less than 1/6 th the flexural wavelength to satisfy the "Boundary wave" conditions.

To the author's knowledge, no theoretical or experimental results have been published to date on the propagation of flexural waves in a floating ice sheet with multiple surface cracks. A similar problem exists in the field of improving the sound insulating properties of plywood panels where machined grooves are utilized to artificially reduce the flexural wave velocity to decrease the radiation characteristics of the panel [51]. Arctic ice has roughness and cracks both causing a decrease in the flexural wave velocity through two different mechanisms namely mass loading and reduced flexural rigidity. The effects of near-closed cracks in Arctic ice plates on low-frequency underwater acoustic waves seem to have been overlooked.

In this section, preliminary laboratory ultrasonic modeling results are presented revealing the potential importance of shallow cracks to Arctic Acoustics [18]. Experimental field data from the Canadian Arctic obtained by G. H. Brooke [52] tend to support the ultrasonic modeling findings. These observations have a bearing on ice reflectivity [53], anisotropy, shear wave attenuation coefficient, and air-coupled flexural waves [54].

5.1 ESTIMATED CRACK PROPERTIES IN SEA-ICE

In the Arctic, different types of cracks exist varying from open cracks (leads) which pass completely through the ice plate to air-filled near-closed shallow cracks on the top surface of the floating ice [46]. Surface cracks can be generated by thermally induced stresses in the upper ice layer due to rapid air temperature changes above the ice. These cracks have a maximum width of about 2 cm but in many cases are near-closed. Thermal crack spacing depends on cracks dimensions; generally, the crack spacing increases as the crack dimensions increase. For example, tiny cracks have spacings in the order of centimeters, whereas, large cracks are separated by tens of meters. In the limiting case of cracks which form pressure ridges, the nominal spacing is roughly 100 m. It is estimated that near-closed crack spacing may vary between 3 - 40 m for crack depth extending from 10 cm to about one-half the plate thickness.

Assur [47] reported on "long-wave cracks" which are closely spaced long fissures in the ice extending virtually from horizon to horizon, parallel to each other and occuring primarily in winter. These cracks do not follow lines of weaknesses in the plate and cut right through old or new pressure ridges. Two other types of cracks were also described by Assur [47] "parallel-edge-cracks" and "perpendicular-edge cracks". "Parallel-edge cracks" run parallel to the edge of the plate some 12-15 m away, and "perpendicular-edge-cracks" form at fairly uniform distances of 50-100 m apart. Both types of cracks occur primarily in the spring and summer. Snow, slush, and water may partially fill the air-filled cracks. An example of an ice bottom crack observed in the Arctic was desribed by Berkson and Clay [48].

5.2 REDUCED FLEXURAL WAVE VELOCITY BY CRACKS IN FLOATING PLATE

Prior to our preliminary 1985 research, interest in cracks in the ice was mainly on safety of operation of aircrafts and vehicles on sea-ice. There were no published papers on dry cracks distribution in sea-ice and their interaction with low-frequency underwater acoustic waves. Upward refraction in the Arctic causes substantial interactions of underwater acoustic waves with the ice cover. Although several research papers focused on the effects of ice roughness on transmission loss, apparently no studies have been reported on the effect of cracks in the ice cover on reducing the flexural rigidity of the ice plate in relation to Lamb waves and on energy exchange between the water and the ice. Coupling between the acoustic waves in the water and the elastic waves in the ice plate is function of the relative densities and phase velocities of the waves. Depending on the number, size, and spatial distribution of cracks, the flexural wave velocity of a low-frequency component may be higher or lower than the water compressional velocity. Laboratory

ultrasonic models are used to provide physical insight into a potentially important low-frequency transmission loss mechanism caused by the effective reduced flexural rigidity of the cracked ice cover.

The first set of experiments were carried out to compare the flexural wave dispersion curve for the following cases: 1) plate in air, 2) floating plate on a water half-space, 3) plate with multiple shallow cracks in air, and 4) floating plate with shallow dry cracks on its top surface. The experimental setup consisted of broadband 2 mm diameter Sonoquest compressional ultrasonic transducers (40-900 kHz) used to generate and detect ultrasonic waves in a 2.26 mm thick Plexiglas plate. The source was excited with either a 2.5 us pulse or with a gated sinusoidal signal at selected frequencies. The receiver was connected to an amplifier, a bandpass filter, and an oscilloscope. Phase velocity measurements were obtained for the four cases mentioned above. The cracks in the plate were machined with the following dimensions: crack depth = H/3, where H = plate thickness, crack width = 0.1 mm, crack length = entire length of the plate ("infinite"), crack spacing was random with a 5 mm average spacing, and all cracks were machined parallel to each other. The flexural waves propagated normal to the cracks. The source and receiver were placed on the top surface of the plate while the bottom surface of the plate was water loaded for cases (2) and (4). The crack spacing was selected to be random and not periodic to avoid resonances of a periodic structure [57,58]. The four models are shown in figure 5.1..

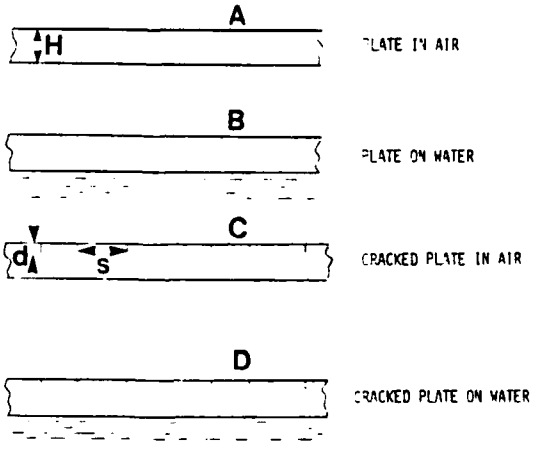

FIG. 5.1. Plate models used in the experiments.

The flexural wave phase velocity was plotted vs frequency (Fig. 5.2) for the four cases. The plate compressional wave velocity was 2345 m/s and the shear velocity was 1388 m/s. The solid smooth plate in air had the fastest flexural wave velocity. The floating cracked plate on water had the lowest flexural wave velocity. The effect of water loading on reducing the flexural wave velocity was comparable to the effect of cracks on reducing the flexural wave velocity. At about 200 kHz, the average crack spacing was about one wavelength. It is interesting to note how an average crack spacing greater than a wavelength can affect the high frequencies above 200 kHz. The effect of cracks on reducing the flexural wave velocity increases as the frequency is decreased. In figure 5.3, the ratio of the flexural wave phase velocity to the shear wave velocity is plotted as function of kH for the four cases. At the low-frequency end of the curves, the average crack spacing is about 1/2 a wavelength of the flexural wave. The dispersion curves extend to kH values greater than 3. Tolstoy's paper [50], on the added scatterers to the plate to form a boundary wave, described boundary wave phenomena valid up to kH of about 1. The cracks reduce the flexural wave velocity by lowering the effective flexural rigidity, while the added scatterers in Tolstoy's paper reduce the flexural wave velocity by mass loading effects.

5.3 ICE THICKNESS DETERMINATION DISCREPANCY

Theoretical and experimental field data on sea-ice taken from Hunkins' 1960 paper [4] are shown in figure 5.4. The flexural waves indicate the sea-ice average thickness of about 2m, however, the average measured thickness from six holes drilled along the wave path was 2.55 m. Hunkins observed that sea-ice thickness determined from flexural wave dispersion or from air-coupled flexural waves is generally lower than the actual thickness. The presence of cracks in the ice plates was not taken into consideration. It seems that the effects of cracks on reducing the flexural wave velocity provide an explanation to the ice thickness discrepancy reported by Hunkins. Hunkins attributed the discrepancy to the anisotropy nature of sea ice and that it is probable that the shear vertical wave SV is slower than the shear horizontal wave SH. Seismograms obtained by Crary [57] on Fletcher's Ice Island indicated that the SV wave velocity is faster than SH. If the cracks provide the explanation to Hunkins' discrepancy, the reduced flexural wave velocity should be more pronounced the greater the distance between source and receiver in general. This stems from interacting with a greater number of cracks along the wave path. Hunkins' results shown in figure 5.4 seem to have these characteristics , namely, the field data recorded at 147 m, 207 m, 268 m, and 328 m progressively have a slower flexural wave velocity as the range was increased. Quantitative field studies on Arctic ice are needed to actually verify the effect of cracks.

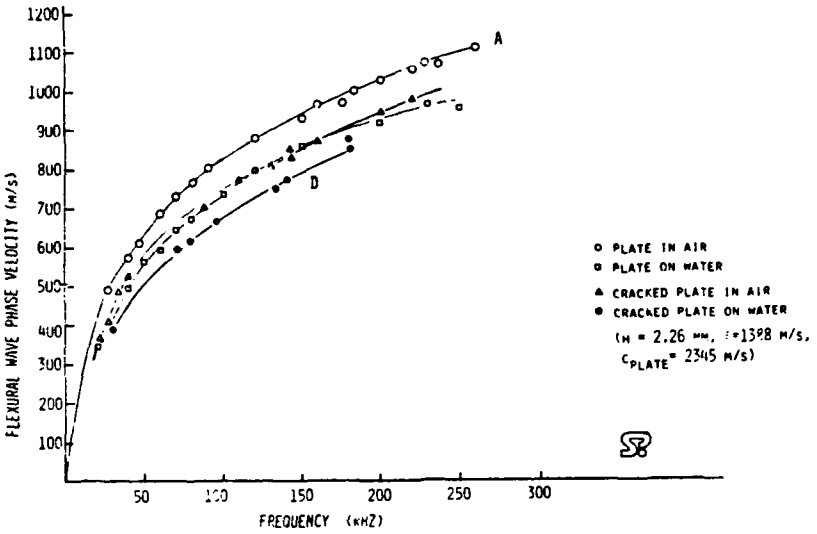

FIG.5.2. Decrease of flexural wave velocity by cracks and water loading. Model consists of a 2.26 mm thick Plexiglas plate. Average crack spacing is 5 mm and crack depth d = h/3 .

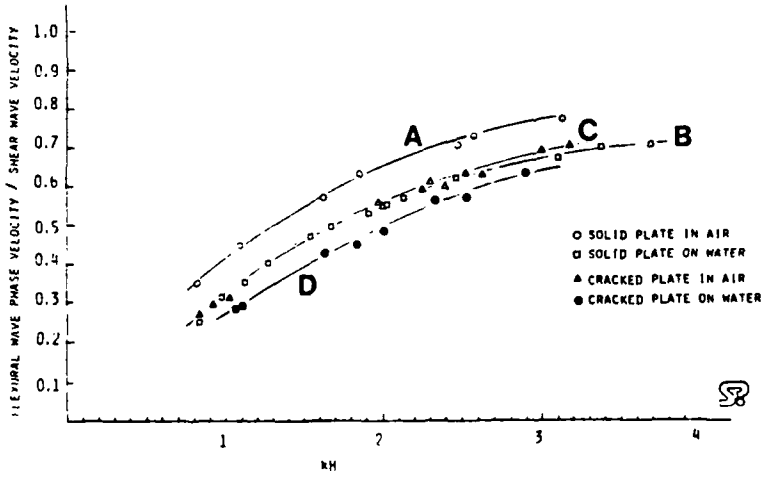

FIG. 5.3. Same as figure 5.2 plotted vs kH.

In the spring of 1986, Brooke [52] obtained preliminary seismic time series plots from smooth and rough ice plates in the Canadian Arctic. Flexural waves were compared from a smooth patch and from a rough patch where the ice plate thickness was uniform. Brooke's preliminary Arctic field data showed an unmistakable decrease in the flexural wave velocity when the propagation is in the rough ice. Figure 5.5 shows a typical set of flexural wave data where the rough ice flexural wave when aligned arrives later than the corresponding smooth ice flexural wave as range was increased by 80 m. Further field and laboratory studies are planned to quantitatively characterize the effects of shallow cracks in the ice plates on Arctic acoustics. The recent preliminary field data seem to support the ultrasonic modeling predictions.

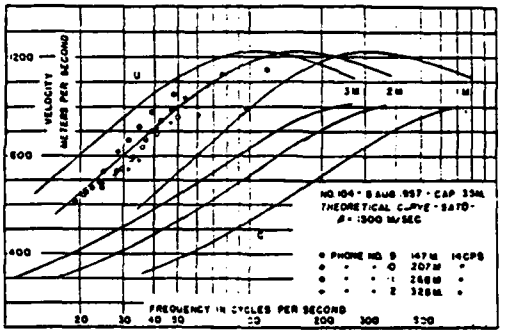

Comparison of observed and theoretical dispersion for record 104, August 8, 1957.

FIG. 5.4. Sea-ice thickness determined from flexural wave dispersion is generally lower than the actual thickness. Fom Hunkins 1960, J. Geophys. Res. 65(10), page 3467. The effect of cracks on reducing the flexural wave velocity in floating ice plates provides an explanation for this discrepancy.

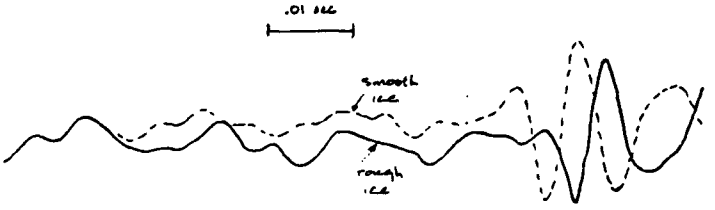

FIG. 5.5. Comparison of flexural waves from smooth ice and rough ice. Geophones separated by 80 m. (G. H. Brooke/DREP 1986).

5.4 LOW-FREQUENCY TRANSMISSION LOSS BY CRACKS

In this section, new ultrasonic modeling findings are presented [18-19] demonstrating that shallow cracks in Arctic sea-ice create substantial backscatter and attenuate near-grazing low-frequency underwater acoustic waves. The new findings provide an answer to the observed discrepancies between measured and predicted backscatter and attenuation of low-frequency waves. Previous theoretical models focused on scattering from the rough ice boundary and did not include scattering from cracks within the ice. Air-filled shallow cracks on the top surface of the floating ice plates extend near-vertically down in the plate causing sharp acoustic impedance discontinuities to the low-frequency waves penetrating the ice. Waves incident on the ice plate beyond the critical angle interact with the cracks. Upward refraction in Arctic water increases the percentage of energy interacting with the cracks therefore enhances the backscatter from each crack. The importance of cracks increases as the effective water waveguide depth is decreased. Experimental results are also presented on the interference of forward-scatter and backscatter, and on air-filled cracks compared with water-filled cracks. The ultrasonic models consist of a layer of water in contact with a smooth acrylic plate having parallel randomly spaced shallow grooves machined at the plate/air interface.

BACKGROUND

In Arctic acoustics, the measured underwater acoustic wave attenuation and backscatter at frequencies below 100 Hz are considerably higher than predicted [11-14]. The attenuation coefficient below 100 Hz is about 4.2×10^{-3} dB/km for the Polar environment and 0.3×10^{-3} dB/km for the Tropics [60]. DiNapoli and Mullen [12] showed that models based on treating the rough ice as a liquid layer results in very low attenuation and backscatter values. Green and Stokes [61] used a composite surface based on diffractive scattering from small-scale roughness on the sides of randomly oriented triangular ridge keels to improve matching the backscatter data at high frequencies (1.28 kHz - 2.56 kHz). Kuperman and Schmidt [13] included the effect of conversion to shear waves and trapping of low velocity shear waves in the ice to increase the predicted attenuation coefficient level. All the above models and others depend on scattering from the ice topography. Sea-ice has a great number of near-vertical shallow cracks extending from the top surface of the floating ice deep into the plate. Air-filled cracks present sharp impedance discontinuities to low-frequency acoustic waves coupled to the plate [18-19] . Upward refraction in the water increases the interaction of the guided water waves with the cracks. In flat ice regions, the effect of cracks would dominate. Sections

5.2 and 5.3 discussed the role of shallow cracks on reducing the flexural wave velocity and creating discrepancies in sea-ice plate thickness determination. The following experimental results show how shallow cracks in the upper surface of a floating plate can create significant backscatter and attenuate low-frequency underwater acoustic waves coupled to the plate.

EXPERIMENTAL SETUP

The ultrasonic model experimental setup consisted of a 2.23 mm thick "h" acrylic plate (60x91 cm) in contact with a water layer of thickness "H". Randomly spaced thin (0.1 mm wide) parallel cracks were machined at the plate/air interface. The depth of the cracks were h/2 and the number of cracks "N" was 90. The cracks were machined over half the width of the acrylic plate as shown in figure 5.6 to provide a crack-free region on the plate to be used as a reference. Figure 5.7 shows a detailed sketch of the cracks. The crack spacing distribution was plotted vs crack spacing over plate thickness in figure 5.8. The average crack spacing was 5.3 mm. The experiments were aimed at investigating the effect of shallow cracks on the acoustic waves propagating in the water layer in contact with the smooth non-cracked side of the plate. Enhanced ultrasonic modeling techniques were used to isolate and determine the role of cracks. The enhancement is generated by utilizing parallel "infinitely long" closely spaced cracks and shallow water. Real cracks in the Arctic have finite lengths and are not all oriented parallel to each other over the entire wave path. In the experiments, the water layer was on top of the plate, however, in figures 5.10-5.19, the acrylic plate is sketched on top of the water layer to match the Arctic floating ice configuration. The water waveguide was bounded by air on one side and by the cracked plate on the other. An air boundary was intentionally used to eliminate wave components associated with a second solid boundary and to confine the acoustic energy to the water layer and the plate.

Pulsed ultrasonic waves were generated and detected with broadband 2.35 mm diameter Sonoquest piezoelectric transducers (50 kHz - 700 kHz). The source/receiver range was selected and fixed in each experiment. The source and receiver were moved simultaneously from the crack-free region to the cracked region for comparison (FIG. 5.6). The receiver detected waves propagating in a direction normal to the cracks along the path connecting the source and receiver. The received signal was amplified, filtered, and displayed on an oscilloscope. The washapes of the received signals were recorded photographically. Spectral analysis of the received signals was accomplished using a 7L5 Tektronix spectrum analyzer. Table 5.1 lists the elastic properties of the modeling materials used.

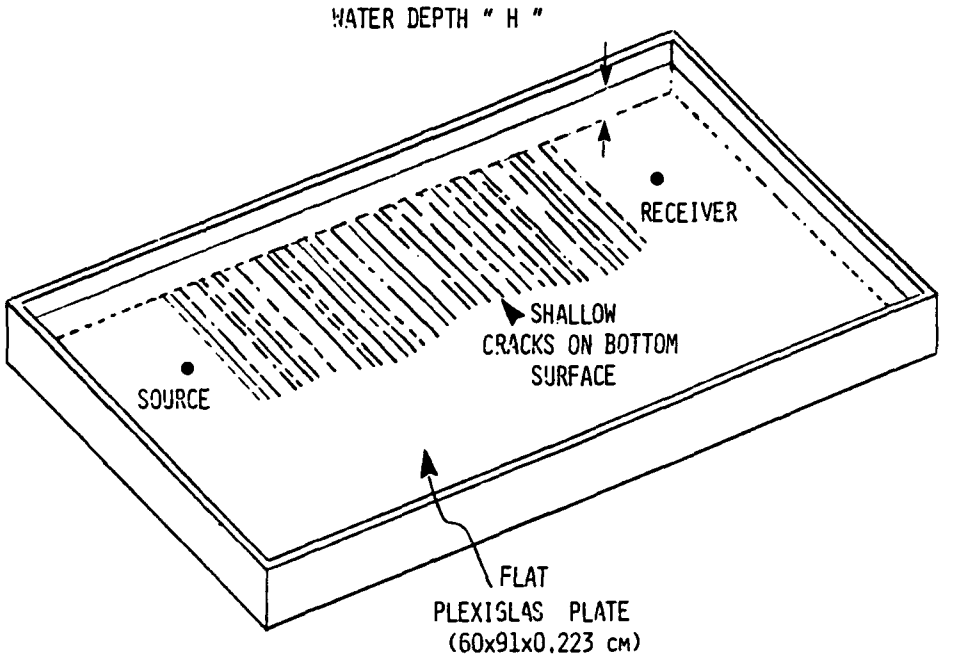

FIG.5.6. Diagram of experimental setup on cracks in floating plate.

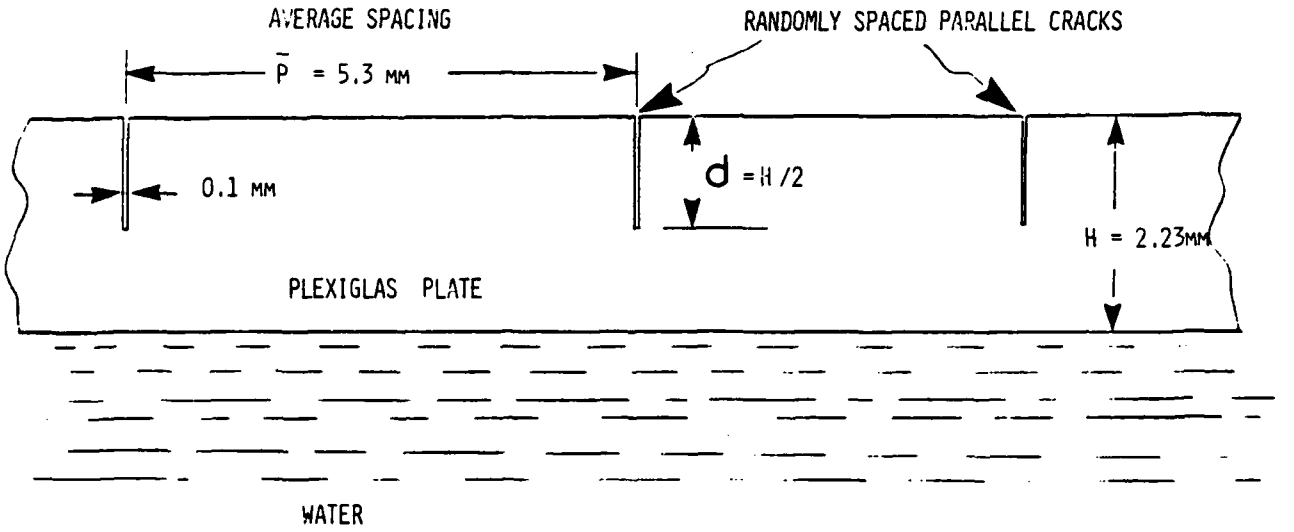

FIG. 5.7. Configuration of machined cracks in Plexiglas plate model. Number of cracks N = 90.

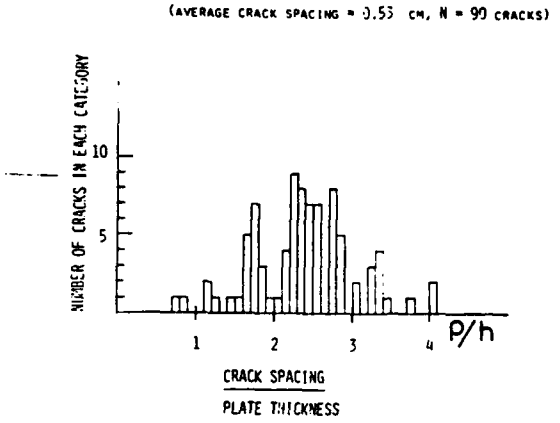

FIG. 5.8. Crack spacing distribution in Plexiglas plate model

EXPERIMENTAL RESULTS

In order to compare the effect of different waveguide boundaries on acoustic wave propagation in a water layer, a reference signal was first obtained from a "perfect waveguide" consisting of a free water layer (air/water/air) as described in reference [25] on an air-suspended water waveguide. Figure 5.9 compares the received acoustic waves from an air-suspended water layer (Fig. 5.9(a)), a water layer in contact with a thin solid acrylic plate (Fig. 5.9(b), and a water layer in contact with an acrylic plate having machined shallow cracks at the air/plate interface (Fig. 5.9(c)). In this experiment, the water depth H = 2 cm, the source/receiver range x = 20 cm (10H), and the plate thickness h = 0.11H. Both source and receiver were located near the water/air boundary. In figure 5.9(a), the "perfect waveguide" signal consisted of large nondispersed pulses similar to the results described in reference [25]. The top left photograph of figure 5.9 shows the waveshape of the received signal arriving at 135 us. The horizontal time scale was 20 us/div. .Introducing a solid flat acrylic plate in contact with the water layer generated early-arriving leaky plate waves and redistributed the acoustic wave energy as shown (Fig. 5.9(b)). Interference of the leaky plate waves with the first-arriving set of water waveguide pulses was noticeable. The bottom trace shows the effect of cracks in the plate on the acoustic waves. The leaky plate waves were almost eliminated and the water waveguide acoustic waves were attenuated (FIG. 5.9(c)). In the 20 cm range along the wave path, 30 cracks were present. Changes in the received signal were due to the characteristics of the acrylic plate.

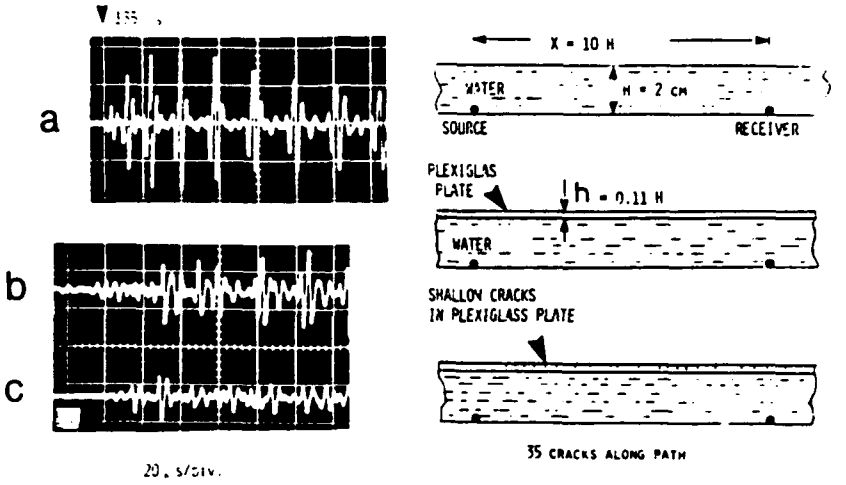

FIG. 5.9. Effects of floating plate on water waveguide waves. Top: air/water/air "perfect" waveguide. Middle: Solid plate in contact with water. Bottom: cracked plate in contact with water.

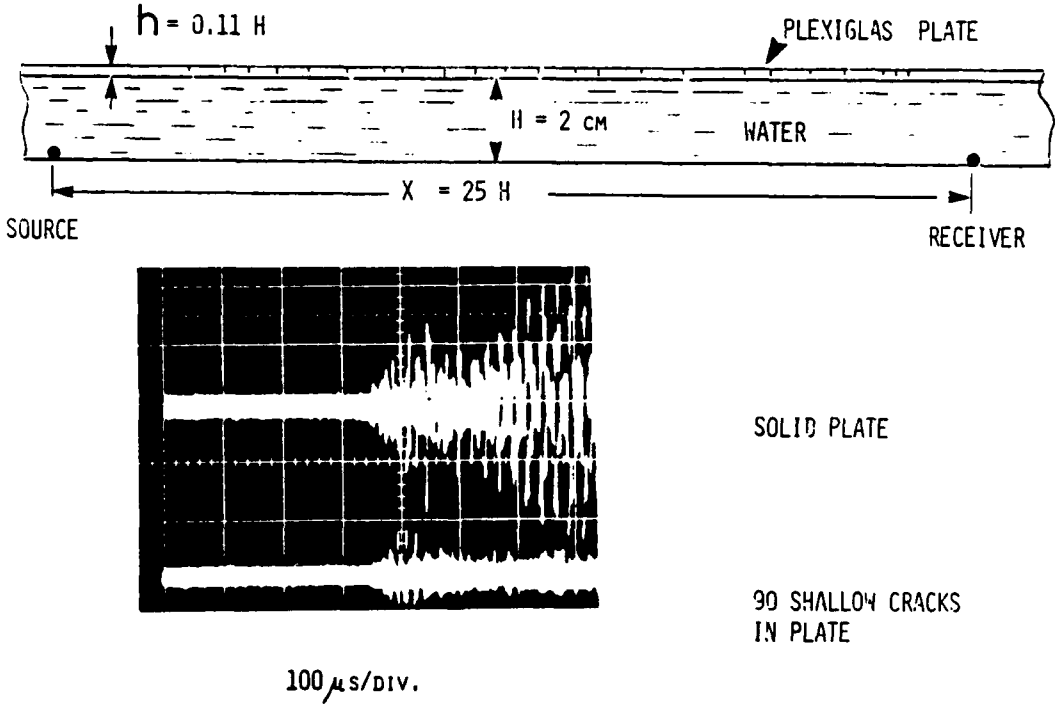

FIG.5.10 Severe attenuation of late-arriving pulses (high-order modes) by shallow cracks in floating plate.

Figure 5.10 shows the attenuation of very late-arriving waveguide pulses by the cracks. In this model, x = 25H, N = 90 cracks along the 50 cm range, H = 2 cm, and the oscilloscope time scale was compressed to 100 us/div. The late-arriving pulses corresponded to waves incident on the plate with large grazing angles. From the normal mode point of view, the late-arriving waveguide pulses are generated by the summing the low-frequency components of the different modes [25]. Attenuation of these late-arriving pulses can be interpreted as attenuation of the low-frequency components of the modes. The transducers were placed near the waveguide boundary to enhance the generation of the late-arriving pulses. In the Arctic, the late-arriving pulses are quickly dissipated to the ocean bottom and the received signal consists mainly of the first few pulses.

Figure 5.11 isolates the first reflection from the cracked plate and compares it with the reflection from the solid plate boundary. The water depth was increased to 5 cm, x = 50 cm, and the time expanded scale was 10 us/div. The reflected pulse shown in figure 5.11 was incident on the acrylic plate with a grazing angle of 9.5°. Although this angle was smaller than the critical grazing angle for water/acrylic, attenuation of the reflected pulse was observed. The spectrum of the gated portion of the received signal belonging to the first reflection from the plate is shown at the bottom right of the figure. The dot frequency was 200 kHz, the vertical scale 10 dB/div., and the horizontal scale 50 kHz/div. A dip in the spectrum of the cracked plate was observed between 200 kHz and 340 kHz from a single reflection.

As the water waveguide depth was decreased, the time separation between the pulses decreased and interference between the waveguide pulses occurred. In figure 5.12, the water depth was reduced to 2.9 cm and the range was again 50 cm. The source and receiver were located in the middle of the water column at H/2 to enhance the generation of the first-arriving pulses. The first three waveguide pulses were gated and recorded for both solid plate and cracked plate boundary models (Fig. 5.12(a) and (b)) with a 10 us/div. time scale. The corresponding spectra are presented at the bottom of figure 5.12. A broad null appeared in the vicinity of 275 kHz for the cracked plate case. Other frequency components were also attenuated but to a lesser degree.

As the water waveguide depth was further decreased to H = 1 cm, the waveguide pulses partially overlapped each other forming a dispersed wavetrain with the high frequencies arriving first (FIG. 5.13). Water wave components with frequencies between 150-400 kHz were attenuated. Maximum attenuation was again in the vicinity of 275 kHz.

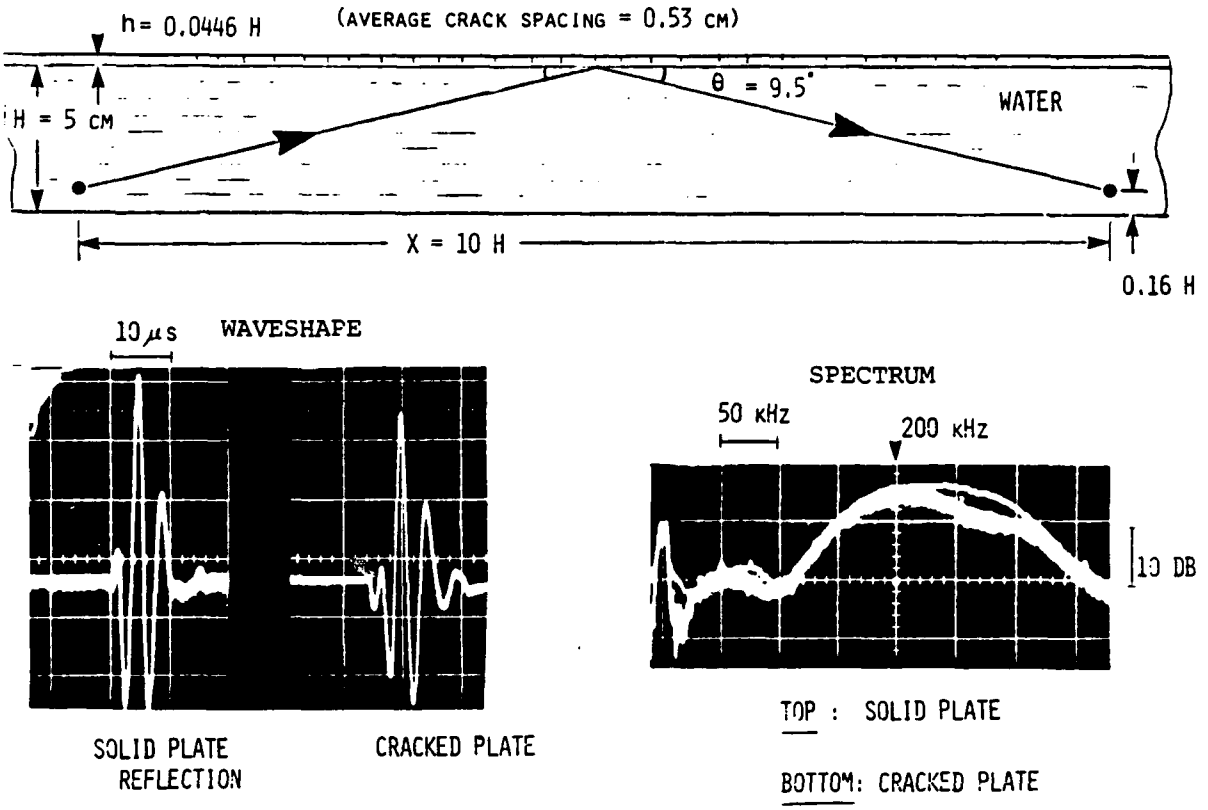

FIG. 5.11. Waveshape and spectrum of first water waveguide pulse reflected from floating plate with shallow dry cracks.

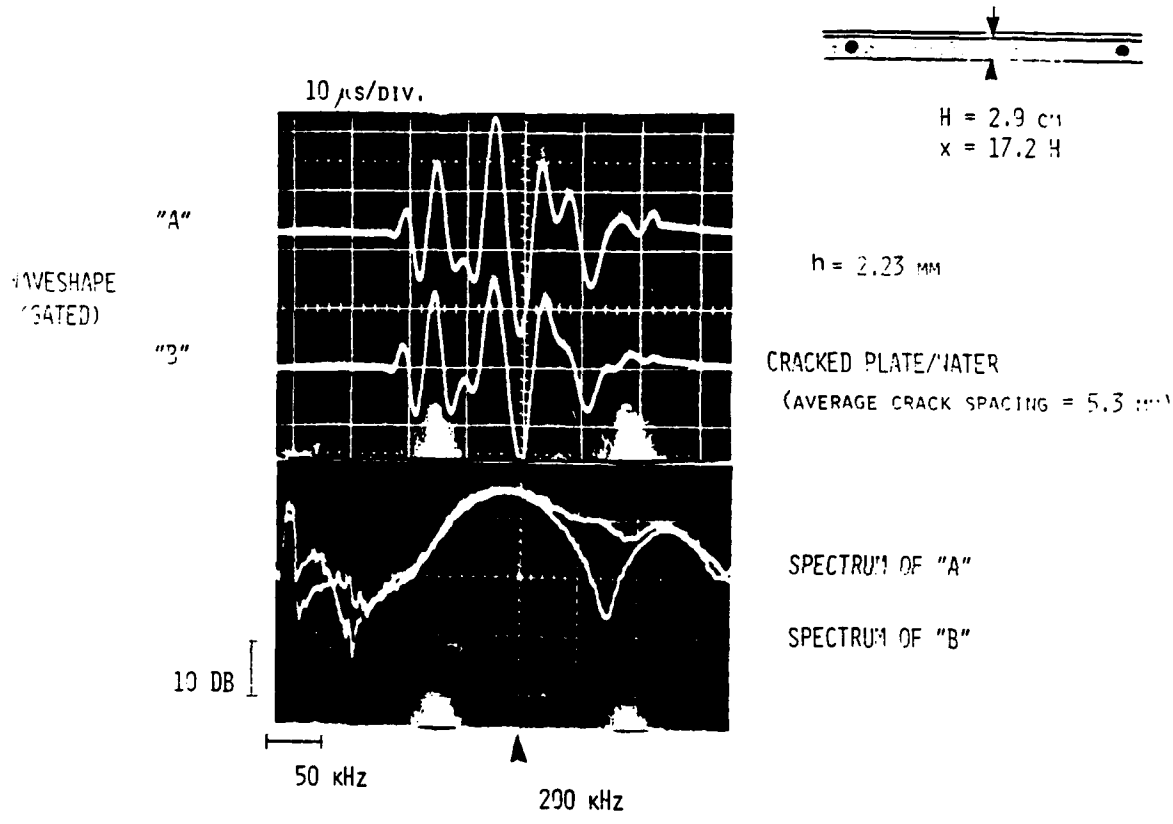

FIG. 5.12. Dip in spectrum of gated first-arriving 3 waveguide pulses from water layer model bounded by cracked floating plate.

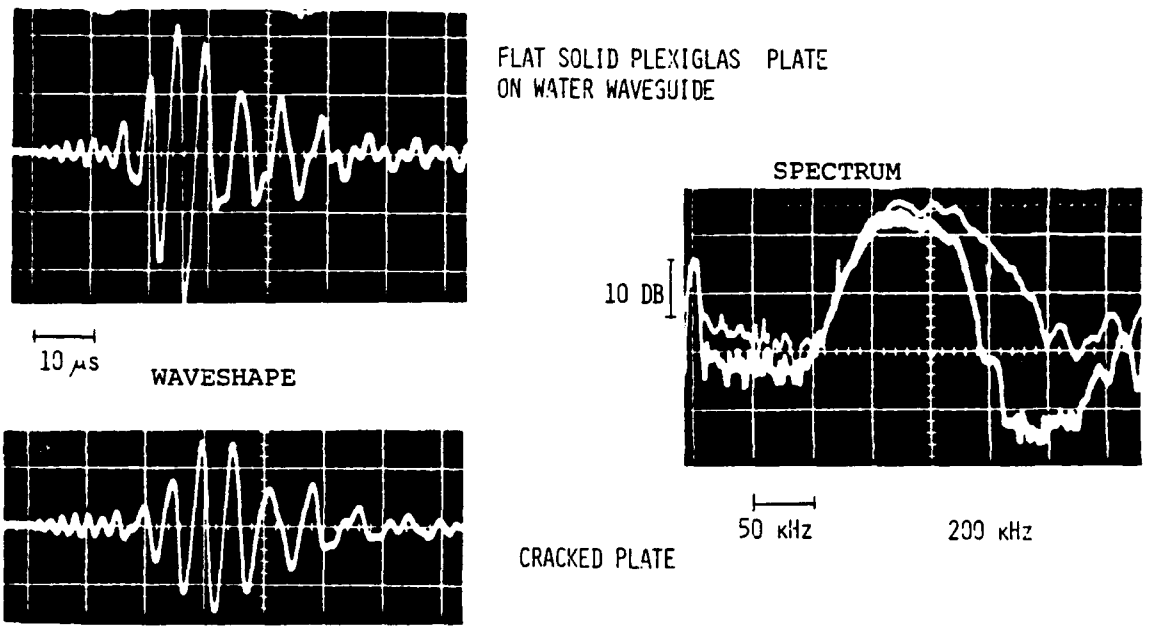

FIG. 5.13. Shallow-water waveguide bounded with floating plate with dry cracks. Low-frequency attenuation by shallow cracks. Range X = 50H , h = 0.223 H, H = 1 cm, $Z_s = Z_r = H/2$.

A very shallow-water example is shown in figure 5.14. The model parameters were H = 5mm, h =0.446 H, x = 100H, N = 90 cracks, and Z_S = Z_R= H/2. In this case, attenuation by the cracks was observed over a broad frequency range as shown. Maximum attenuation occurred also around 275 kHz.

The effect of varying the water waveguide depth on the attenuation of underwater acoustic waves by the dry cracks in the floating plate is plotted in figure 5.15 for H = 4, 3, 2, 1, and 0.5 cm. The range was 50 cm and the transducers were placed at H/2. The top four traces have a 5 us/div. time scale, while the last trace has 10 us/div. .The solid line and the dotted line plots correspond to the cracked and solid plates, respectively. Figure 5.15 demonstrates how the importance of cracks increases as the effective water waveguide depth is decreased either by a) upward refraction , b) shallow water regions, c) combination of both upward refraction and shallow water.

The reflection coefficient is close to unity for waves incident beyond the critical angle on a flat floating ice plate (ideal), however, the presence of shallow dry cracks creates backscattering and attenuates the incident waves even beyond the critical angle. The presence of shallow cracks also introduces a dependence of the reflection coefficient on frequency and angle of incidence. The effect of cracks is greatly enchanced by the presence of upward refraction which confines the acoustic waves to a shallow water waveguide underneath the cracked ice plates.

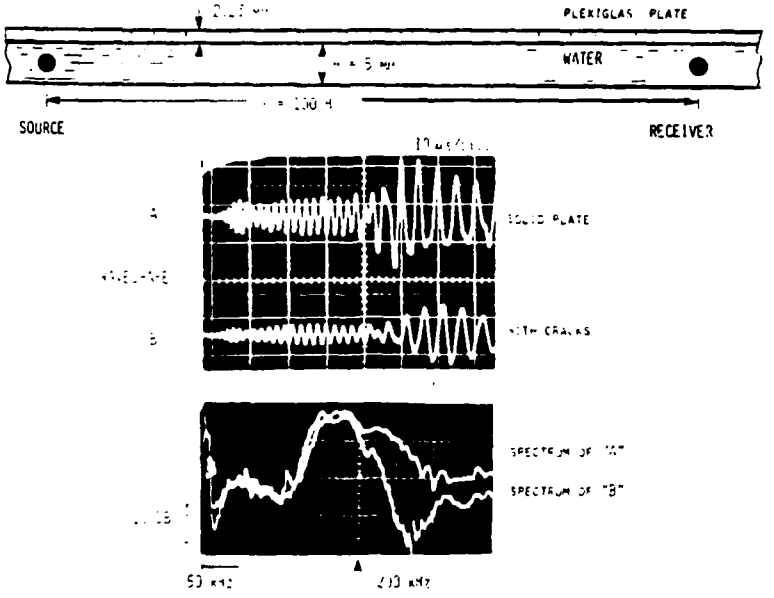

FIG. 5.14. Attenuation of low frequency acoustic waves in a shallow water waveguide by cracks in floating plate.

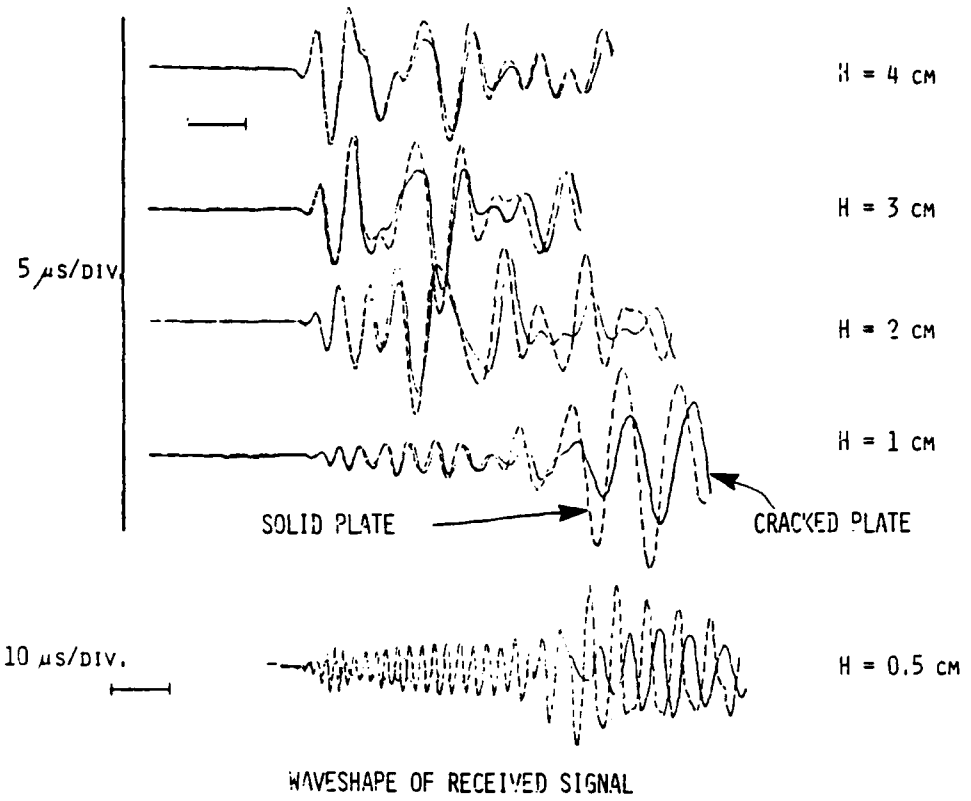

FIG. 5.15. Effect of varying water waveguide depth on attenuation of underwater acoustic waves by shallow cracks in floating plate. As the water depth is decreased, the relative importance of cracks increases. (X = 50 cm, $Z_S = Z_R = H/2$, 2.23 mm thick Plexiglas plate on water)

The enhanced ultrasonic modeling results, previously obtained on the cracks were measured from models with a crack spacing of about twice the plate thickness. Since cracks in the Arctic may be 100 m apart in some cases (30-40x ice plate thickness), another experiment was carried out to demonstrate the potential long range effect of widely spaced dry cracks on the transmission of low-frequencies. Using a modeling scale of 2000:1, the model consisted of a 3.065 m long water waveguide with a water depth of 5.08 cm. The floating plate thickness was 1.67 mm, and the crack spacing was about 5 cm as shown in figure 5.16. At this scale this corresponds to Artic crack separation of 100 m , ice plate thickness of 3.34 m, and a 6.13 km range. Enhanced upward refraction was roughly represented by a finite depth water waveguide equivalent to 101.6 m. In order to increase the effective range, we looked at the reflection of the water waveguide from its far end "A" resulting in a 12.3 km propagation path for the round trip. In the experiment, the water waveguide consisted of a long rectangular plastic channel with machined cracks at the boundaries. Source and receiver transducers were mounted at one end of the waveguide and a lexan reflector at the other end of the waveguide. A reference signal was first obtained from the waveguide without cracks (Fig. 5.16(a)). Introducing the cracks attenuated the propagated waves and also created backscattered plate waves and water waves (Fig. 5.16(b)). An expanded view of the reflected waves is shown in figure 5.16(c) and (d). Waves incident on the boundary at angles beyond the critical angle were also attenuated by the cracks.

Two separate attenuation mechanisms may be present. The first increases steadily with frequency, while the second is centered at a specific frequency originating from multiple scattering, combined waveguide and crack spacing configuration [26], or coupled liquid/solid wave components as described later in section 7.1.

Another interesting experiment was devised to examine only the effect of randomly spaced small vertical discontinuitites along the boundary of a waveguide on long range transmission. In this experiment, seismo-acoustic wave components associated with a floating plate were subtracted. The model consisted of examining the transmission of elastic waves in a free solid waveguide with machined shallow grooves along one boundary (FIG. 5.17). Longitudinal waves were propagated along a 3 mm x 5 cm x 2.44 m aluminum bar. Source and receiver transducers were mounted on opposite ends of the bar along its longitudinal axis as shown. The source was excited with a single broadband pulse. The received waveform was recorded together with the corresponding spectrum. Randomly spaced shallow grooves were machined along one boundary of the waveguide (75 grooves, 0.2 mm wide and 1 mm deep). The received waveform from the grooved model was recorded and compared to the nongrooved waveguide. Figure 5.17 shows dips in the spectrum of the grooved model. The shallow grooves

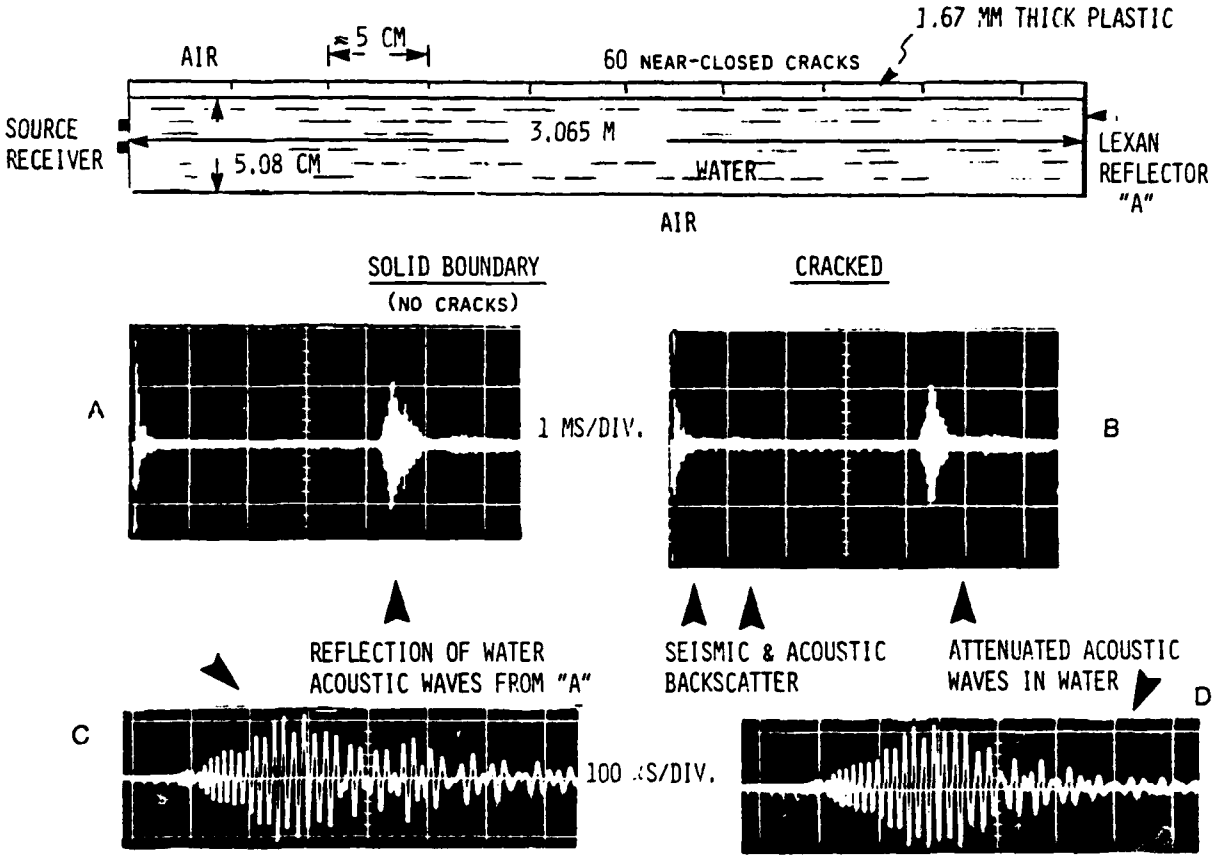

FIG.5.16. Backscatter and attenuation of underwater acoustic waves by shallow cracks in floating plate. Long-range transmission is simulated by round trip propagation of end reflected waves.

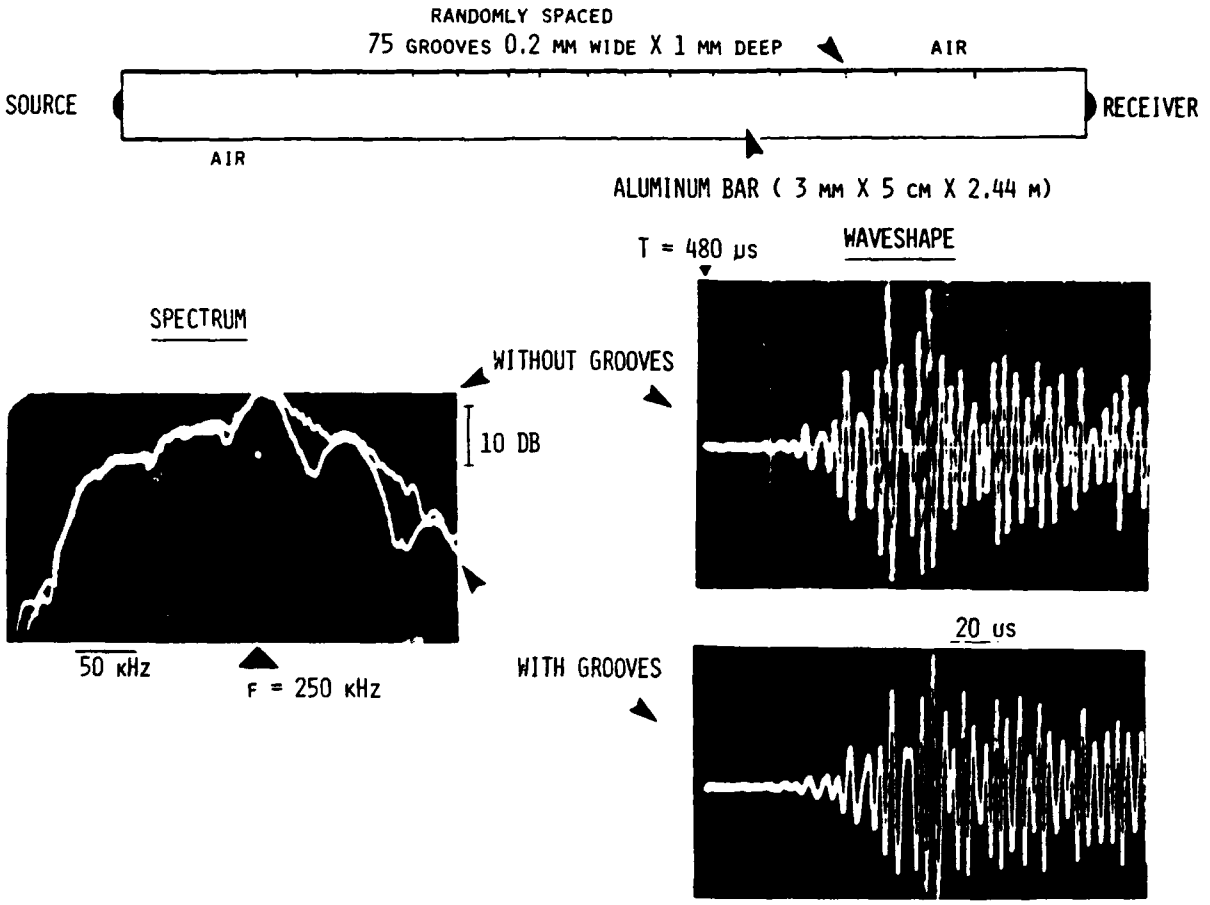

FIG. 5.17. Enhanced ultrasonic modeling simulation of effect of dry cracks in floating sea-ice plates on attenuating horizontally propagating low-frequency underwater acoustic waves in upward refracted water waveguide. In this model, the ice is integrated with the water waveguide and the cracks are represented by vertical air-filled shallow grooves interrupting longitudinal waves in an aluminum waveguide. The groove depth is H/50, where H is the waveguide depth. The average groove spacing is 0.586H and the range X = 50H. With only 75 cracks, most frequencies shown were attenuated by at least 2 dB, while some selected frequencies were attenuated by about 10 dB. The wavelength at the dip around 300 kHz corresponds to H/3 .

were only 1/50th of the wave guide depth. With only 75 grooves, most frequencies were attenuated by at least 2 dB, while some selected frequencies were attenuated by about 10 dB. The wavelength at the dip around 300 kHz corresponded to H/3. These findings demonstrate the importance of cracks when combined with waveguide phenomena [26].

Propagation over a 300 km range would increase the number of cracks to over 3000 (assuming a 100 m spacing) therefore enhancing the effect of cracks. Our models have infinitely long parallel cracks yielding an upper limit on estimating the attenuation effect by cracks. Enhanced modeling is a great tool to identify and isolate the effect of a particular phenomenon. Other studies on crack orientation and length need to be investigated.

5.5 BACKSCATTER FROM DRY AND WET CRACKS

In the previous examples, the cracks existed along the waveguide boundary only between source and receiver. No cracks were present before the source or after the receiver. Results on backscattering measurements are described in this section. Source and receiver transducers were placed adjacent to each other in a crack free region of the waveguide and were directed towards the cracked region as shown in figure 5.18. The distance between the transducers and the first crack was 2.4 cm, the water depth H = 1 cm, and the transducers depth was H/2. The source was excited with a single broadband pulse and the received waveshapes and spectra were recorded as before. In the absence of any cracks along the waveguide, the received signal consisted of a rapidly decaying wavetrain having no significant components beyond about 50 us from the beginning of the water wave arrival. The model with cracks created large backscatter that filled the same time window which was previously free of signals (FIG. 5.18(b)). Gated backscattered waves were compared to the background noise from the crack-free model. The spectrum of the backscatter had a peak near about 279 kHz.

In the Arctic, cracks may exist on both sides of the source and receiver. This condition can create additional forward-scatter and backscatter. As the transducers were moved to different locations along the waveguide, interference of the forward-scattered and backscattered waves caused the spectrum of the total scattered waves to vary (FIG. 5.19). Scattered waves from cracks that are closer to the source or receiver have a greater effect on the acoustic waves.

All the experimental results presented so far were obtained from models with air-filled cracks. These cracks act as near-vertical sharp acoustic impedance discontinuities to the propagating waves coupled to the plate. The effectiveness of the cracks is due to the high contrast between the plate impedance and the air impedance in the cracks. Shallow surface cracks in the Arctic may be filled with snow, ice crystals, or water. Figure 5.20 shows the effect of filling the shallow cracks in the ultrasonic model with water. The

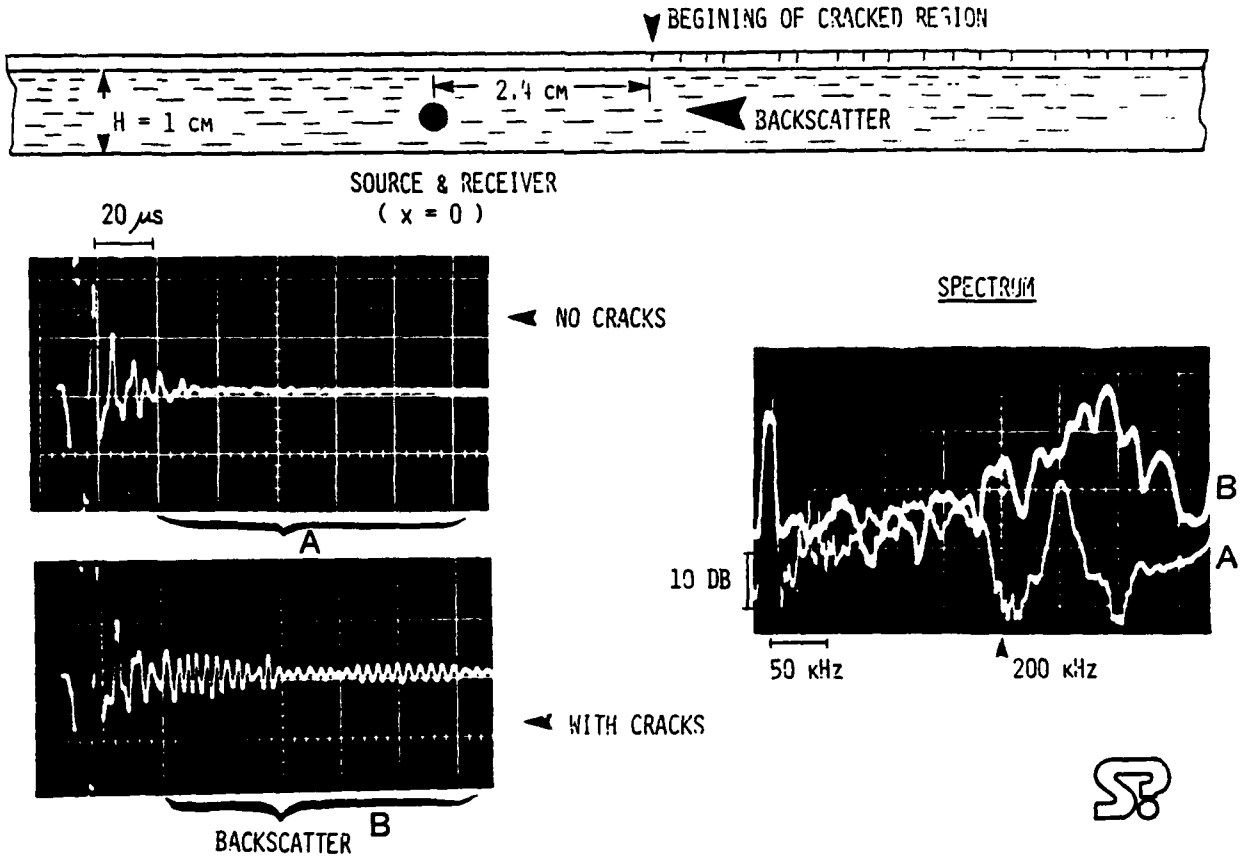

FIG.5.18. Backscatter from shallow cracks in floating plate.

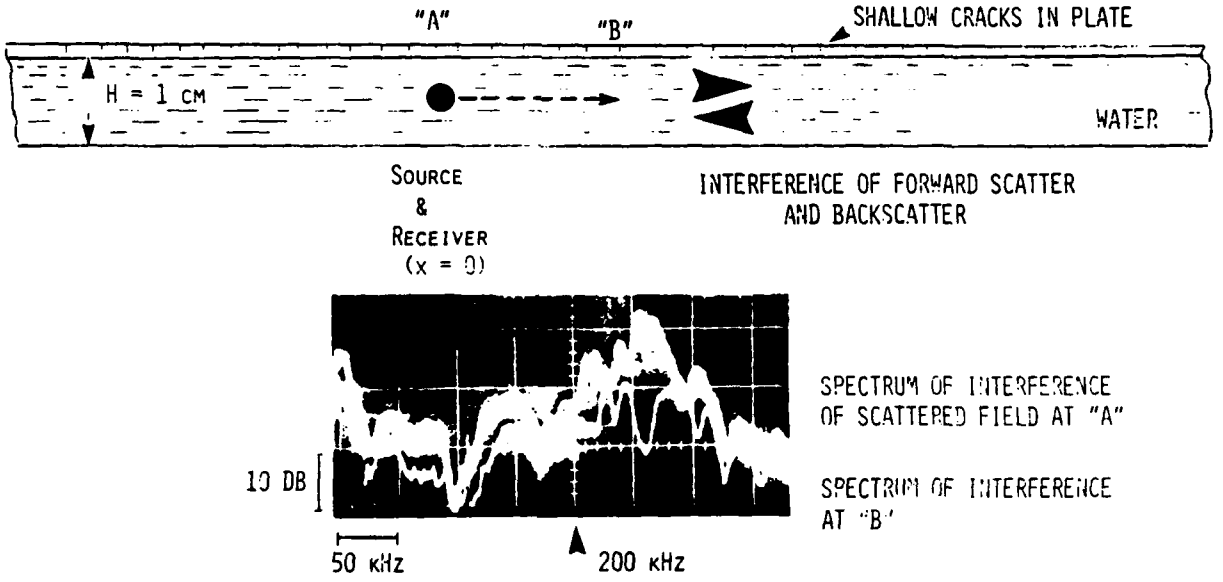

FIG.5.19. Range dependent interference of forward and backscatter from shallow cracks in floating plate. Spectrum of received waves at two different locations along water waveguide.

spectrum of the backscattered waves from the air-filled cracks is compared to the water-filled cracks. The bottom reference spectrum was obtained from the solid boundary case without cracks. Water in the cracks reduced the backscatter at around 275 kHz by almost 10 dB in this example (H = 1 cm, h = 0.223H, x = 0, $Z_S = Z_R = H/2$, distance to crack region = 2.4 cm, and average crack spacing 5.3 mm).

Yang and Votaw [62] reported on under ice reflectivities at frequencies below 1 kHz an found that the reflection coefficient from large smooth ice floes in the Arctic is strongly dependent on frequency and grazing angle. Our ultrasonic modeling results clearly indicate a strong frequency dependence of the reflection coefficient of underwater acoustic waves interacting with a smooth floating plate with shallow cracks on its top free surface. Smooth ice floes are not homogeneous solid plates free of internal cracks. The number of cracks intercepted by the acoustic waves increases with range. Furthermore, the greater the range is the larger the number of deep and long cracks encountered along the wave path. Therefore lower frequencies would be more affected as range is increased. Arctic experiments conducted at short ranges would give correct reflection coefficient only for high frequencies. The reflection coefficient approaches unity for acoustic waves incident at near-grazing angles on a smooth solid plate, however, in the presence of cracks in the plate the reflection coefficient would not approach unity. Further research is needed to assess finite length cracks, randomly-oriented cracks, oblique incidence, and combined effects of cracks with other scattering features.

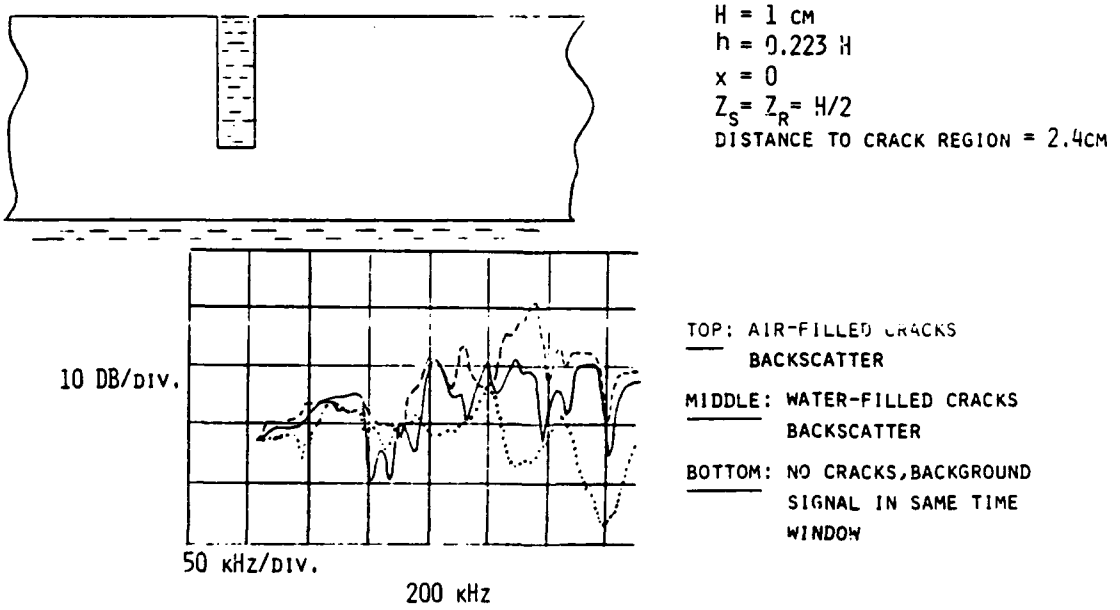

FIG. 5.20. Backscatter decrease with presence of water in cracks.

6. WAVES ALONG EDGE OF FLOATING SEMI-INFINITE PLATE

6.1 PLATE EDGE LEAKY RAYLEIGH WAVE

Leaky Rayleigh waves propagating along the bottom side of floating sea-ice plates experience cylindrical geometrical spreading and have their low-frequency limit determined by the ice plate thickness which corresponds to about 500 Hz. A second type of leaky Rayleigh wave can exist along ice plate edges with particle motion in the horizontal plane (FIG. 6.1) . The plate edge Rayleigh wave has no geometrical spreading and has its low-frequency limit determined by the large horizontal dimensions of the plate. Laboratory ultrasonic modeling results demonstrate underwater detection of low-frequency plate edge Rayleigh waves radiated by the edge of a floating "semi-infinite" ice plate. In one experiment, the detected plate-edge leaky Rayleigh wave had a wavelength greater than 12 times the ice plate thickness. The results suggest that a 3 m thick ice plate in the Arctic may radiate 10 -100 Hz components from its edges. The active portion of the plate edge acts as a finite length linear source producing a directional radiated field in the water. The low-

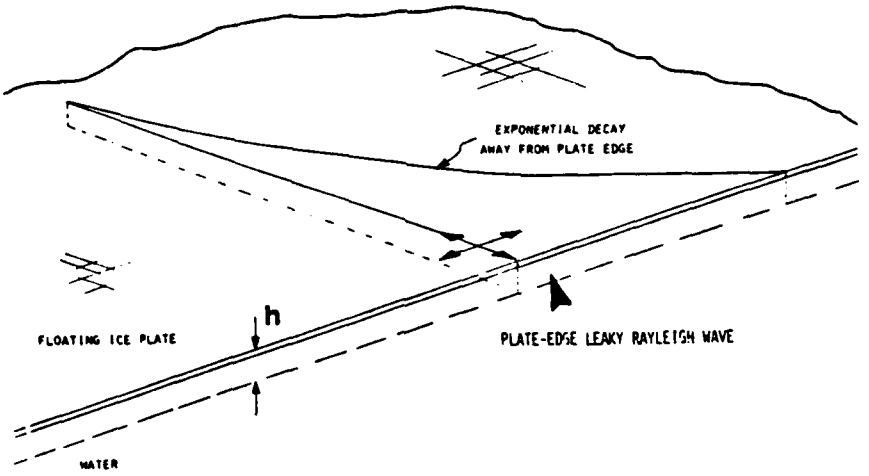

FIG. 6.1. Plate-edge leaky Rayleigh wave in floating plate.

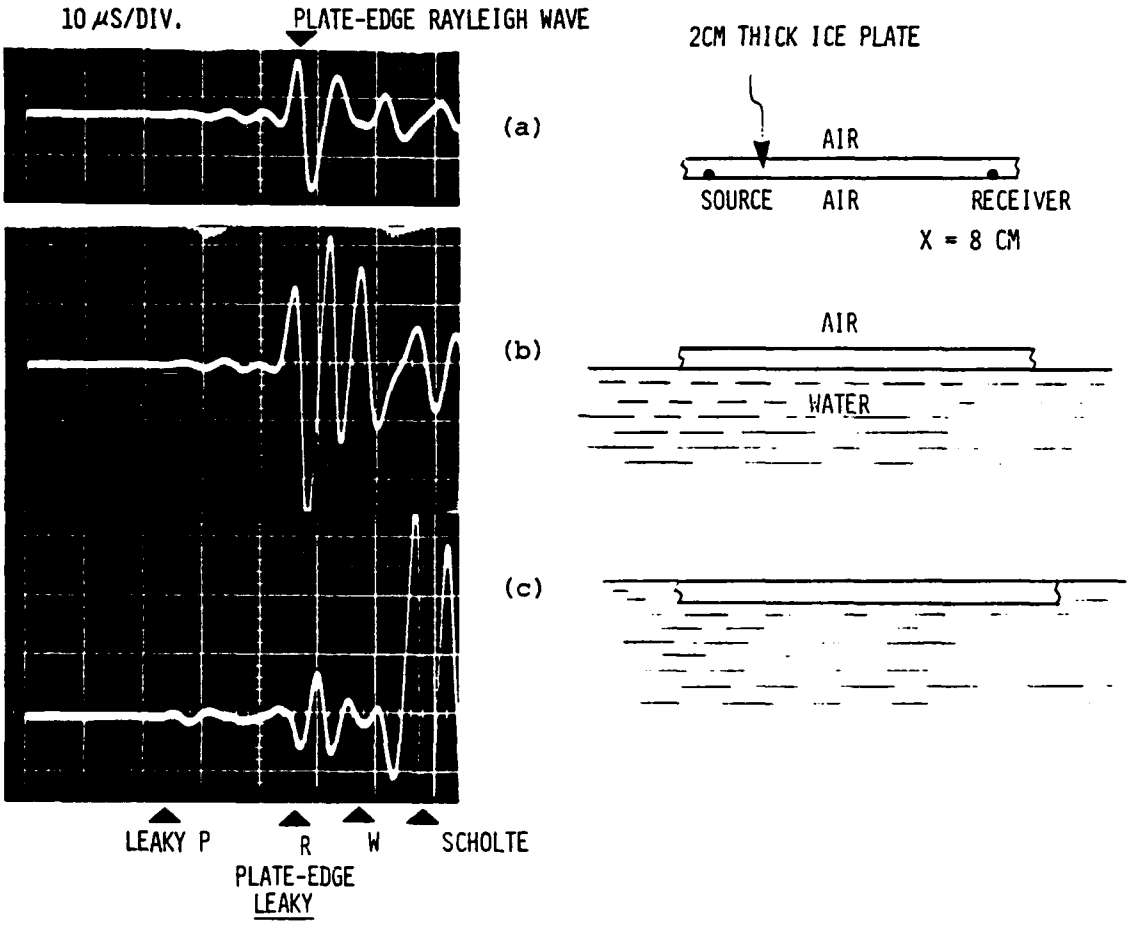

FIG. 6.2. Horizontal edge Rayleigh wave along plate edge for a) free plate, b) floating plate with free side edges, c) floating plate with only top surface of plate free.

frequency plate-edge leaky Rayleigh wave may be detected in the water at significant distances from the ice edge. Similar to the leaky Rayleigh wave, the edge leaky Rayleigh wave leaks its energy to the water, however, since only 9/10th of the vertical edge surface is immersed in water, the edge leaky Rayleigh wave is attenuated to a lesser degree.

Figure 6.1 shows a diagram of a floating plate with an edge leaky Rayleigh wave. The leaky Rayleigh wave decays exponentially away from the edge in the solid plate as shown. The plate-edge Rayleigh wave from a 2 cm thick ice plate in air is displayed in figure 6.2(a). Source and receiver transducers were positioned along the edge of the plate to induce and detect horizontal particle motion normal to the vertical face of the plate edge. The distance between the transducers was 8 cm. The bottom surface of the ice plate was then placed on a water "half-space" without allowing the water to cover the vertical face of the plate edge. The corresponding detected waveshape is shown in figure 6.2(b). The bottom trace of figure 6.2 was obtained with both the bottom surface and vertical face of plate edge in contact with the water similar to the floating sea-ice condition. The observed wave components included a leaky compressional wave, a leaky Rayleigh wave, a direct water wave, and a Scholte wave. The Scholte wave was rapidly attenuated as the receiver was moved away from the edge of the plate in the water.

Figure 6.3 shows how a thin floating ice plate can radiate low-frequency plate edge leaky Rayleigh waves having a wavelength much greater than the plate thickness. In this model, a 1.5 mm thick floating ice plate radiated leaky Rayleigh waves having a wavelength almost 12 times the plate thickness. These results suggest that a 3 m thick ice plate in the Arctic may radiate low-frequency plate-edge leaky R wave components between 10-100 Hz. Further studies are needed to determine the radiation properties of the plate edge. The laboratory experiments on thin floating ice plates are difficult to conduct. Other solid materials such as glass may be used to characterize the general radiation properties of plate edge leaky Rayleigh waves. The glass to ice velocity and density ratios are as follows: Rayleigh wave velocity ratio = 1.72, compressional plate velocity ratio = 1.6, shear wave velocity ratio = 1.78, and density ratio = 2.5.

Remote detection of low-frequency plate-edge leaky Rayleigh waves in the water away from the plate edge is illustrated in figure 6.4. A 2.57 mm thick glass plate was used in the experiment instead of an ice plate to enhance the plate-edge leaky Rayleigh wave and to achieve better control of the measurements. The plate compressional velocity, the edge Rayleigh wave velocity, and the glass plate density were 5415 m/s, 3104 m/s and 2300 kg/m^3, respectively. The glass plate was fixed on top of the water half-space simulating a floating ice sheet. The source transducer was fixed at the edge of the plate and the receiver was located in the water as shown at x = 14.7 cm, y = 6.15 cm, and z = 4.7 cm. The received signal consisted

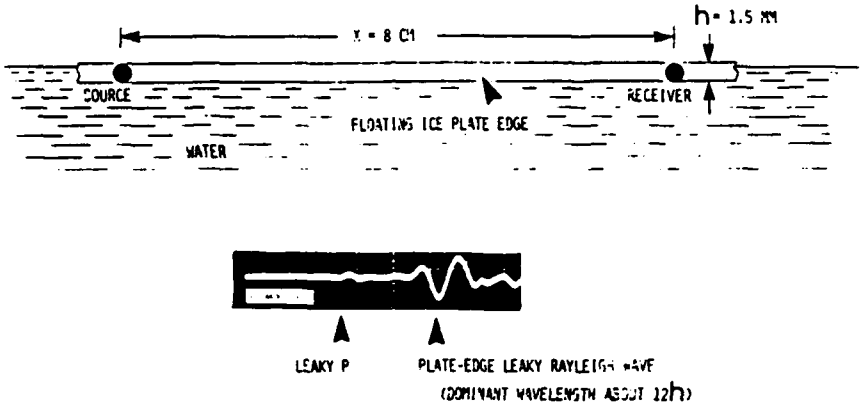

FIG. 6.3. Low-frequency plate-edge leaky Rayleigh wave in ice plate.

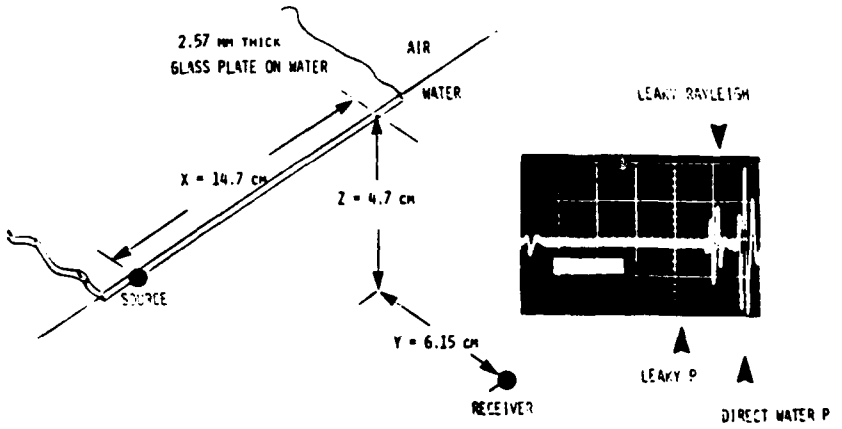

FIG. 6.4. Underwater remote detection of low-frequency plate-edge leaky Rayleigh wave. Glass plate model on water to enhance the leaky Rayleigh wave.

of a plate-edge leaky compressional wave, a plate-edge leaky Rayleigh wave, and a direct water wave. The time delay of these wave components depended on the relative position of the transducers. At large distances, the plate-edge leaky Rayleigh wave merged with the direct water wave. The plate-edge leaky Rayleigh wave contributed significantly to the underwater signal.

Plate-edge leaky Rayleigh waves can easily couple to other adjacent floating plates as shown in figure 6.5. In this experiment, a reference leaky Rayleigh wave was obtained from one floating glass plate with the source and receiver separated by 30 cm along the edge of one plate (FIG. 6.5(a)). The receiver remained on the original plate and the source was positioned at the edge of a second plate as shown in figure 6.5. The two plates were aligned in such a way to allow acoustic coupling to occur between the two plates over a region "D" common to both plates as shown. The distance between source and receiver was fixed at 30 cm. The length of region "D" was varied and the detected waves were recorded. In figure 6.5, four traces are displayed corresponding to a) single floating plate, b) two floating plates with D = 3.5 cm, c) D = 13.6 cm, and d) D = 20 cm. The coupled plate-edge leaky Rayleigh wave arrived at the same time as the reference wave. The signal level of the coupled leaky Rayleigh waves was high indicating significant coupling occurred between the edges of the floating glass plates. In the Arctic, plate-edge leaky Rayleigh waves can be generated by bumping of floes, ice cracking, and conversion of plate waves and underwater acoustic waves from irregular plate boundaries.

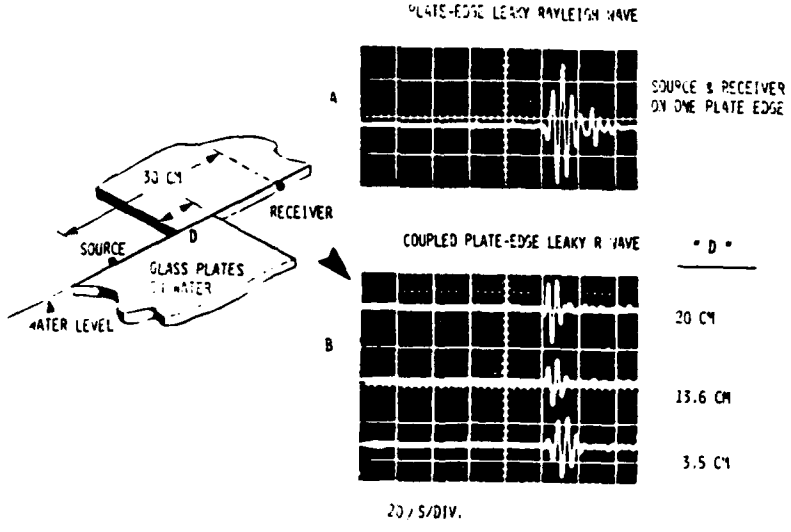

FIG. 6.5. Plate-to-Plate coupling between floating plates dominated by plate-edge leaky Rayleigh wave. Glass plates model.

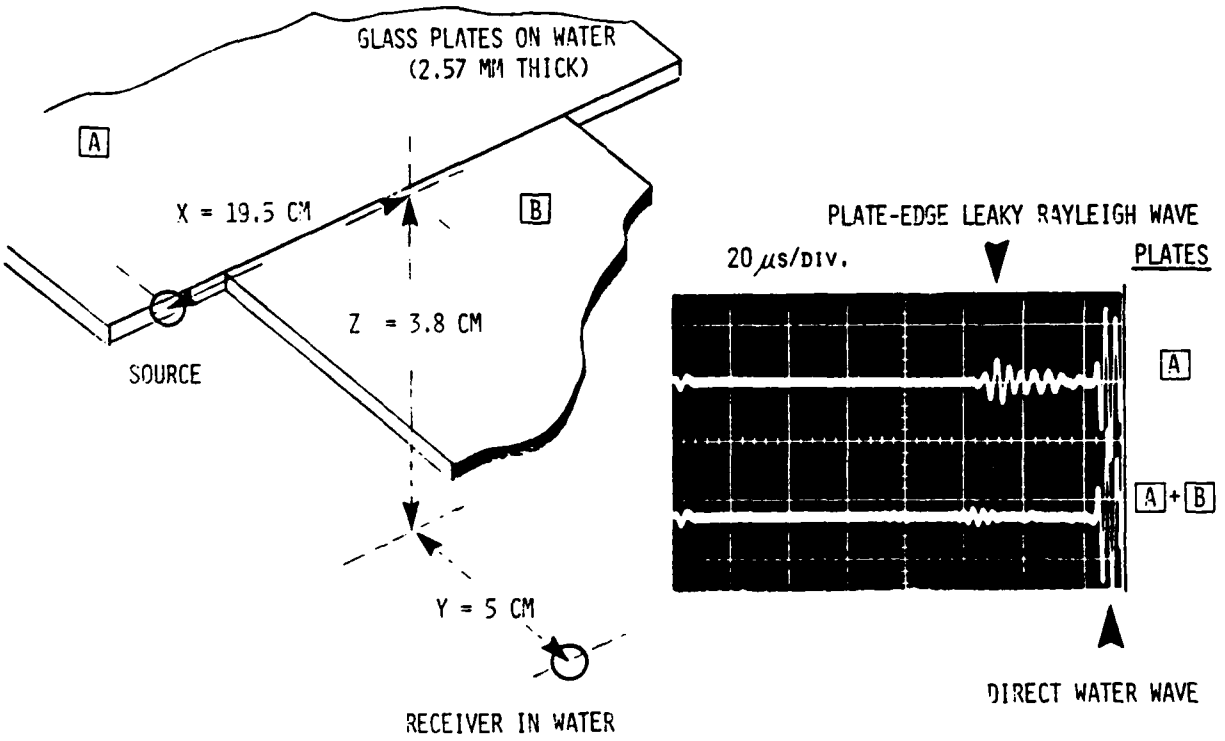

FIG.6.6. Detection of plate-edge leaky Rayleigh wave in the water. Top trace obtained with only one plate "A" present. Bottom trace from two plates in contact as shown.

The effect of gap closure between floating plates on the radiated plate-edge leaky Rayleigh wave in the water is shown in figure 6.6. A pulsed source transducer was placed along the edge of a first floating plate "A" and a receiver transducer was placed in the water at x = 19.5 cm, y = 5 cm, and z = 3.8 cm as shown. The received leaky Rayleigh wave radiated by the edge of plate "A" alone was recorded (FIG.6.6(a)). The edge of a second plate "B" was placed in contact with the first plate as illustrated. The presence of the second plate simulated a near-closed wet crack and greatly reduced the detected plate-edge leaky Rayleigh wave (FIG.6.6(b)) deep in the water. The direct water wave, however, remained unchanged with this configuration.

Kouzov and Luk'yanov [63] analyzed the problem of a plate separated into two parts by a near-closed rectilinear crack. They described a special case where no radiation occurs from waves propagating along the two sides of the crack. In view of the presence of plate-edge leaky Rayleigh waves, it would be expected that Arctic ambient noise should be higher near the edges of floes. Field measurements, laboratory studies, and theoretical formulation are needed to quantify the role of edge leaky Rayleigh waves.

6.2 PLATE-EDGE FLEXURAL WAVE

Our studies on edge waves reveal a gap in Arctic acoustics on plate-edge flexural waves in floating plates. The plate-edge flexural wave decays exponentially with distance from the edge into the plate.

Konenkov [63] presented theoretical results on plate-edge flexural waves propagating along the edge of a thin semi-infinite plate in vacuum. Using thin plate theory, Thurston [64] independently obtained a dispersion expression for the plate-edge flexural wave matching Konenkov's results. The ratio of the plate-edge flexural wave velocity C_E to the flexural wave velocity C_F as given by both Konenkov and Thurston is:

$$(C_E/C_F)^4 = (1-\sigma)[(3\sigma-1)+2(1-2\sigma+2\sigma^2)^{\frac{1}{2}}]$$

where σ is Poisson's ratio of the plate. Since this equation is based on the classical thin plate approximation, we expect to observe deviations from the predicted edge flexural wave velocity in laboratory measurements.

In order to obtain a baseline on the characteristics of edge flexural waves, an ultrasonic experiment was carried out on a 4.35 mm thick polycarbonate plate. The measured plate parameters were:

plate thickness h = 4.35 mm
compressional plate velocity C_{pl} = 1593 m/s
shear wave velocity C_s = 879 m/s
calculated bulk compressional velocity C_p = 2078 m/s
density = 1.207
Poisson's ratio σ = 0.391

The flexural wave phase velocity C_F and the plate-edge flexural wave phase velocity C_E were then measured at different frequencies (25, 30, 40, 50, 60, and 70 KHz). Table 1 summarizes the results. The measured edge flexural wave velocity is slower than predicted by the thin plate theory and the ratio C_E/C_F is frequency dependent. The importance of this apparently trivial small reduction in velocity is in its role in guiding substantial low-frequency energy along the plate edge with no geometrical spreading and creating large wave amplitudes near the plate edge. Figure 6.7(a) shows the conventional flexural wave from a 2.31 mm thick acrylic plate. The source-receiver range was 26 cm. The edge flexural wave for the same range is displayed in figure 6.7(b). The amplitude of the edge flexural wave was about 4X greater than the flexural wave at X = 26 cm in this configuration.

TABLE 1

f (KHz)	C_F (m/s)	C_E (m/s)	C_E/CF Experimental	C_E/CF Theoretical (thin plate)
25.000	492.61	486.74	0.9881	0.99668
30.000	525.16	519.11	0.9884	0.99668
40.000	583.09	575.31	0.9867	0.99668
50.000	624.99	613.79	0.9820	0.99668
60.000	646.56	656.45	0.9849	0.99668
70.000	686.22	676.79	0.9867	0.99668

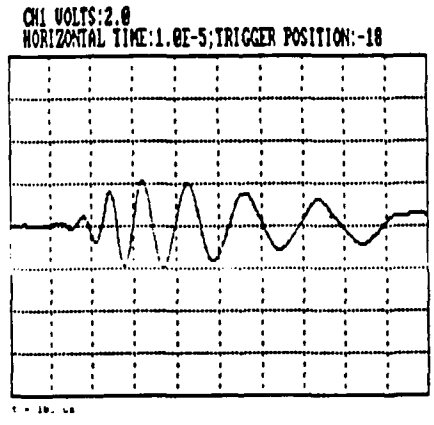

h = 2.31 mm, X = 26 cm

(a) FLEXURAL

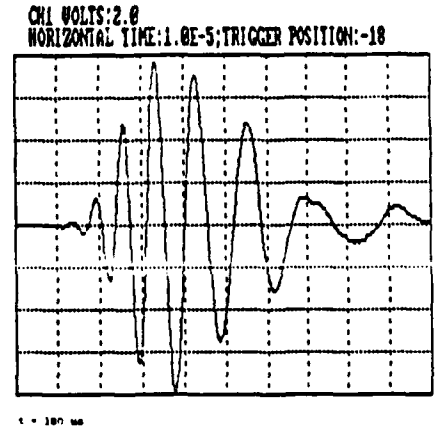

h = 2.31 mm , X = 26 cm

(b) EDGE FLEXURAL

FIG.6.7. Comparison of flexural wave in free plexiglas plate (a) and edge flexural wave propagating along edge of semi-infinite plate (b).

Figure 6.5(a) shows the conventional flexural wave from a 2.31 mm thick acrylic plate. The source-receiver range was 26 cm. The edge flexural wave for the same range is displayed in figure 6.5(b). The amplitude of the edge flexural wave was about 4X greater than the flexural wave at X = 26 cm.

Similar edge wave behavior occurs in floating plates. Kouzov and Luk'yanov [65] analyzed the model of a thin floating plate separated into two parts by a closed rectilinear crack, and derived the dispersion relation for a trapped edge wave under the assumption that the plate is denser than the fluid. To the author's knowledge, no exact theory exists for the plate-edge flexural wave in a floating semi-infinite ice plate.

An experiment was conducted on flexural and edge flexural waves in a vertical large diameter polycarbonate cylindrical shell filled with water as shown in figure 6.8(a). The source was fixed on the outer surface of the cylindrical shell near the edge. The water loaded flexural wave was detected with the receiver located at position "B" (Fig. 6.8(b)) 180° around the cylinder circumference and vertically down 3 cm from the top edge as shown. An expanded display of this flexural wave component is given in figure 6.8(c). The receiver was then moved to position "A" near the edge, and the water loaded edge flexural wave was recorded (Fig. 6.8(d)). A large edge flexural wave was observed. This particular experimental configuration was selected because the vertically oriented cylinder could be easily filled with water or emptied without disturbing the transducers and their coupling to the cylinder. The large diameter cylinder (22.143 cm O.D. and 2.81 mm wall thickness) partially simulated the effect of a large thin floating plate at this frequency range. The large high-frequency wave component arriving at about 150 μs in figure 6.8(b) is the direct water acoustic wave travelling across the diameter of the cylinder.

In the presence of plate edge discontinuities such as cracks, plate thickness variations, and topographical boundaries along the edges of the floating plate, low-frequency underwater acoustic waves are converted into plate waves and also plate waves radiate back to the water contributing to ambient noise characteristics. In Arctic field experiments, it is not sufficient to measure the elastic properties of the ice plate, but it is essential to know the geometry of the plate boundaries including cracks, leads, and outer edges. We need to understand the conversion of elastic waves in the ice into edge waves and the conversion of underwater acoustic waves into edge waves.

a

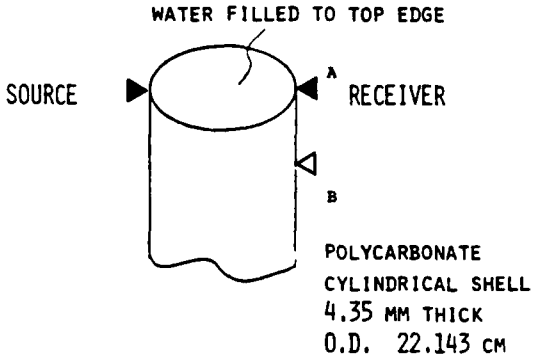

water filled

b

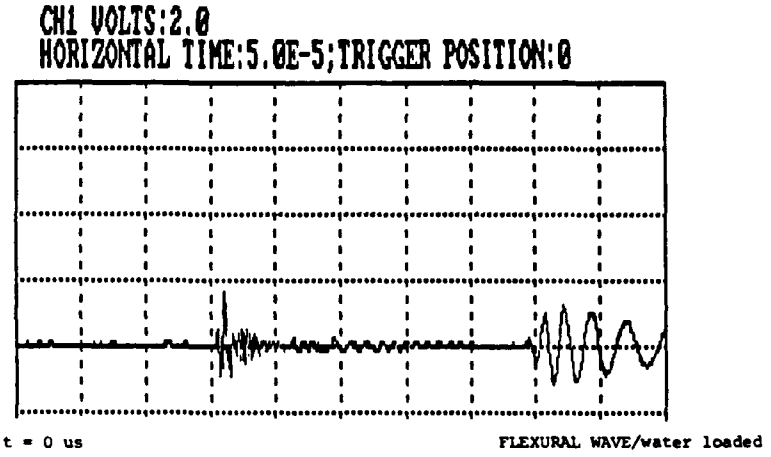

Received flexural wave with receiver at point "B" 3 cm below edge.

c

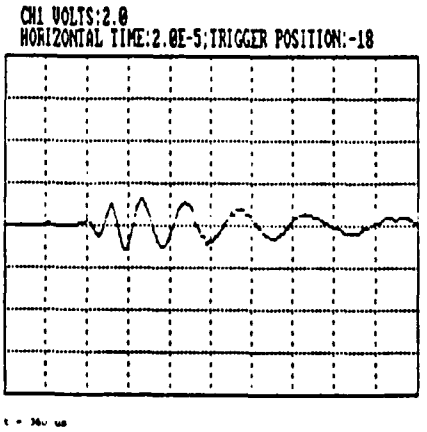

Expanded display of water loaded flexural wave shown above.

d

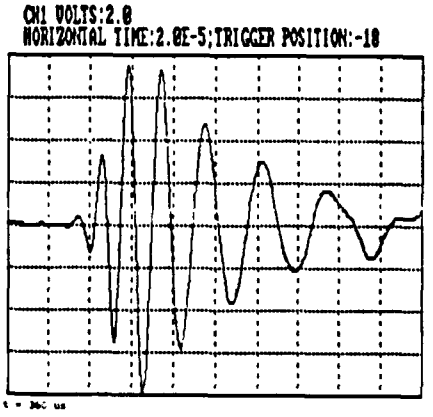

Received edge flexural wave with receiver at point "A"

FIG.6.8. Comparison of trapped edge flexural waves and flexural waves in finite floating plate simulated by water filled large diameter cylindrical shell. Notice large amplitude of edge wave. The dispersion curve for the edge flexural wave is also slower than the flexural wave away from the edge.

7. BACKSCATTER FROM EDGES OF FLOATING PLATES

The Arctic ice cover is composed of a very large number of floating ice sheets with immersed edges. Sea-ice has a shear wave velocity that may vary over a wide range depending on environmental conditions and ice plate history. Our ultrasonic modeling studies on cracks in floating plates [18-19] raised fundamental questions on the characteristics of scattered wave components by vertical plate discontinuities. A series of experiments were conducted to study the interaction of near-horizontally propagating pulsed underwater acoustic waves with straight edges of floating plates. Two general cases were investigated: Case I plates with a shear wave velocity $C_s < C_w$, and Case II plates with $Cs > C_w$, where C_w is the water compressional wave velocity. The results consistently demonstrated that backscatter of underwater acoustic waves incident at small grazing angles on a finite-width floating plate is dominated by backscatter from the lagging edge of the plate. This is caused by coupled seismo-acoustic wave components associated with underwater waves [20-21] . The time of arrival and properties of backscattered waves from the lagging plate edge greatly depends on the ratio C_s/C_w and plate thickness as described below.

The reflection of Lamb waves (eigen modes of an infinite free plate) by a free plate edge has been studied by several investigators [66-70]. The Lamb modes are not coupled to each other as they propagate along the homogeneous plate. Mode conversion occurs when the plate has discontinuities such as edges. Auld used the variational method to obtain a solution to the edge resonance in a semi-infinite plate, and also presented a detailed review of plate-edge resonance [68]. Gazis and Mindlin [66] demonstrated that edge resonance cannot be represented by the addition of incident and reflected propagating modes alone, and that complex modes have to be used. Auld's theory explains that when a fundamental symmetric plate wave is incident normal to the free edge of a plate, the summation of incident and reflected fundamental waves cannot satisfy the traction free boundary condition at the edge face. This is based on the fact that a component of shear stress reflects with a change in sign, while a longitudinal stress component does not change sign upon reflection [68]. Auld's theoretical expression for edge resonance frequency generated by evanescent waves in a plate with a Poisson's ratio of 0.31 is

$$f = 1.43\ C_s / 2h \quad , \qquad (7.1)$$

where C_s is the shear wave velocity, and h is the plate thickness. Zhang et al. used photoelastic techniques to study the reflection of Lamb waves by a free glass plate edge [70]. To the author's knowledge, the theory for edge resonance of floating semi-infinite plate has not yet been published.

7.1 PLATE WITH SUBSONIC SHEAR WAVE VELOCITY : CASE I $C_s < C_w$

The first experiment on backscattering from the edges of a floating plate was conducted in a water waveguide with depth H = 3 cm bounded on top and bottom with air "perfect waveguide" [25]. Source and receiver transducers were located next to each other in the middle of the water column at a depth of 1.5 cm. The transducers were oriented horizontally along the centerline of the waveguide. A 2.45 mm thick acrylic plate was placed on the top surface of the water waveguide as shown. The measured wave velocities were: C_w = 1480 m/s, the longitudinal plate wave velocity C_{pl} = 2422 m/s, and C_s = 1360 m/s. The plate was 7 cm wide, and its first edge was 88.5 cm from the transducers and oriented parallel to the wavefront. The acrylic plates were allowed to float using surface tension. The use of any vertical walls along the edges would disturb the boundary conditions at the edges. The source was excited with a single broadband pulse (Fig. 2.1). Figure 7.1 shows the relative amplitude of backscattered waves from the leading and lagging edges of the floating acrylic plate. The water/plate edge (leading edge) will be referred to as edge "A", and the plate/water edge (lagging edge) as "B". Edge A produced backscatter in the form of a high-frequency nondispersive pulse, while B generated a large amplitude low-frequency backscatter. Figure 7.2 shows an expanded view of the waveshape of backscattered waves from edges A and B obtained from a different model (plate thickness h = 2.41 mm, and width W = 7 cm). The backscatter from edge B was in the form of near-sinusoidal ringing. The spectrum of the ringing is displayed in figure 7.2. The measured ringing peak frequency was 282 kHz which is much lower than the calculated free edge resonance frequency f = 418.43 kHz from equation (7.1).

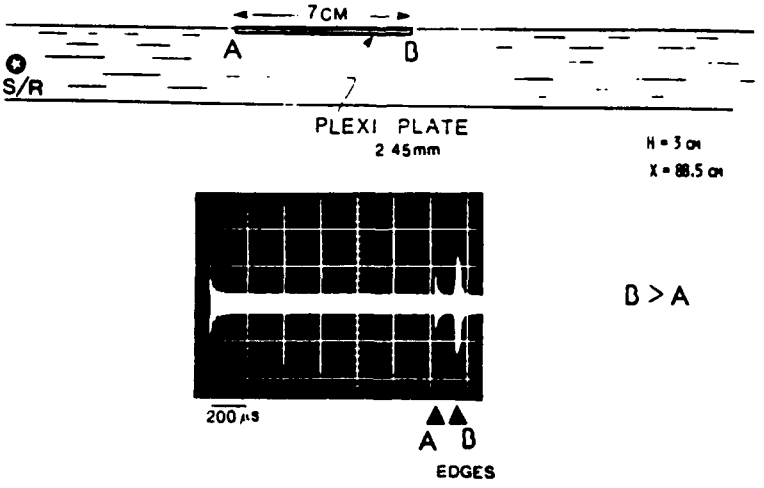

FIG. 7.1. Relative backscatter from edges of floating plate. Notice dominant backscatter from lagging edge "B".

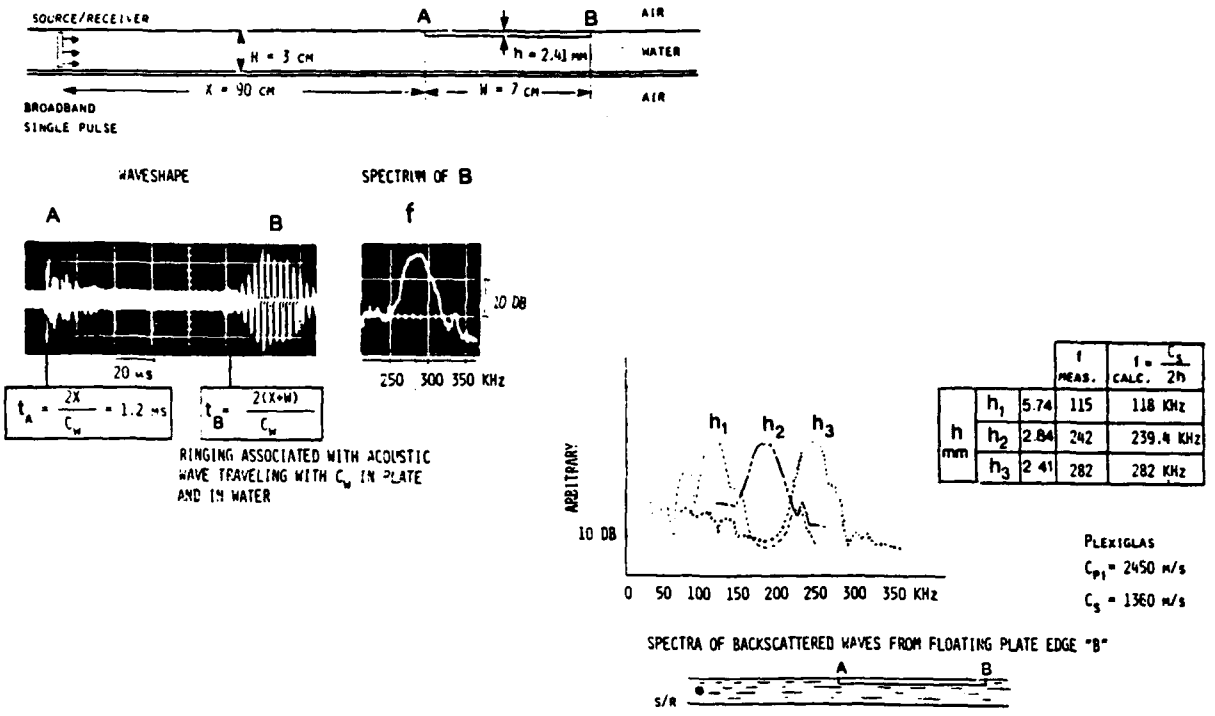

FIG. 7.2. Waveshape and spectra of backscatter from trailing edge "B" of floating plate. Notice ringing frequency increases as plate thickness is decreased.

Figure 7.2 compares the spectra of ringing obtained from floating plates having different thicknesses. The ringing shifted to lower frequencies as the plate thickness was increased. The 2.41, 2.84, and 5.74 mm plates produced a peak ringing frequency at about 282, 242, and 115 kHz, respectively. The measured ringing frequency from these models was found to be nearly equal to $C_s/2h$.

The above experiments were conducted using a shallow water waveguide in contact with a plate, and the waves were detected at a range greater than 70 wavelengths from the plate. Three examples from a water half-space model measured at close range are shown in figure 7.3. The distance between the transducers and edge A was 20 wavelengths. Plexiglas plates had a shear wave velocity C_s = 1360 m/s while other lower quality acrylic plates had a smaller shear wave velocity C_s = 1342 m/s. At close range, other converted wave components became mixed with the backscattered ringing. The received waveform appeared dispersed as shown in figure 7.3. The time marked t_w corresponds to the round trip travel time of an acoustic wave reaching edge B.

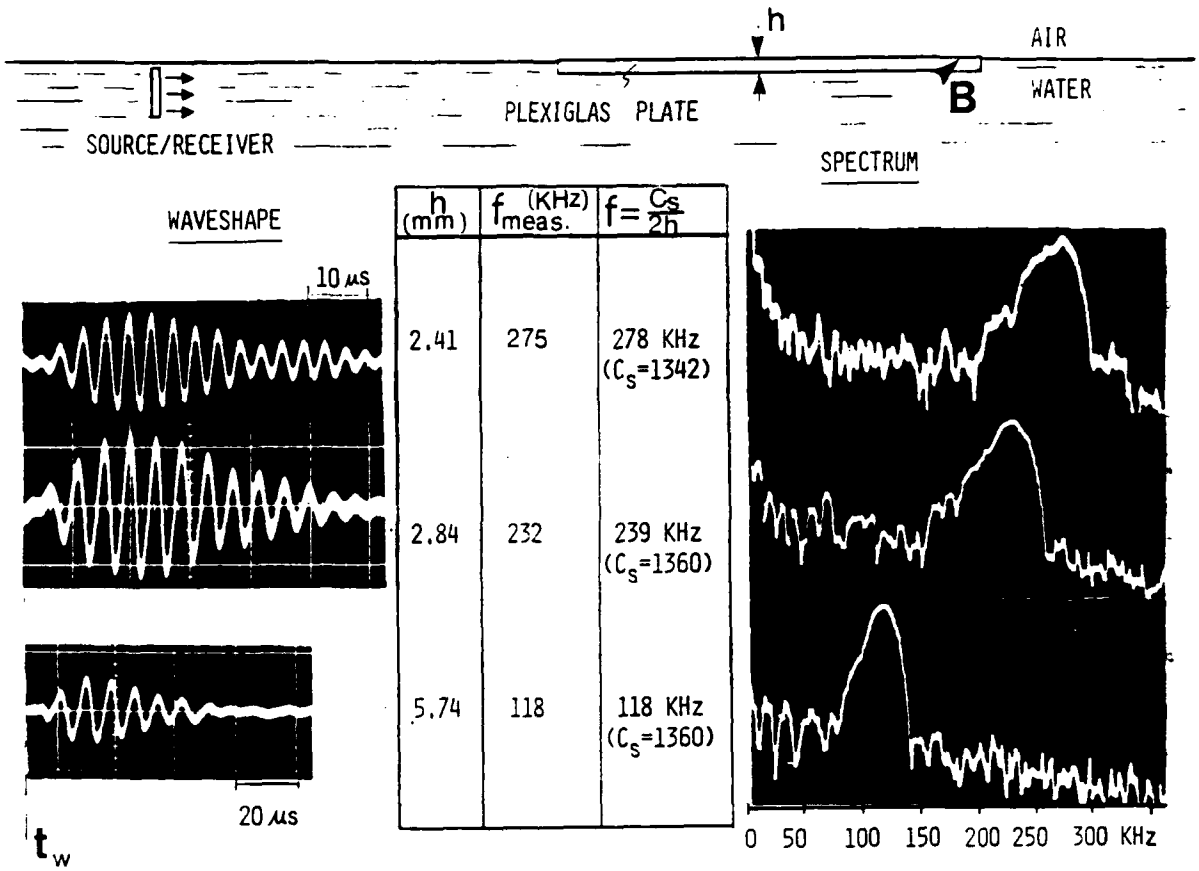

FIG.7.3. Backscatter from trailing edge of floating plate. Effect of plate thickness and shear wave velocity on ringing frequency is demonstrated.

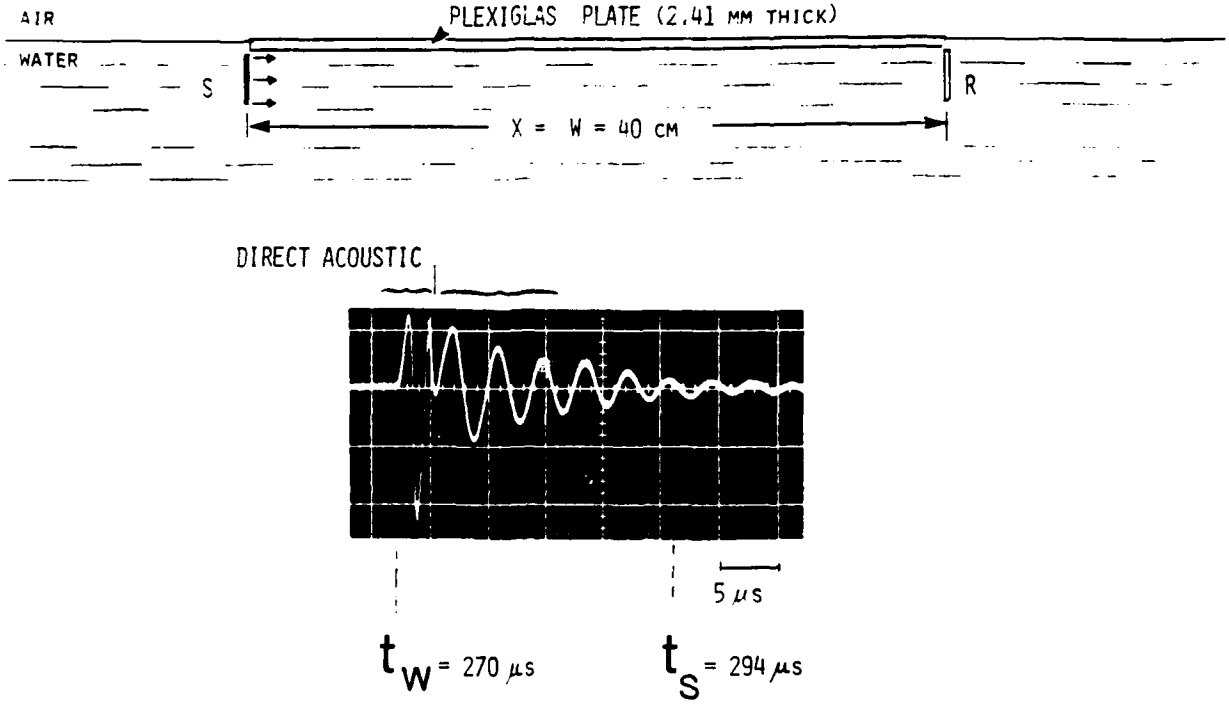

FIG. 7.4. Direct underwater acoustic wave and its associated coupled plate ringing detected in the water. Notice that ringing starts before the shear wave arrival and is initiated by the water wave.

Great care was exercized in the work to isolate the backscatter. from the lagging edge and determine that the ringing was not due to the particular experimental setup. Several experiments were performed to further characterize the observed backscatter ringing. Figure 7.4 shows a 40 cm wide floating acrylic plate (2.41 mm thick) on a water half-space, and the source and receiver transducers were placed in the water on opposite edges of the plate. By pulsing the source with a single broadband pulse similar to figure 2.1, the received signal consisted of ringing following the direct water wave pulse (FIG. 7.4). The observed ringing started before the travel time of a shear wave in the plate, and was initiated by the coupled underwater acoustic wave. The initial portion of the ringing partially overlapped the direct underwater acoustic wave, and the tail portion overlapped the shear wave component. The dominant frequency of the ringing was again close to $C_s/2h$.

In order to minimize the detection of the initial direct acoustic pulse and also to avoid the effect of plate edges, the transducers were placed on the top surface of an "infinite plate" away from any edges as shown in figure 7.5. A reference waveform was first obtained with the plate in air (FIG. 7.5(a)). The received signal was composed of a dispersive longitudinal wave followed by a

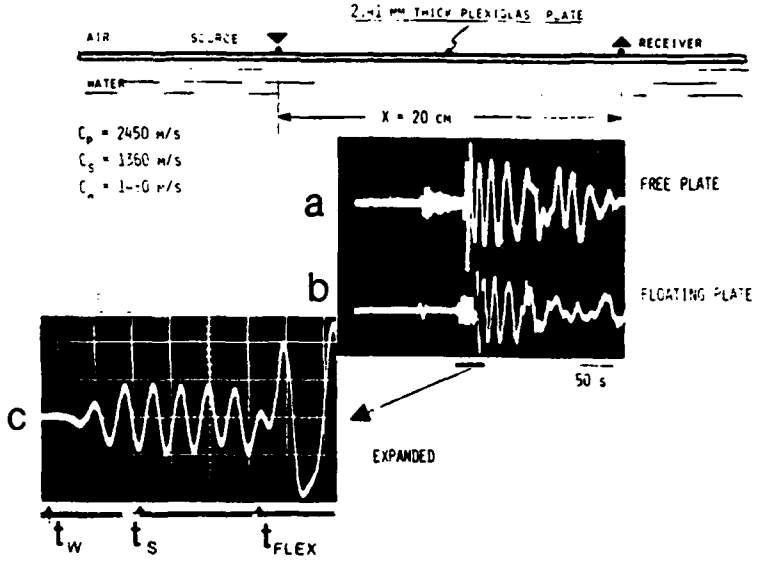

FIG. 7.5. Ringing in floating plate initiated by the water acoustic wave, propagating with the water compressional velocity, and arriving before the shear wave.

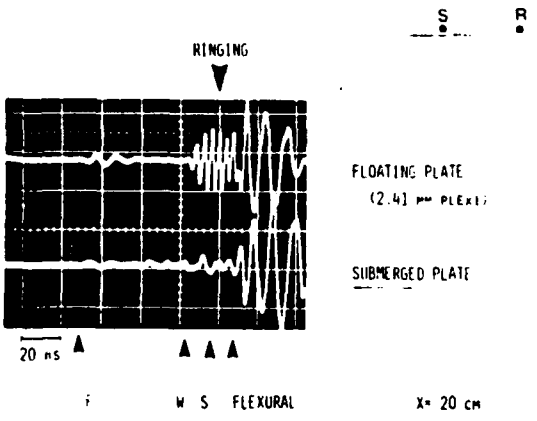

FIG. 7.6. Disappearance of ringing described in figure 7.5 by submerging the plate.

flexural wave as expected. Figure 7.5(b) shows the waveform from the floating plate model. Slightly before the flexural wave, a ringing appeared starting at the acoustic wave arrival time t_w and blended with the flexural wave. The peak ringing frequency matches $f = C_s/2h$, and it arrived before the shear wave.

Figure 7.6 illustrates that the near-sinusoidal ringing in the floating plate disappears if the plate is totally submerged in water. Figure 7.7 shows that a thin rigid barrier in the water underneath the floating plate can interrupt the propagation of the ringing revealing that it is associated with the underwater acoustic wave. Figures 7.8 and 7.9 compare the received waveforms detected by vertical and horizontal receiver transducers at the edge of the floating plate. The leaky compressional plate wave did not reverse polarity while the ringing associated with the water wave did as the horizontal receiver was moved from bottom to top along the vertical face of the plate edge (FIG. 7.9). The compressional wave component showed a phase reversal in figure 7.8 as the receiver was relocated from the horizontal free surface of the plate to the vertical plate edge surface.

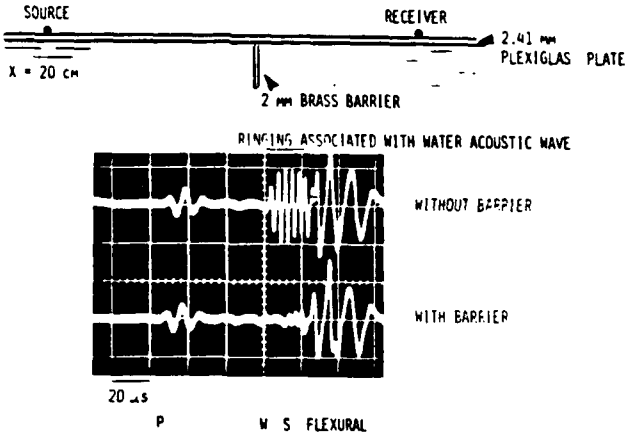

FIG . 7.7. Use of barrier in water to demonstrate that ringing is associated with the water acoustic wave and that it is not an independent shear wave in the plate.

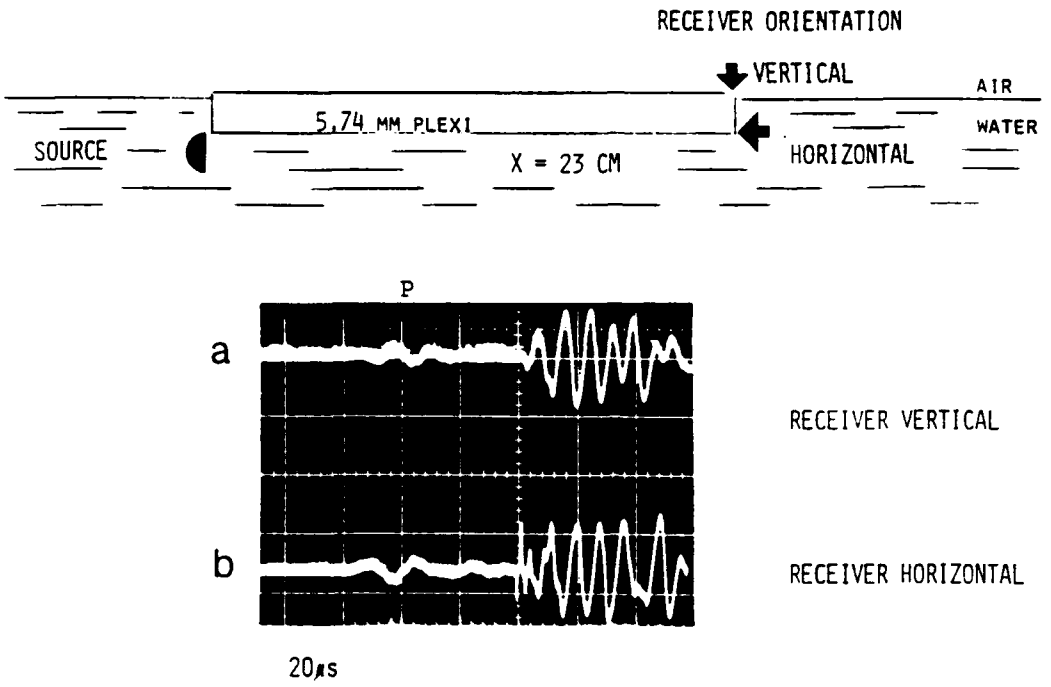

FIG. 7.8. Detection of plate ringing associated with water wave. Compare received signal with vertical and horizontal receivers at plate edge. Notice phase reversal of compressional wave component P

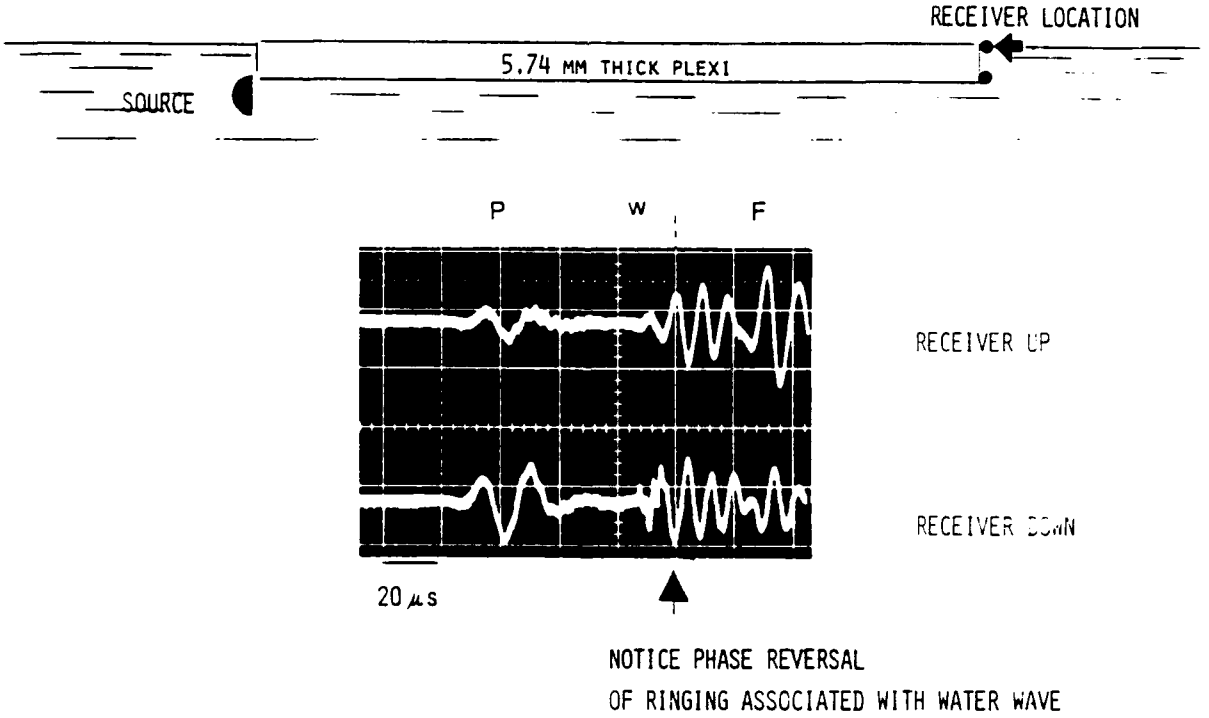

FIG. 7.9. The floating plate ringing associated with the water acoustic wave has opposite polarity near top and bottom of plate edge.

A plot of measured group velocity dispersion curves vs fh for low-frequency elastic wave components propagating in floating acrylic plates on water is shown in figure 7.10. The horizontal lines in the plot indicate the compressional wave velocity, the water sound velocity, the plate shear wave velocity, the Rayleigh wave velocity, and the Scholte wave velocity, from top to bottom respectively. The measured dispersion curve for the symmetric Lamb wave in the free plate is also plotted. The group velocity of the longitudinal waves in the plate dropped very rapidly as fh was increased. The circled dispersion curve formed by the black dots is a coupled seismo-acoustic wave obtained from the floating "infinite" plate. The dispersion characteristics of backscattered waves originating from the plate edge matched the circled dispersion curve of figure 7.10.

A different experiment was performed to demonstrate that the observed ringing is a resonant seismo-acoustic wave mode strongly coupled to the underwater acoustic wave (FIG. 7.11). Source and receiver transducers were placed on opposite edges of a floating 2.42 mm thick acrylic plate. The plate width was 23 cm. By pulsing the source, the received waves consisted of a low-frequency leaky compressional wave followed by high amplitude ringing as before (Fig. 7.11(a)). Without disturbing the setup, a layer of spread-out small air-bubbles was introduced underneath the plate to partially decouple the underwater acoustic waves from the plate waves. The presence of air bubbles eliminated the seismo-acoustic ringing associated with the water wave, and increased the amplitude of the compressional wave in the plate. By further increasing the number of air bubbles per unit area underneath the plate, the amplitude and velocity of the plate compressional wave components increased, while the direct acoustic wave amplitude decreased.

Figure 7.12 is a theoretical group velocity dispersion curve provided by G. H. Brooke for a flexural wave in a floating Plexiglas plate. The group velocity maximum which is independent of the plate thickness is slower than the experimentally observed ringing associated with the water wave. Using the SAFARI program [28], Brooke obtained a synthetic waveform for floating Plexiglas plate on water (FIG.7.13). Similar to the experimental results, a wavepacket arrived shortly prior to the flexural wave. The SAFARI program being limited to range independent layers, could not be used to obtain backscattering from cracks and plate edges.

The ultrasonic modeling experiments demonstrated that when $C_s < C_w$, backscatter of near-grazing underwater acoustic waves from vertical discontinuities in the plate is dominated by a water coupled seismo-acoustic wave component having a velocity near C_w and a spectrum with a peak frequency near $C_s/2h$. The trailing edge of floating plates produce major backscatter. It is evident from the experimental results that combined boundary scattering and waveguide phenomena affect the apparent dispersion characteristics of the detected ringing as previously reported [26]. A normally dispersed

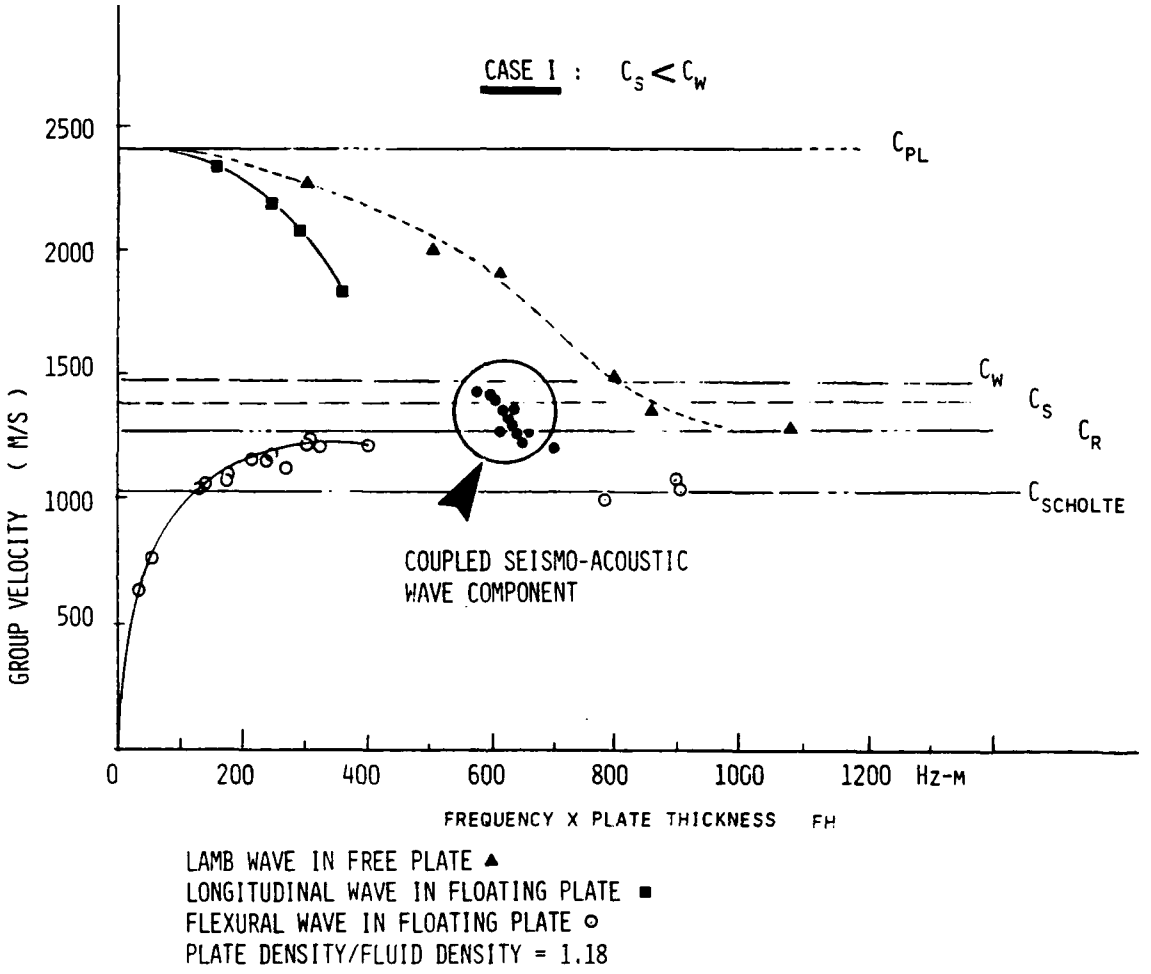

FIG. 7.10. Plot of measured group velocity dispersion curves for low-frequency elastic wave components in floating plate on water. The circled dispersion curve formed by the black dots is a coupled seismo-acoustic wave obtained from the floating "infinite" plate. This components dominates the backscatter from the trailing edge of floating plate.

wavetrain may be modified by the waveguide dispersion characteristics to look like a near-sinusoidal ringing. Medwin et al. reported other experimental observations on backscattering from a trailing edge of a floating acrylic plate [66].

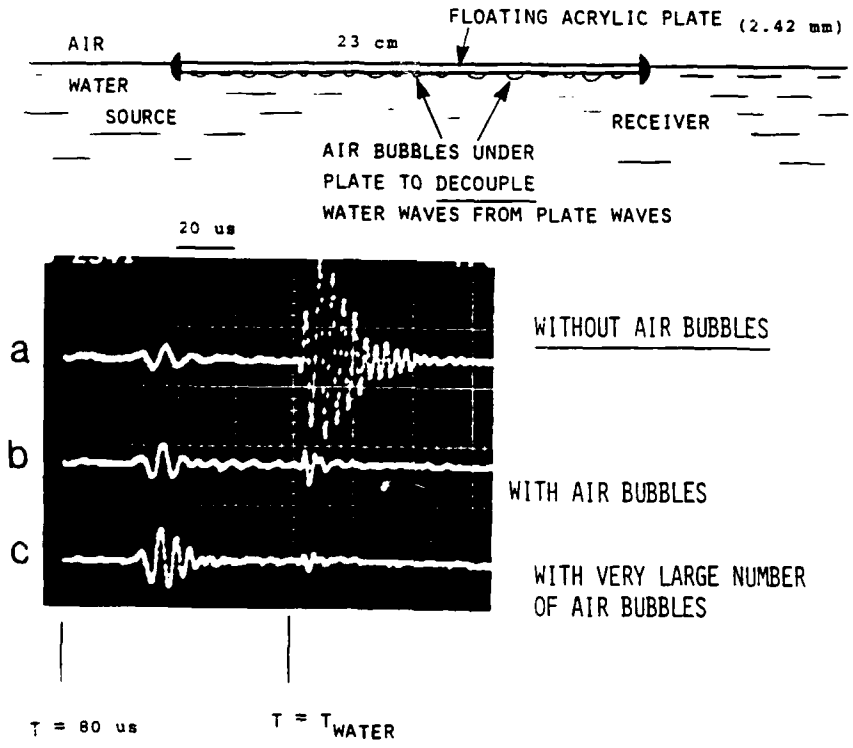

FIG.7.11. Resonant seismo-acoustic mode traveling with water compressional velocity and has peak resonant frequency = $C_s/2h$. Experimental results demonstrating that the ringing is a coupled liquid/solid phenomenon. By introducing air pockets underneath the floating plate the ringing disappears by decoupling the water waves from the plate waves. Notice also increase of amplitude and velocity of first-arriving normally dispersed longitudinal plate wave as the number of air bubbles is increased.

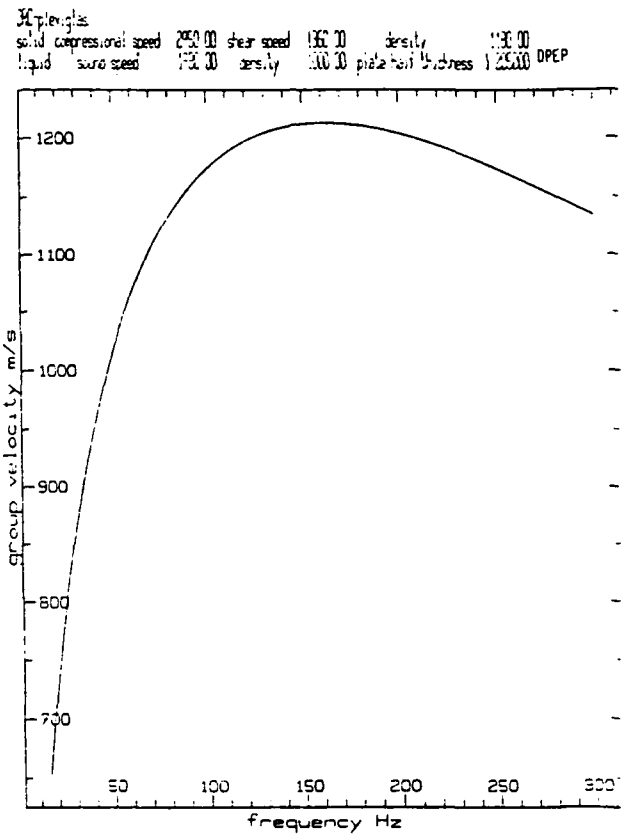

FIG. 7.12. Theoretical group velocity dispersion curve for flexural wave in floating Plexiglas plate (G. H. Brooke/DREP). Group velocity maximum is slower than the experimentally observed ringing associated with the water wave.

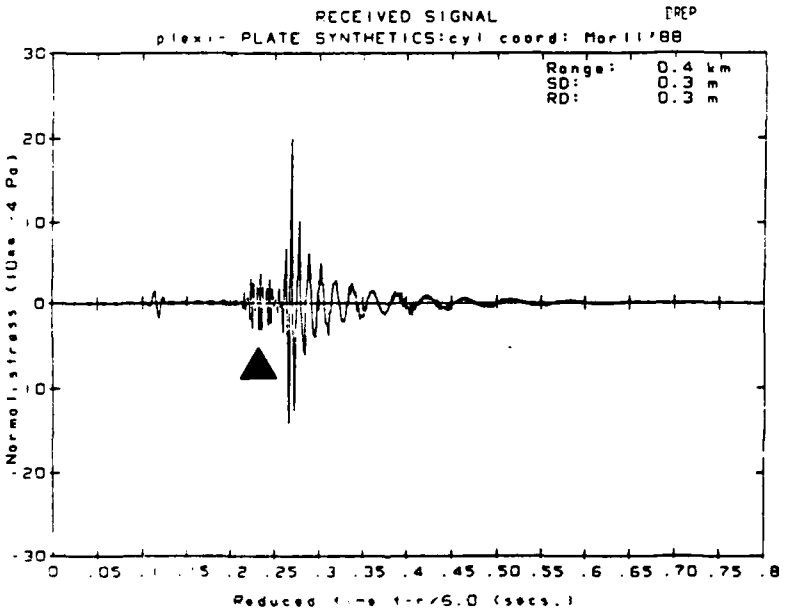

FIG.7.13 Synthetic time waveform for floating Plexiglas plate (G. H. Brooke/DREP). Similar to the experimental results, the SAFARI calculations predicts a wavepacket arriving shortly prior to the flexural wave.

7.2 PLATE WITH SUPERSONIC SHEAR WAVE VELOCITY : CASE II $C_s > C_w$

Ultrasonic modeling experiments were conducted to characterize the backscatter from edges of floating plates having a shear wave velocity greater than the water compressional wave velocity (CASE II). Glass plates of different width and thickness were used in this study (C_p = 5772 ms, C_s = 3355 m/s, C = 1480 m/s). The glass plate was fixed on top of a water half-space simulating a floating plate condition.

Figure 7.14 shows the effect of plate width on the waveshape of backscattered waves from edges of a floating glass plate (h = 2.18 mm). The source and receiver were located in the water as shown at a distance 6.5 cm from the first plate edge "A". The plate edges were oriented parallel to the wavefront. Similar to CASE I, backscatter from the trailing edge "B" was the major received component. The top waveform was obtained from a narrow plate W = 5.14 cm (FIG. 7.14(a)). The slightly dispersed pulse marked with an arrow was the backscattered wave from edge B. To the right of it, other smaller waveforms appear separated by about 50 us. As the plate width was increased, the backscattered waves became more dispersed indicating that the acoustic waves penetrated the glass plate. The low-frequency components arrived first in the dispersed wavetrains.

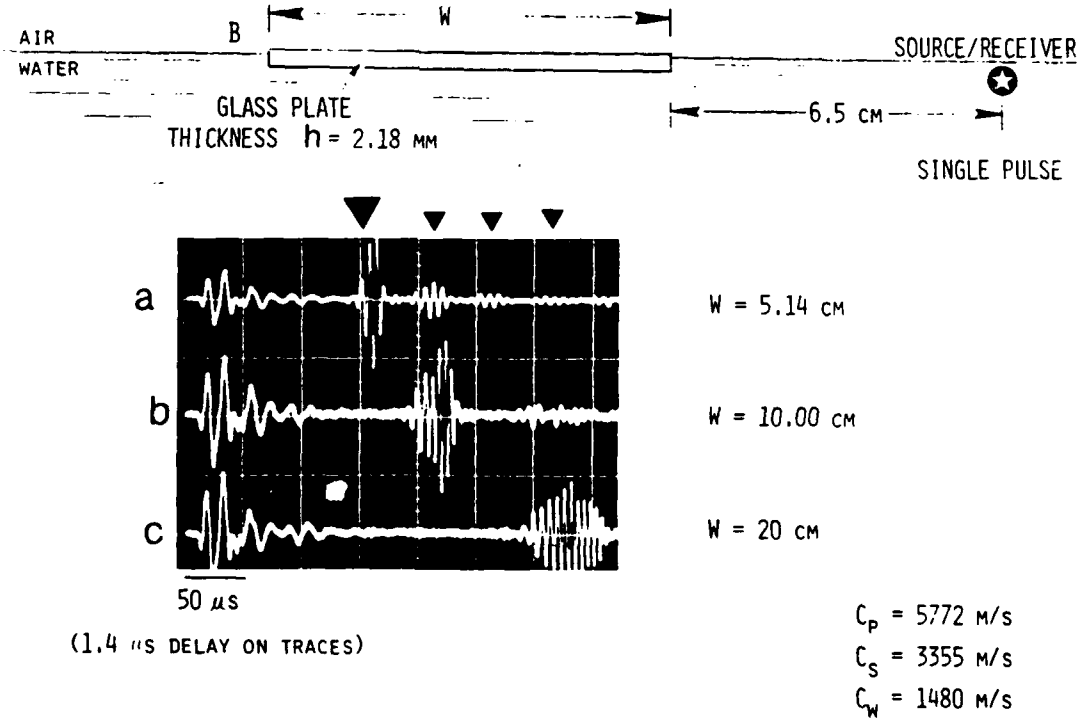

FIG. 7.14. Backscatter from edges of floating "hard" plate as function of plate width. The major dispersed wavetrain corresponds to flexural waves in floating plate radiated by plate edges. Notice distance between source/receiver and plate edge is fixed.

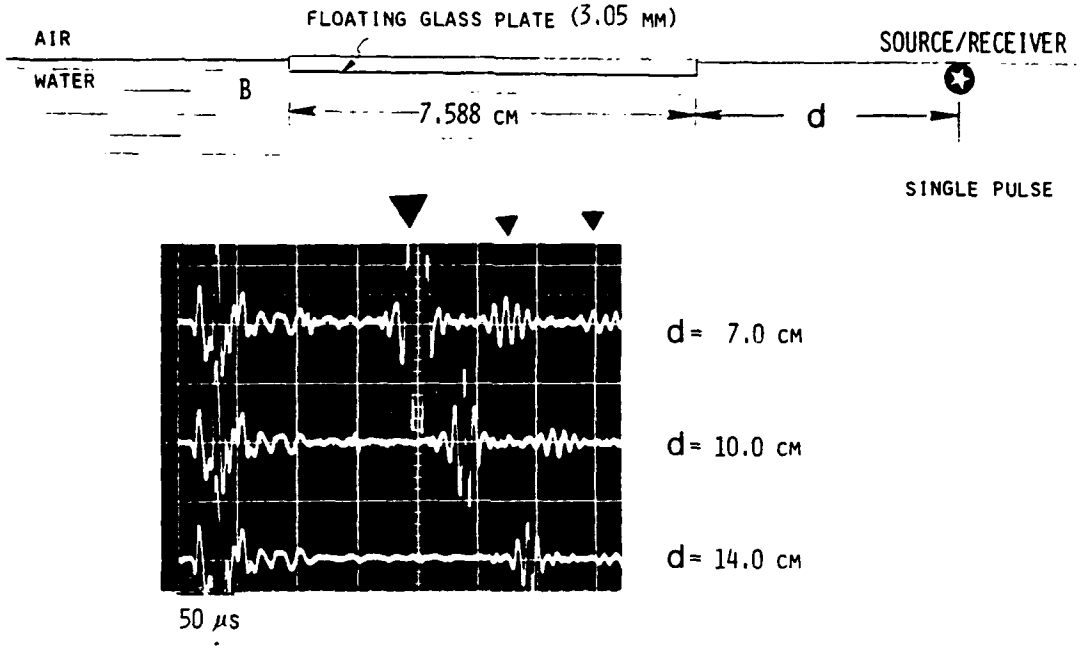

FIG. 7.15. Effect of distance between source/receiver and floating plate edge on backscattered waves. Notice plate width is fixed.

In figure 7.15, the plate width remained fixed at W = 7.588 cm and the distance "d" between the transducers and the first plate edge was varied. The received backscatter from edge B (arrow marker) was again followed by a series of smaller waveforms now separated by about 75 us. Varying the distance "d" reduced the amplitude of the backscattered waves but did not drastically change the waveshape.

Evaluation of the above results was initially puzzling because the backscattered waves travelled with a velocity much slower than the plate longitudinal velocity and their dispersion did not look like the conventional flexural wave were the high frequency components arrive first.

A vertical source was fixed at one edge of a floating glass plate (h = 2.18 mm, W = 10 cm), and a receiver was placed very near the water surface at a distance of 13 cm from the other edge of the plate in the water as shown in figure 7.16. The received waveform and its expanded view are displayed. It was first surprising to see that the vertical source which was intended to generate a flexural wave with the high-frequency components arriving first created a waveform at the receiver with opposite dispersion properties (low-

frequencies arriving first). Plotting the dispersion of the waveform shown in figure 7.16 revealed that it matched the segment of the theoretical flexural wave group velocity (FIG. 3.3) to the right of the maximum group velocity peak. This indicated that the received backscattered waves travelled in the plate with the maximum flexural wave group velocity of 2017 m/s and that the low-frequency components travelled with greater speed than the high-frequency components. The calculated round-trip travel time of the multiple reflections discussed in figures 7.14 and 7.15 also matched the theoretical maximum group velocity. The calculated time separation between multiple reflections from the 5.14 cm and 7.588 cm wide models was 50.96 us and 75.2 us, respectively.

Plate-edge backscatter from a floating plate with a shear wave velocity greater than the water compressional velocity (glass) consists of normally dispersed wavetrain belonging to the portion of the first antisymmetric mode group velocity to the right of the peak group velocity. Other converted components also exist.

A comparison of backscatter obtained from leading and trailing edges of different floating plates (CASE I and CASE II) is presented in figure 7.17.

One implication of the above findings concerns the effect of a floating finite plate on the returned reflections from an object in the water. The reflection of a single broadband pulse from an object in the water (vertical glass plate reflector) at a distance of 28 cm from the source/receiver transducers is shown in figure 7.18(a). In the absence of the object (vertical plate) and having only a thin floating glass plate (23 cm wide) present, the received signal consisted of a dispersed ringing backscattered from the trailing edge of the floating plate as expected in view of the above results (FIG. 7.18(b)). When both object and floating plate were present simultaneously, the reflection from the object appeared to have changed and acquired a precursor in the form of ringing (FIG. 7.18(c)). The same behavior was observed from other small targets in the water. The explanation of the phenomenon is that a fraction of the reflected waves became guided by the floating plate and travelled back towards the receiver with supersonic speed in the plate along the portion of the path covered with the floating plate. Therefore depending on the relative location of a target in the water with respect to floating plates, a substantial low-frequency precursor to the backscattered water waves may occur.

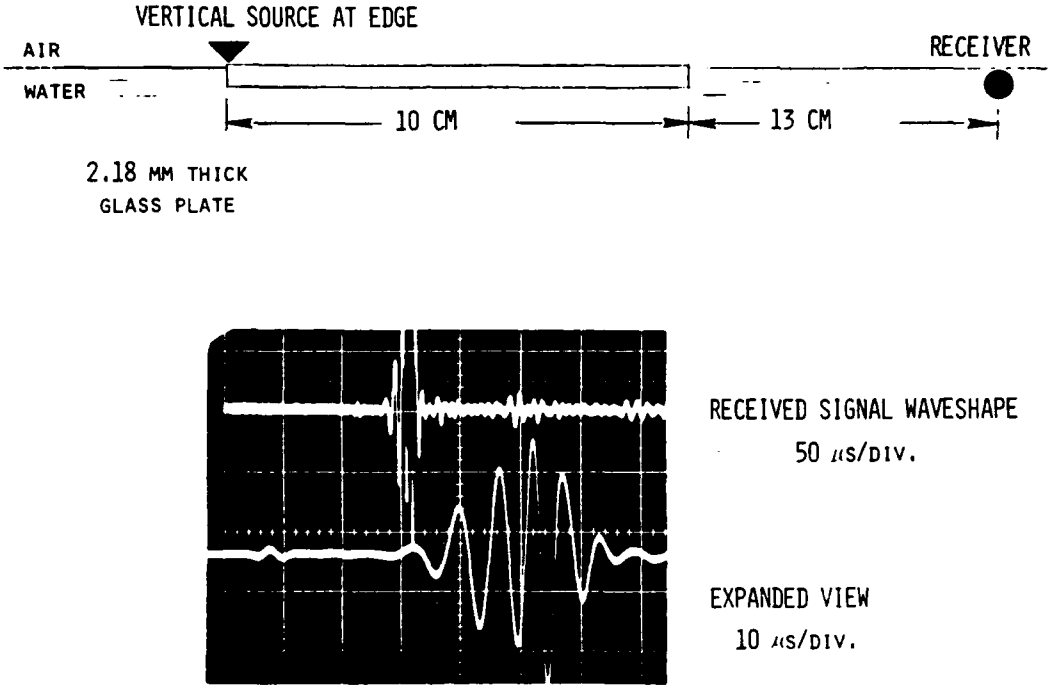

FIG. 7.16.Underwater acoustic waves detected close to the water surface with a pulsed source on the floating "hard" plate and the plate covers a portion of the wave path. The large dispersed wavetrain consists of a leaky flexural wave, portion of the Scholte wave branch of the flexural wave to the right of the maximum group velocity, and a direct water wave. Thermal cracking noise in the Arctic may be explained with this model. Other leaky plate compressional waves also exist.

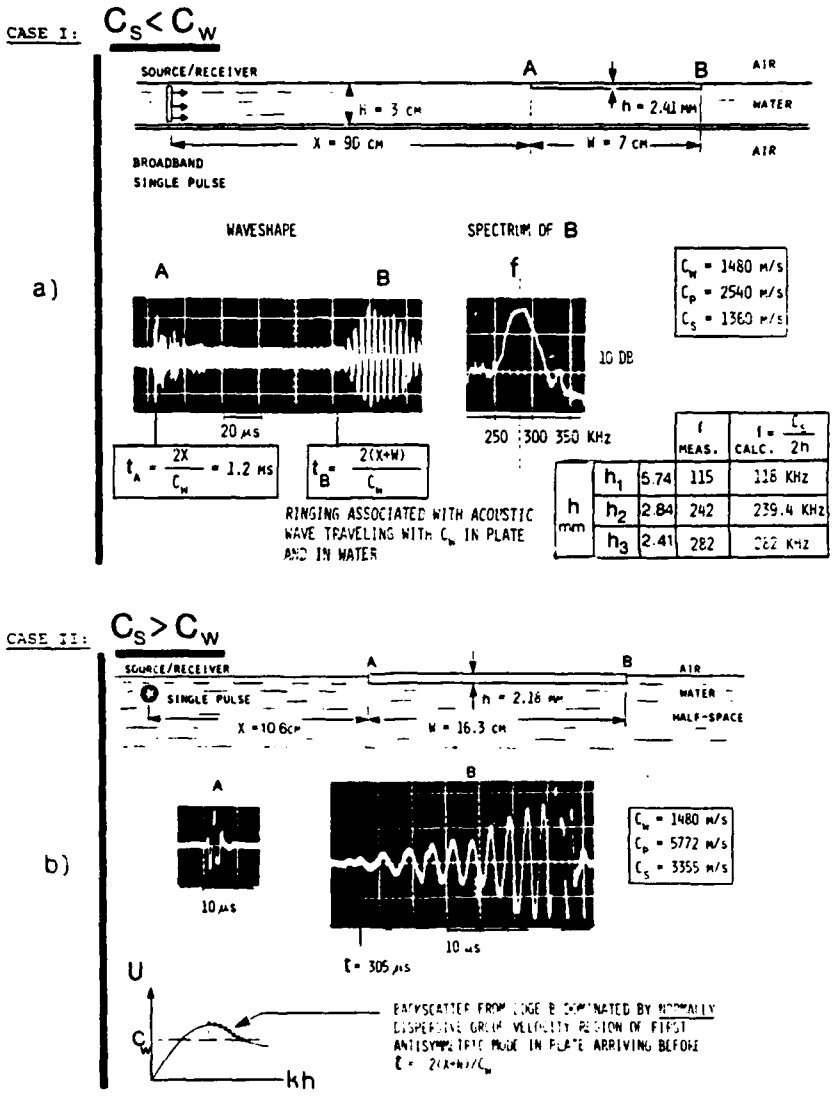

FIG. 7.17.Comparison of backscatter from leading and trailing edges of finite floating plate. Top: $C_s < C_w$. Bottom $C_s > C_w$.

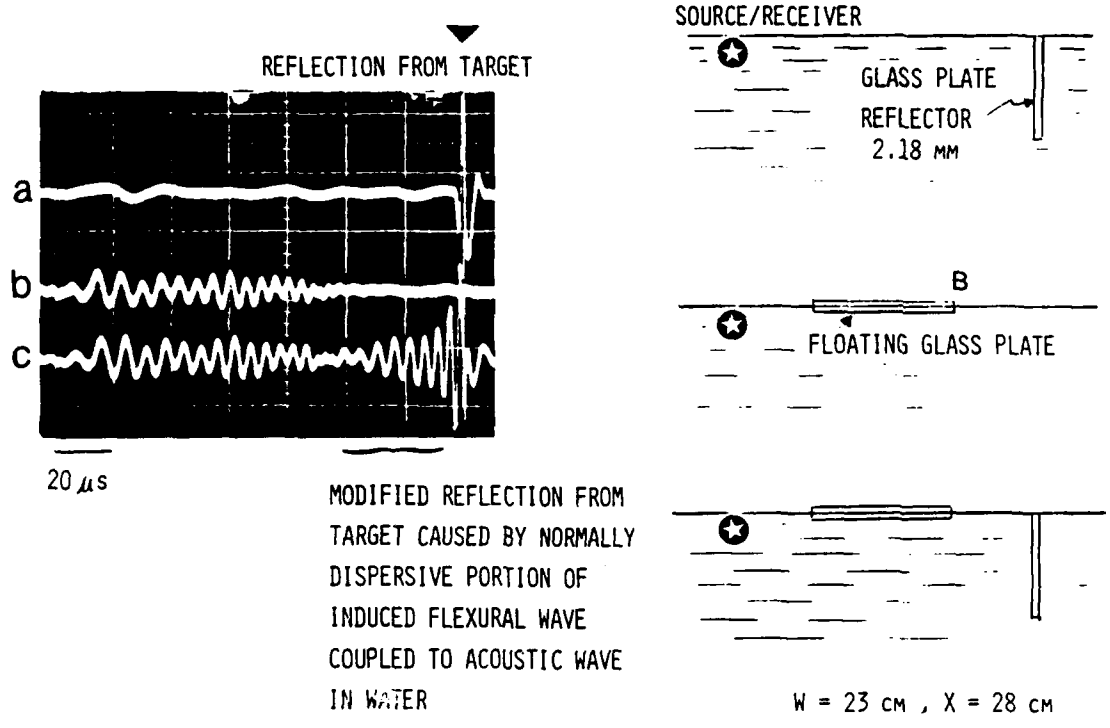

FIG. 7.18. Modified reflection from target caused by floating plate.

8. INTERACTION OF ACOUSTIC WAVES WITH ICE KEELS

8.1 UNDERWATER ACOUSTIC WAVE CONVERSION INTO PLATE WAVES

The problem of the interaction of underwater acoustic waves with penetrable ice keels having dimensions comparable to the wavelength has not yet been solved theoretically. At the Spring 1986 Meeting of the Acoustical Society of America preliminary laboratory experimental results were presented (FIG. 8.1) showing the effect of a keel underneath a floating plate on converting pulsed underwater acoustic waves into plate waves [18] .

In this preliminary qualitative investigation, an ultrasonic model was utilized to enhance the generation of flexural waves by the conversion of underwater acoustic waves by a vertical keel under a floating plate. Figure 8.1(a) shows a reference flexural wave generated by a vertically oriented source in the water underneath a uniform floating plate. When the source was rotated to point in the horizontal direction, the received waveform was dominated by a direct water wave pulse (Fig. 8.1(b)). The introduction of a vertical keel underneath the plate caused conversion of underwater acoustic waves into flexural waves (FIG.8.1 (c)). In this enhanced model, the keel width was equal to the plate thickness.

Recent results taken from a scaled ultrasonic model are shown in figure 8.2. A 2.4 cm diameter source radiating in the horizontal direction was placed near the water surface underneath an edge of a floating 2.41 mm thick acrylic plate. A 2 mm diameter receiver was placed on the top surface of the plate at a distance of 16.6 cm from the plate edge. The received signal was composed mainly of a direct underwater acoustic wave with its associated plate waves (FIG. 8.2(a)). The experiment was repeated with a triangular acrylic keel (9 mm deep and 17 mm wide) welded to the bottom surface of the plate as shown in figure 8.2(b). The relative position of the source and receiver transducers with respect to the plate was not changed. The keel generated a plate compressional wave arriving before the direct underwater acoustic wave and a flexural wave arriving after the water wave. The range of wavelengths used was comparable to the keel dimensions.

If we consider a scale of 1000:1, the model described in figure 8.2 would correspond to a 17 m wide X 9 m deep solid ice keel in a 2.41 m thick floating ice sheet. These results may be considered as an upper limit on the effect of an ice keel on converting underwater acoustic waves into plate waves because Arctic ice keels are inhomogeneous and have cracks which would reduce the coupling between the keel and the floating plate. Combined effects of cracks and keels will be investigated in the next phase of the ultrasonic modeling research. It is expected to find that cracks in the floating plate would tend to decouple the keel from the plate.

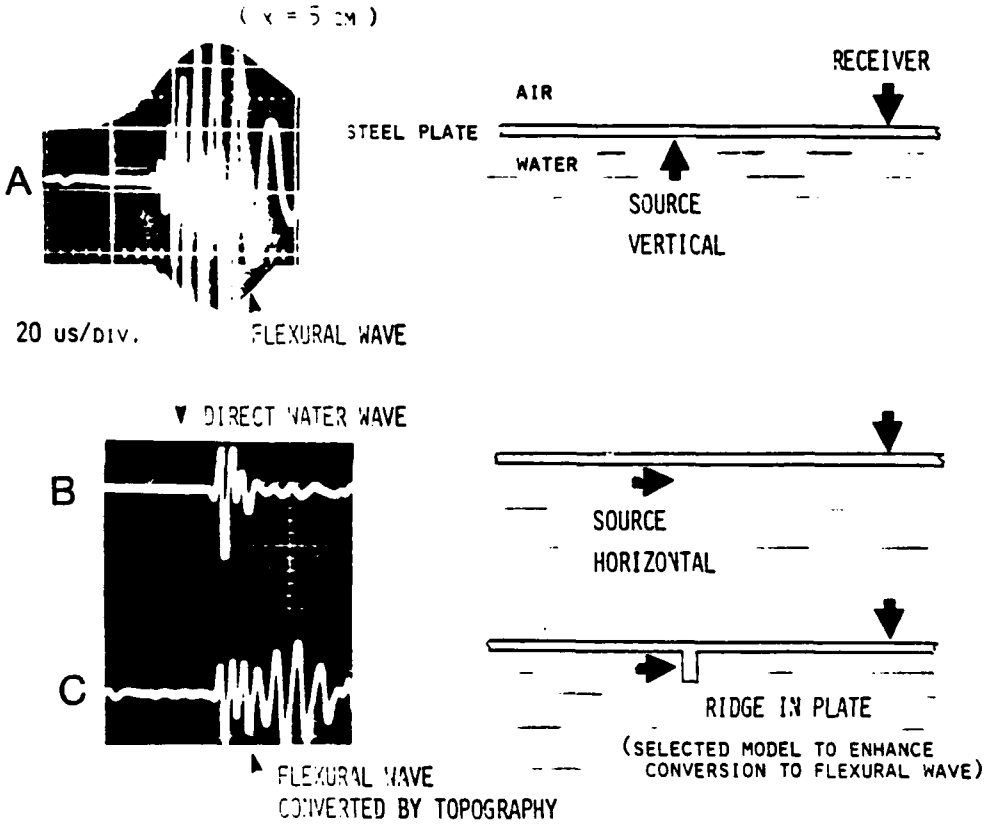

FIG. 8.1. Preliminary laboratory experimental results showing conversion of underwater acoustic waves into plate waves by keel underneath a floating plate.

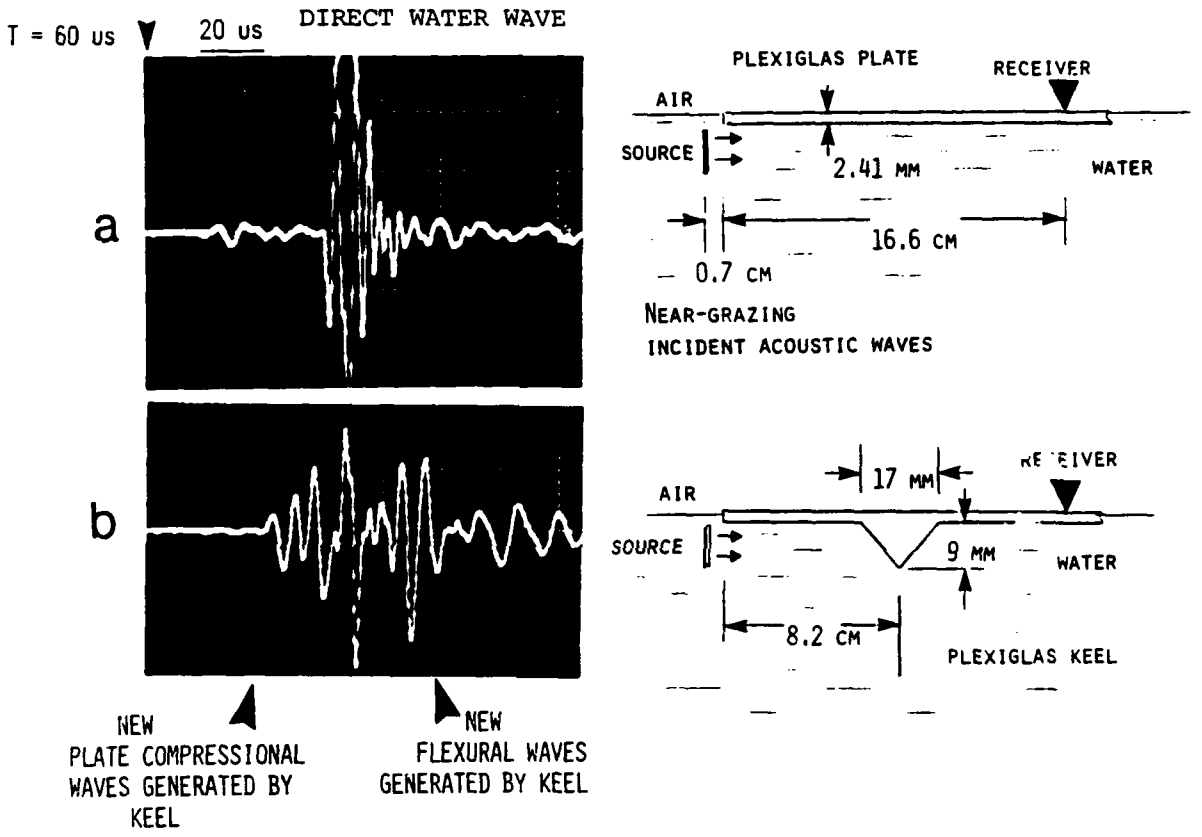

FIG. 8.2. Conversion of underwater acoustic waves into compressional and flexural waves in floating plate by keel. Notice arrival of new compressional wave in plate before the direct underwater acoustic wave.

Figure 8.3 demonstrates the effect of a crack in a floating plate on reducing the backscatter from the trailing edge of the plate. A similar behavior may occur when combining cracks and keels. The drawback of using acrylic in the experimental modeling is that its shear wave velocity is slower than the water compressional wave velocity, while sea-ice may have a supersonic shear wave velocity. Models with elastic properties similar to sea-ice would generate more leaky wave components contributing to ambient noise.

Further studies are needed to quantify the conversion of underwater acoustic waves by ice keels. A major step in this direction has been achieved by the impressive finite difference numerical modeling results obtained by J. R. Fricke et al. [73]. Our experimental ultrasonic modeling studies also revealed the presence of guided waves along the keel axis. In section 9, edge waves along apex of solid immersed wedges are discussed. In this preliminary study, we have simply demonstrated the potential role of keels on converting near-grazing underwater acoustic waves into leaky and trapped plate waves.

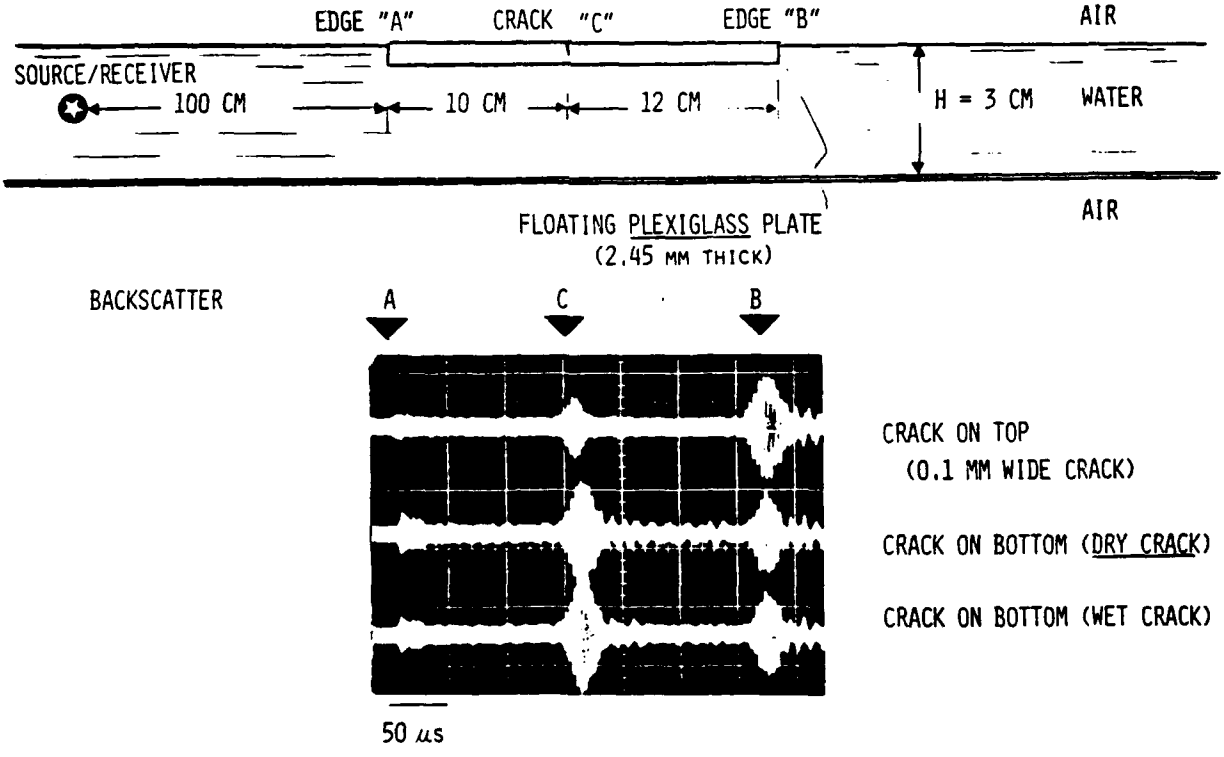

FIG. 8.3. Effect of combined cracks and plate edges on backscattering. Presence of crack in floating plate decreased backscatter from trailing edge of plate.

8.2 TRANSMISSION LOSS BY SEA-ICE KEEL WIDTH RESONANCES

The common viewpoint on scattering from ice ridges has been in terms of kd where k is the wavenumber and d is the depth of the ice keel. At small kd, shallow ridges were considered to create little backscatter. The ultrasonic modeling studies indicate that shallow Arctic keels may significantly contribute to the attenuation of low-frequency underwater acoustic waves (10-100 Hz) due to seismo-acoustic components controlled by the keel width "w" which is comparable to the wavelength. Therefore although kd is small, kw is large.

Ice keels have usually been represented by either triangular, circular, or elliptical cross section. Flattened ridge keels due to ablation increases the ratio of ridge width to ridge depth. The enhanced ultrasonic models used keels with a rectangular cross section approximating typical ridge keel contours Fig. 8.4. The ultrasonic model consisted of a water layer bounded with air on one side and by a 2.45 mm thick acrylic plate on the other side. Parallel identical keels were used in a shallow water waveguide (H = 3 cm) to magnify the backscattering from keels and focus on keel width resonances. The keels were made of long rectangular strips of acrylic and were in sliding contact (not welded contact) at the bottom of the floating plate to eliminate the possible conversion of

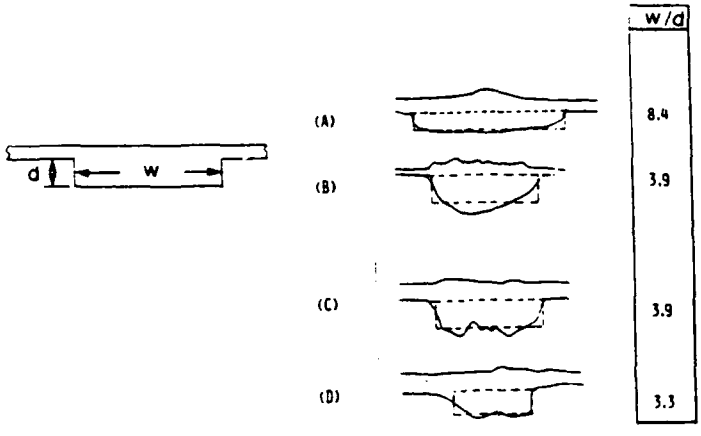

FIG.8.4. Representing ice keels by approximate rectangular ridges. Ridge profiles "a" and "b" by Kovaks, and "c" and "d" by Francois as referenced by Diachok 1976.

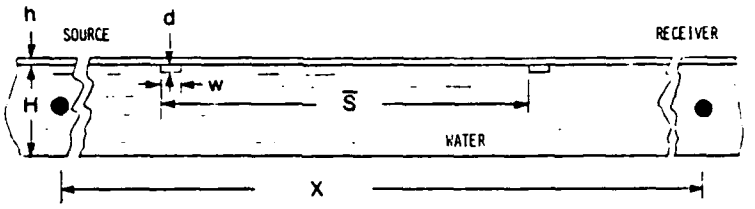

FIG. 8.5. Configuration of experimental setup for ridges.

underwater acoustic waves into plate waves as described in section 8.1 above. Models with shallow keels welded to the plate did not significantly change the characteristics of the backscattered waves in this study. The keels were oriented with their axis parallel to the wavefront. Figure 8.5 shows the geometry of the experimental model. The source was pulsed with a single broadband pulse, and the distance between source and receiver was 2.76 m.

EFFECT OF KEEL WIDTH

Three different sets of keels were used having a width w = 6.77 mm, 8.47 mm, and 15.28 mm. Figure 8.6(a) displays a reference waveform obtained from the waveguide without keels. The dispersed received wavetrain was generated by the water waveguide dispersion characteristics. Twenty parallel keels (w = 6.77 mm) were randomly placed along the boundary underneath the floating plate with an average separation of 11.6 cm. The model with keels produced the waveform shown in figure 8.6(b). The corresponding spectra are also displayed. The keels attenuated a broad range of frequencies and had a major effect on components centered around 111 kHz.

Results from the second set of keels (w = 8.47 mm) are presented in figure 8.7. The transmission loss increased and two closely spaced dips appeared near f = 92 kHz and 105 kHz as shown in figure 8.7.

The widest keels (w = 15.28 mm) generated the largest attenuation of the transmitted underwater acoustic waves and had a dip at about 62 kHz (FIG. 8.8)). Figure 8.9 compares the spectra obtained from the three models (w = 6.77 mm, 8.47 mm, and 15.28 mm). Attenuation in dB vs frequency was obtained by subtracting the spectrum of "B" from the spectrum of "A" for the three cases. The dip shifted to lower frequencies as the ridge width was increased.

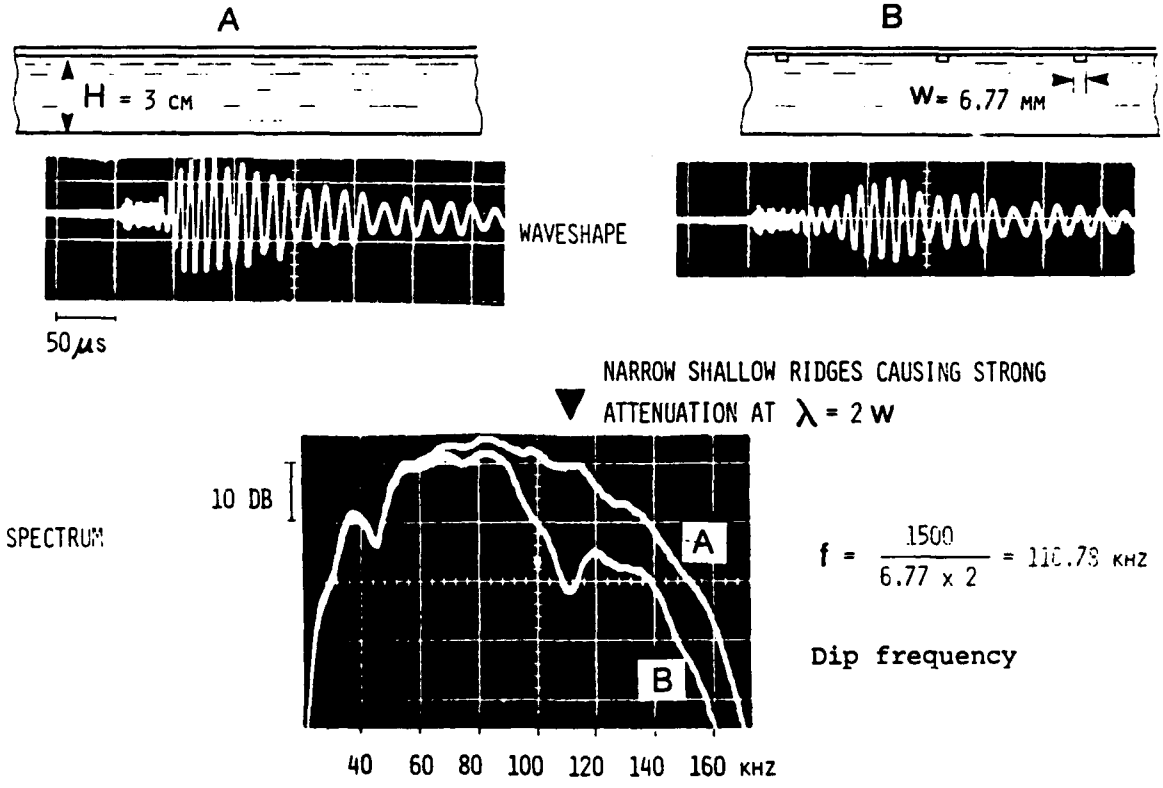

FIG. 8.6. Attenuation of underwater acoustic waves by narrow shallow ridges under floating plate.

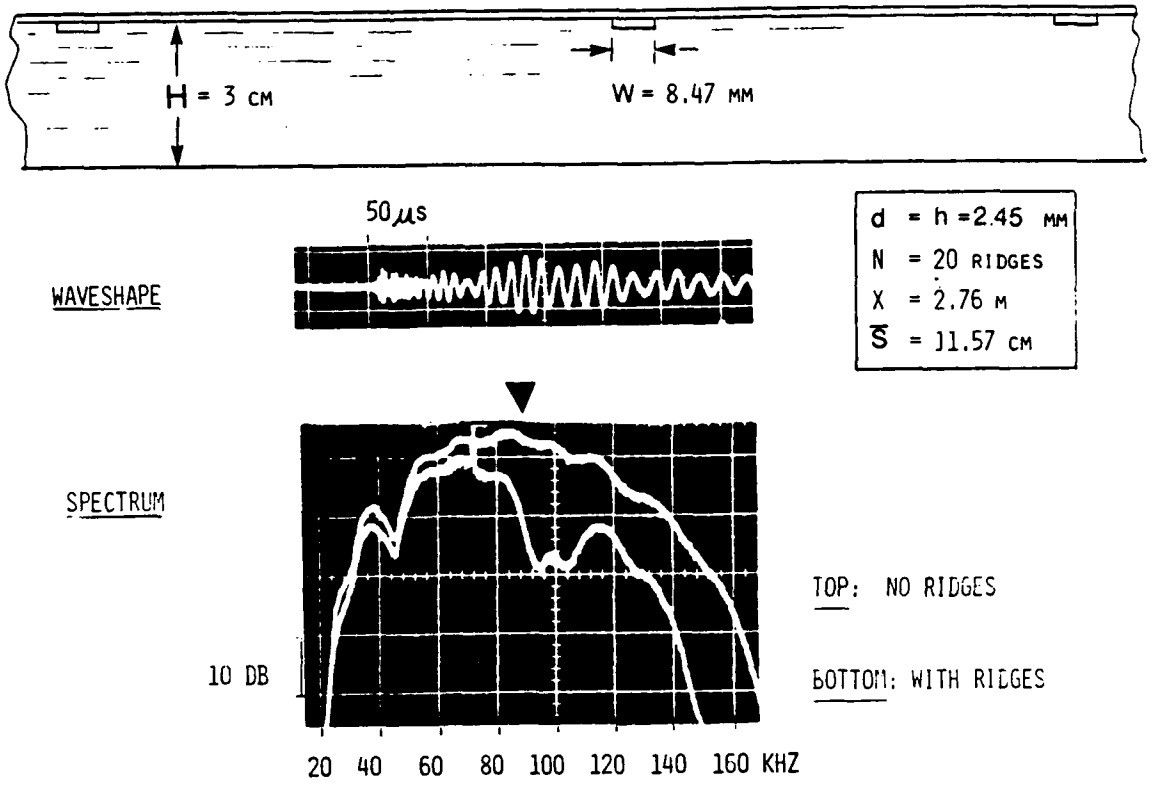

FIG . 8.7. Attenuation of transmitted underwater acoustic waves by ridge width resonances.

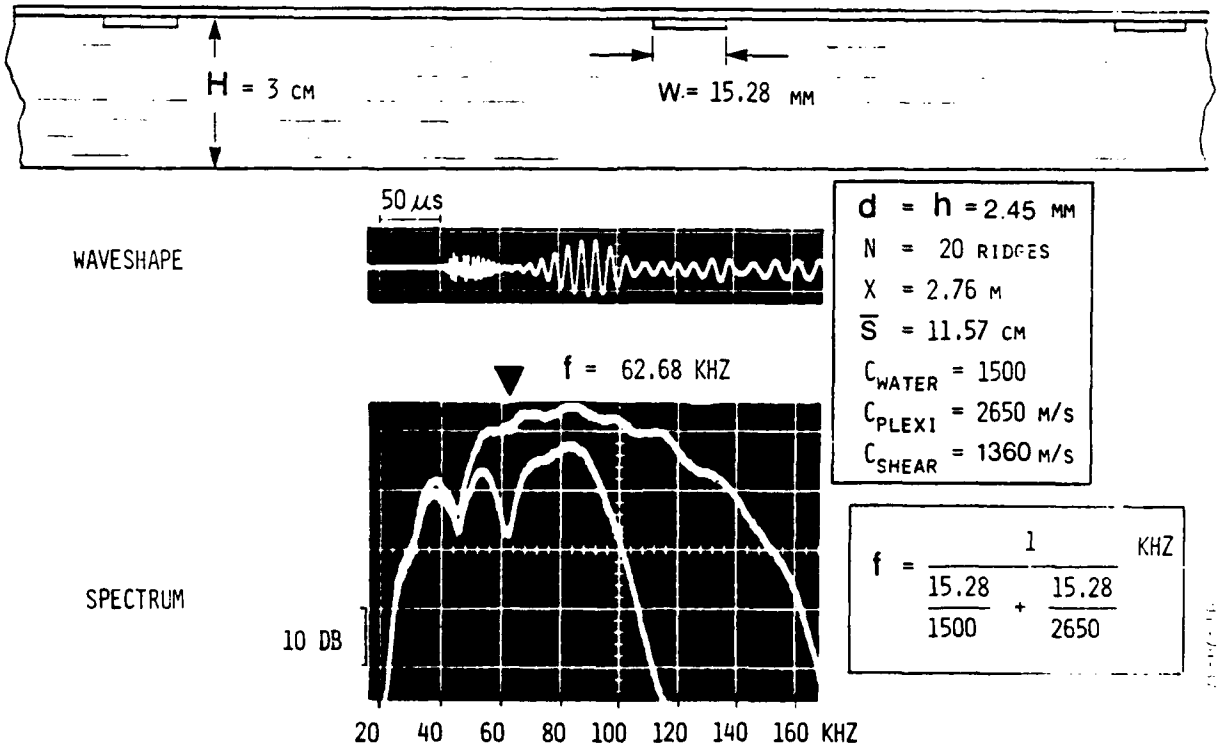

FIG. 8.8. Hybrid ridge width resonance corresponding to traveling one way with the compressional velocity in the solid ridge and returning with the water compressional velocity.

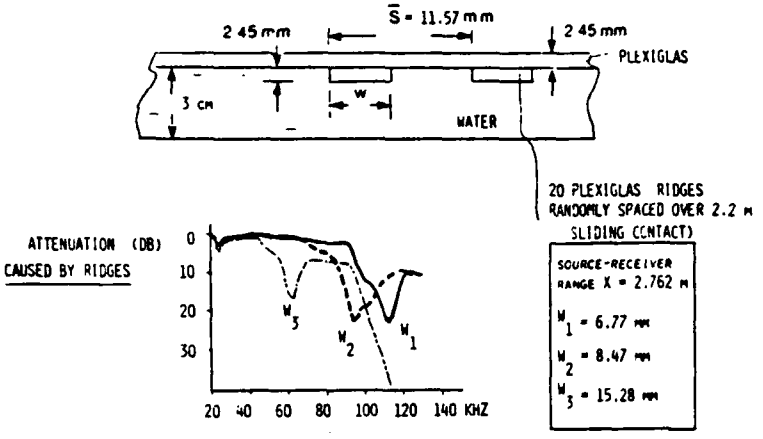

FIG. 8.9. Transmission loss affected by ridge width. The attenuation peak shifts to lower frequencies as ridge width is increased. Notice all ridges are shallow and have the same depth.

The spectrum of backscattered waves from one single wide ridge (W = 15.28 mm, x = 53.4 cm, N =1, H = 3 cm) had a large peak near 62 kHz as shown in figure 8.10 corresponding to the dip of figure 8.8. This experiment demonstrated that transmission loss is due to backscattering of low-frequency wave components by shallow wide keels.

The effect of the number of keels "N" along the wave path on the transmitted low-frequency waves is shown in figure 8.11 (w = 15.28 mm, H =3 cm, d = h = 2.45 mm, x = 2.3 m, and N = 0, 2, 4, 6, 8, 10, 12, 16, 18, and 20). The dip frequency remained fixed near 62 kHz as the number of keels was increased from 2 to 20. The transmission loss also increased with N.

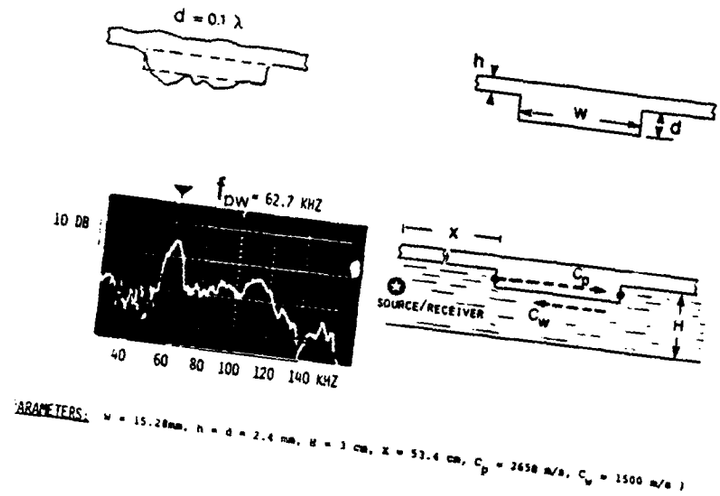

FIG. 8.10. Low-frequency backscatter from ridge width resonances.

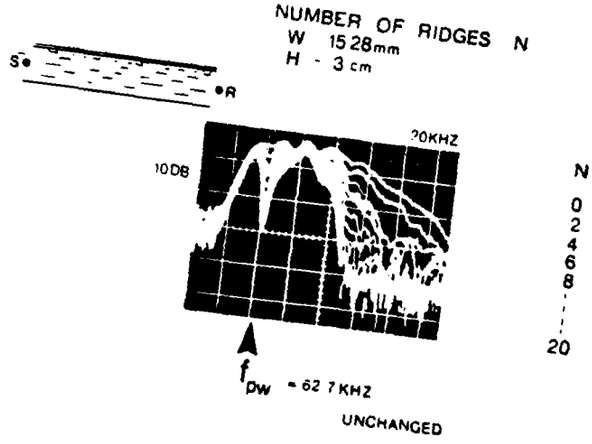

FIG. 8.11. Effects of number of identical ridges along path on attenuating low-frequency underwater acoustic waves.

Figure 8.12 reveals that as the water depth was decreased, not only the transmission loss increased, but the dip frequency remained fixed at 62.7 kHz (W = 15.28 mm, H = 3,4,6 cm, x = 2.3 m, N = 20). This observation is important since it proves that the dip frequency is dominated by the ridge characteristics and not by the water waveguide dispersion characteristics.

The results clearly indicated that the keel width played a major role in the attenuation of low-frequency components, although the keels were shallow and had the same depth. The narrow keels (6.77 mm) of figure 8.6 had a resonance near $f_{ww} = C_w/2w$. The widest keels (15.28 mm) had a resonance f_{pw} that seem to originate from a hybrid mode propagating in one direction in the keel with the compressional velocity of the solid and returning with the water compressional velocity. The medium width keels had the two types of resonances f_{ww} and f_{pw} coexisting. In some models a third resonance f_{pp} also appeared corresponding to the round trip travel time in the keel with the compressional wave velocity of the solid (FIG. 8.13). The exact complicated resonances of these water loaded elements depend on the actual wave path of the converted, reflected and radiated waves and their corresponding velocities.

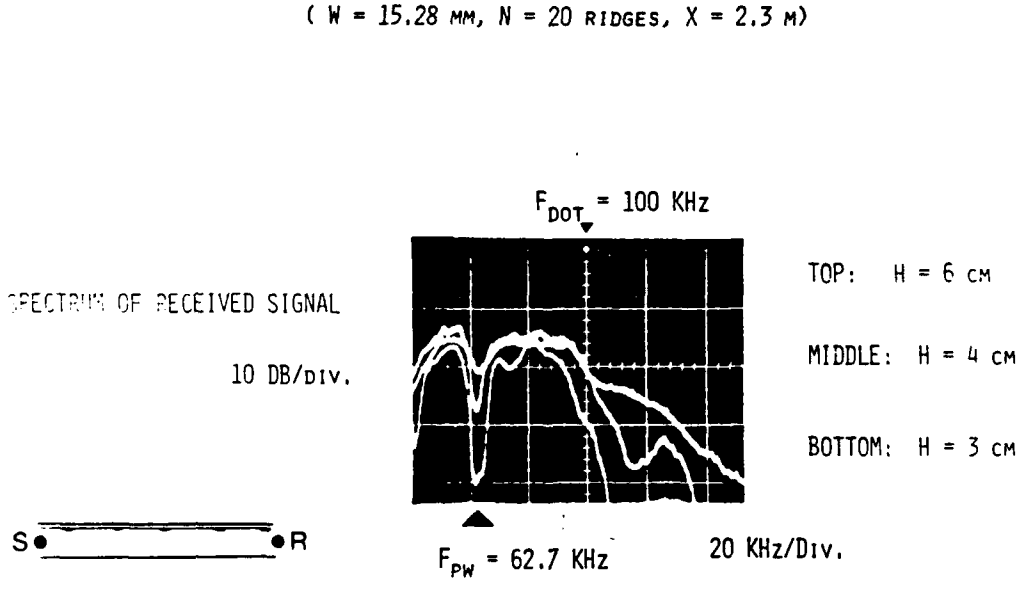

FIG. 8.12.Effect of water depth on attenuation of underwater acoustic waves by shallow ridges under floating plate.

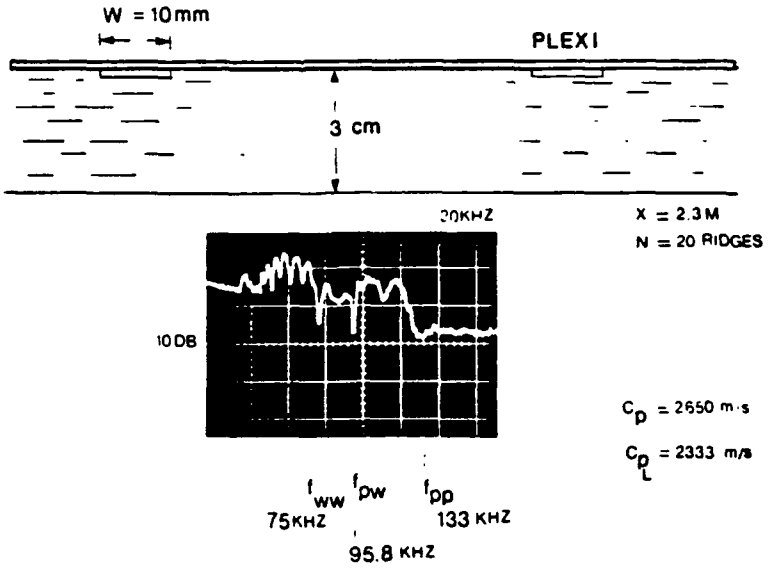

FIG. 8.13. Multiple ridge width resonances observed in some models.

Fig. 8.14 shows the attenuation plot for the case where a mixture of two types of keels were used (20 keels 6.77 mm wide and 10 keels 15.28 mm wide). Two distinct dips were detected at 62.7 kHz and 111 kHz corresponding to the two keel widths.

RIDGE SHAPE

Semi-cylindrical keels (diameter = W) produced a f_{pw} dip at a slightly higher frequency than the corresponding rectangular ridge of width W (Fig. 8.15). The measured f_{pw} from the cylindrical ridge was 77 kHz and the calculated f_{pw} for the rectangular ridge was 74 kHz. The increase in frequency was expected since the effective width of the ridge was decreased by the curved ends relative to a rectangular cross section.

The above results were obtained with the wavefront parallel to the length of the keels. The effect of oblique incidence remains to be investigated.

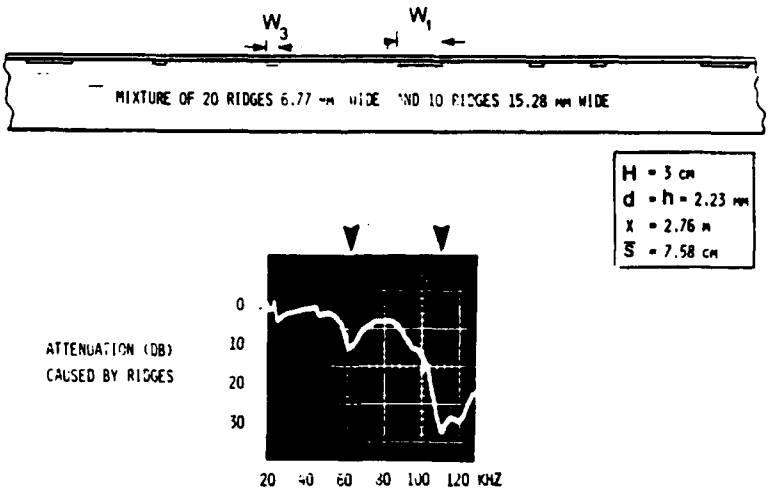

FIG. 8.14.Mixture of two types of ridges creating corresponding transmission loss peaks.

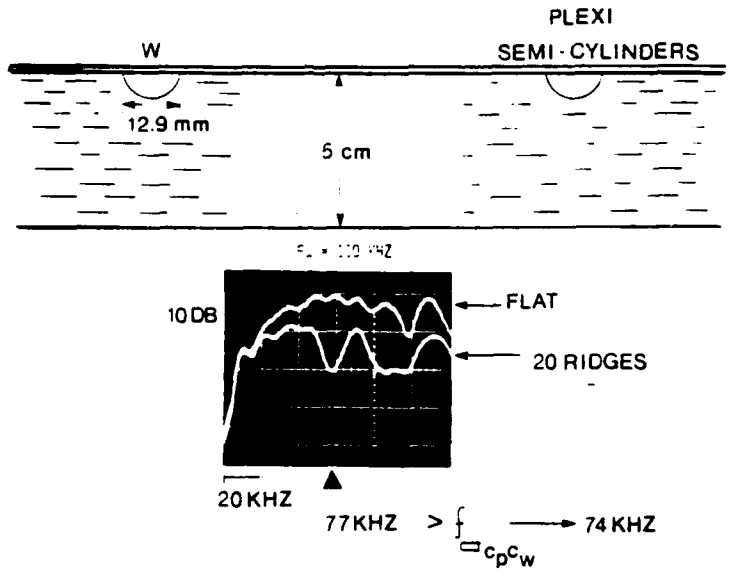

FIG. 8.15. Spectrum of transmitted waves showing attenuation caused by semi-cylindrical ridges. Top trace was a reference signal obtained without ridges. The frequency dip at 77 kHz was slightly higher than calculated based on a rectangular cross section ridge (74 kHz) as expected due to the shorter effective width by the curved edges.

9. SEISMO-ACOUSTIC WAVES ALONG APEX OF IMMERSED SOLID WEDGE

Little is known about the effect of edge waves propagating along cracks, keels, plate edges, and other lineal topographical boundaries on Arctic acsoustics. Most previous Arctic research focused on transmission across surface discontinuities and not on waves guided along ice discontinuities.

The experimental ultrasonic modeling investigations discovered the existence of a substantially large edge leaky Rayleigh wave guided along the apex of an immersed ice quarter-space (90° wedge) in water [23]. The potential importance of edge waves propagating along plate edges, ice keels, cracks, and hard ocean bottom discontinuities became apparent in regards to mode conversion, energy partitioning, trapping, ambient noise, and 3-D underwater acoustic wave characteristics. The presence of a source in the water close to an ice keel can create obscure seismo-acoustic wave phenomena which need to be quantified.

In this section, experimental results from different ultrasonic models are presented on broadband pulsed edge waves propagating along an edge of a free or immersed solid in the form of a quarter-space (90° wedge), a small-angle wedge, or truncated wedge. The type of waves studied include the antisymmetric edge-Rayleigh wave, the nondispersive flexural wave, the leaky edge-Rayleigh wave, and the edge-Scholte wave. The laboratory models used were aluminum, acrylic, limestone, and ice in air or water. The studies indicate that all edge surface and interface waves travel with a velocity slower than their corresponding waves on a solid half-space. The measured ratio of the quarter-space edge-Rayleigh wave velocity to the half-space Rayleigh wave velocity was 0.9617 for aluminum-6061, 0.9665 for acrylic, and 0.9954 for limestone. The pulsed nondispersive edge flexural wave is also demonstrated using a "sharp" wedge apex. The effect of wedge apex truncation on the dispersion of the antisymmetric edge-flexural wave is also shown. These are the first published experimental waveshapes and velocities on single broadband pulsed edge waves propagating along apex of free or immersed solid wedge. No published theoretical papers exist on the immersed solid wedge.

THEORETICAL BACKGROUND

Ash et al. [77] suggested the presence of a slow edge wave along tip of triangular ridge. P.E. Lagasse discovered in 1972 nondispersive flexural edge waves propagating along the apex of a

small angle "ideal" solid wedges using a computer finite element approach (FIG. 9.1) [74-75]. The same year, Maradudin et al. [76] independently presented theoretical results on edge modes in finite crystals. Lagasse's results show that the wedge antisymmetric edge waves may travel with a velocity much slower than the Rayleigh wave velocity without dispersion (FIG. 9.1) according to the approximate empirical relation

$$V_m = C_R \sin m\theta, \quad m = 1,2,3,\ldots \; m\theta < 90°$$

where V_m = antisymmetric mode velocity,
C_R = Rayleigh wave velocity,
m = mode number
and θ = wedge angle.
The number of antisymmetric edge modes is determined by the relation $m\theta < 90°$.

Edge waves exist in addition to other surface and body waves. They propagate along an edge formed by two semi-infinite free

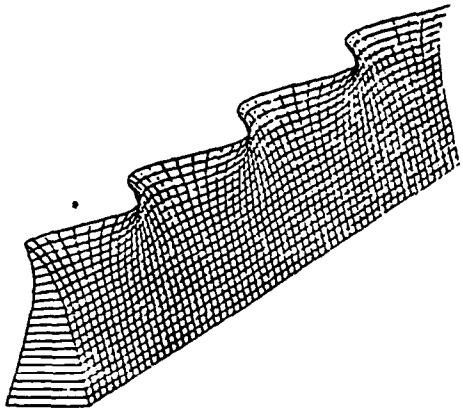

Fig. 9. Computer-generated perspective view of propagation in the lowest order mode on a narrow apex wedge. Wave motion is predominantly antisymmetric flexural.

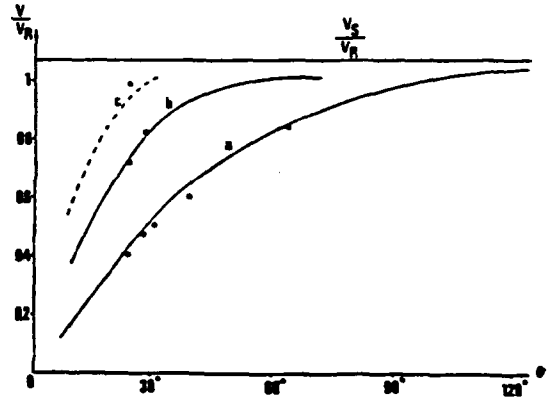

Fig. 8. The effect of varying apex angle on the propagation velocity the three lowest order nondispersive wedge waves. Curves were co puted using fourth-order finite elements for Duralumin 175. Circ represent experimental results.

FIG. 9.1. Wave motion and velocity of nondispersive flexural wedge apex waves copied from IEEE TRans. on Microwave Theory and Techniques MTT-21(4), 1973. Results by P. E. Lagasse, I. M. Mason, and E. A. Ash.

surfaces. Edge waves have three components of displacement, and decay inside the solid and away from the edge [74-87]. In an ideal infinitely sharp edge, symmetric and antisymmetric edge waves exist. The symmetric edge waves are dispersive while the antisymmetric edge waves are nondispersive because there is no characteristic length involved.

Edge waves are slower than Rayleigh waves. The 90° wedge has a single nondispersive antisymmetric mode slower than the Rayleigh wave. The two approaches used so far to study wedge waves include the method of finite elements and the microwave circuits method which is semi-empirical.

Bondarenko and Dubovitskii (1976) derived an equation for the dispersionless edge wave along the edge of a free solid 90° wedge [equation (9) in reference 83]. The calculated edge wave velocity for an aluminum quarter-space (C_p= 6328 m/s, C_s = 3126 m/s) based on this equation yields an unrealistic velocity of V = 9425 m/s. Maradudin's derivation based on $\lambda = \mu$ (Lame's constants) predicts an edge wave velocity $V = 0.9013C_s$ = 2817 m/s for the aluminum quarter-space [76]. Bestuzheva and Durova (1981) derived an expression for the small-angle wedge for different Poisson's ratio, and also explained the limitations of Bondarenko's derivation [78]. Bozhenko et al. (1985) presented experimental results (no waveforms) on continuous edge waves. For a steel quarter-space, their measured ratio of edge Rayleigh wave to Rayleigh wave velocities was 0.984. Pajewski et al. (1987) presented gated sinusoidal (tone burst) edge Rayleigh wave experimental results from a free glass wedge [80].

Comparison of predicted edge wave velocity using Mckenna's equation

$$C = C_s \tan\theta \, [2/3(1-\sigma)]^{\frac{1}{2}} \, [4n^2 + 8n + 6\,(1-\sigma)]^{\frac{1}{2}}$$

and Lagasse's empirical equation for an aluminum full wedge with an apex angle $\theta = 20.75°/2 = 10.375°$, C_s = 3126 m/s, C_p = 6328 m/s, C_R = 2952 m/s, σ = 0.338,

n	2(n+1)θ	V (McKenna)	V (Lagasse)
0	20.75°	1144	1046 m/s
1	41.5 °	2294	1956 m/s
2	83.0 °	3442	2612 m/s.

EXPERIMENTAL SET-UP

The basic experimental set-up has been previously described [58-59]. Broadband pulsed ultrasonic waves in the frequency range 50kHz-1MHz were generated and detected by small piezoelectric

compressional transducers (Sonoquest, 2 mm in diameter) directly placed on a flat surface of a large solid block away from any edges to characterize the properties of surface waves. The dimensions of the solid block were very large compared to the wavelength to avoid interference of wave components reflected by the edges of the block in the time window under study. Experiments were conducted on different free blocks of ice, aluminum, and acrylic. In other experiments, the blocks were totally immersed in water to study solid/liquid interface waves. The waves obtained from the large blocks were used as reference to be compared with other waves generated and detected along the apex of an "infinite" solid wedge. The apex angle θ was 90° in models representing the quarter-space, and 20.75°± 0.25° in a thin wedge aluminum model. Ice, aluminum, and acrylic were chosen for the quarter-space models. The elastic properties of the modeling materials are listed in Table I.

EXPERIMENTAL RESULTS

I. NONDISPERSIVE EDGE FLEXURAL WAVE ALONG APEX OF SMALL-ANGLE SOLID WEDGE

Flexural waves in thin plates are well known to be highly dispersive (Section 3) . Flexural waves along the edge of a semi-infinite thin plate are also highly dispersive (Section 6.3). Dispersive flexural edge waves from a thin truncated aluminum wedge with an apex angle of 20.7° and a wedge thickness of 0.2 mm is shown in figure 9.2(a). It is difficult to physically achieve a real sharp edge. Truncation of the edge causes dispersion as was observed in figure 9.2. An ideal wedge has zero thickness at the tip and has no characteristic dimension. Figure 9.2 demonstrated the severe dispersion from an apex about $\lambda/20$ thick . Theoretical results on the truncated wedge were derived by Lagasse [84] and also by McKenna et al. [81] (no experimental results).

These wedge edge flexural waves were severely attenuated either by simply touching the wedge apex or by adding a vinyl adhesive tape along the wedge apex (Fig. 9.2(b)). As the tip of the truncated wedge was sharpened, the wedge flexural edge wave dispersion decreased. Figure 9.3(a) shows the waveshape of the received flexural edge waves from a sharpened wedge apex with a tip thickness of 5 μm ≈ one thousandth of a wavelength. Three nondispersive flexural edge modes resulted from the sharp wedge with the apex angle of 20.7° in agreement with Lagasse's prediction [74]. It is interesting to note how a minute amount at the tip of the wedge can affect the velocity of very low frequency components. These textbook quality experimental results on pulsed edge waves are available for the first time.

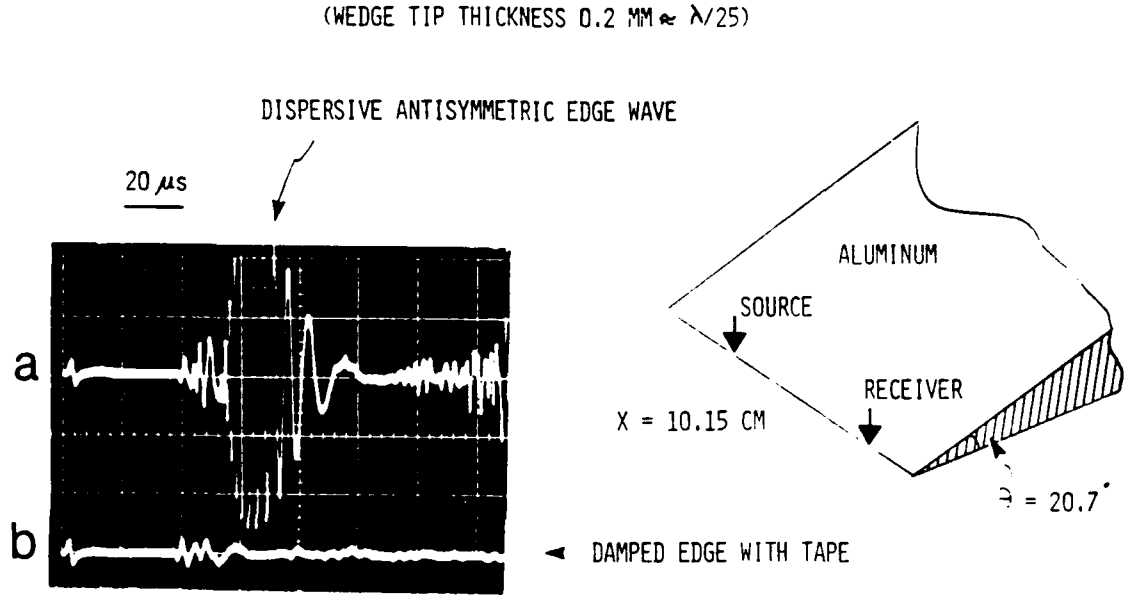

FIG. 9.2. Dispersive antisymmetric edge wave along truncated apex of aluminum wedge.

(WEDGE TIP THICKNESS $5\mu M \approx \lambda/1000$)

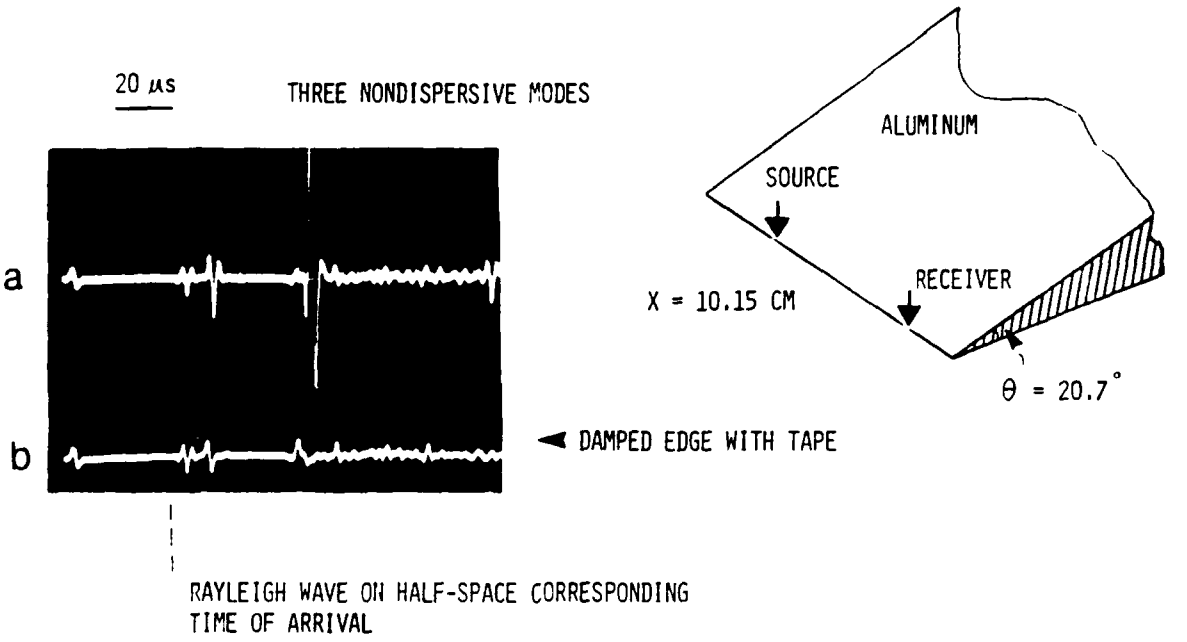

FIG. 9.3. Nondispersive antisymmetric edge waves along very sharp apex of aluminum wedge.

II. COMPARISON OF WAVES ALONG EDGE OF FREE AND IMMERSED SOLID QUARTER-SPACE (90° WEDGE)

WATER/ICE MODEL

The attenuation of the leaky Rayleigh wave at a lossless liquid/solid interface depends on its geometrical spreading and radiation to the liquid. At a water/steel interface, the water loading effect on the Rayleigh wave is small mainly due to the small density ratio of water to steel. In the water/ice case, the water loading effect is dramatic since the water has a greater density than the ice, and the ice shear wave velocity is only slightly greater than the water compressional wave velocity. As was described in Section 4, controversial issues exist regarding the leaky Rayleigh wave at a water/ice interface. Laboratory experimental results on fresh water ice revealed the existence of a leaky Rayleigh wave [6,22,23] . Figure 9.4(a), shows the leaky Rayleigh wave from a half-space water/ice model. The source-receiver range was 7.1 cm and the source was energized with a 4 μs pulse. The cylindrical geometrical spreading of the leaky Rayleigh wave and the severe water loading yield a small amplitude leaky Rayleigh wave at this range. Figure 9.4(b) shows a large edge leaky Rayleigh wave obtained when the source and receiver were located along the edge of an ice quarter-space in water. The range was fixed at 7.1 cm. The experiment was repeated several times using different blocks of ice. The edge leaky Rayleigh wave was very sensitive to the condition of the ice edge. The effect of a shallow saw cut on interrupting the edge leaky Rayleigh wave is demonstrated in figure 9.5. In this model, the range was 10.1 cm.

The amplitude of the Scholte wave from the half-space model was large, however, the edge Scholte wave amplitude was small. Near the ice edge, it was observed that a decrease in the Scholte wave signal was accompanied by an increase in the leaky Rayleigh wave signal. The edge wave had no geometrical spreading and dominated the received signal as the receiver was moved slightly away from the ice edge.

WATER/LIMESTONE MODEL

In this experiment, the elastic properties of a dry limestone block were first determined. The free Rayleigh wave velocity was C_R = 1970 m/s. By wetting the limestone block, (simply filling the pores with water), the Rayleigh wave increased to 1989 m/s. The limestone block was covered with a water half-space, and the leaky Rayleigh wave was recorded (FIG. 9.6(a)). The measured leaky Rayleigh wave velocity was 2103 m/s. The transducers were positioned

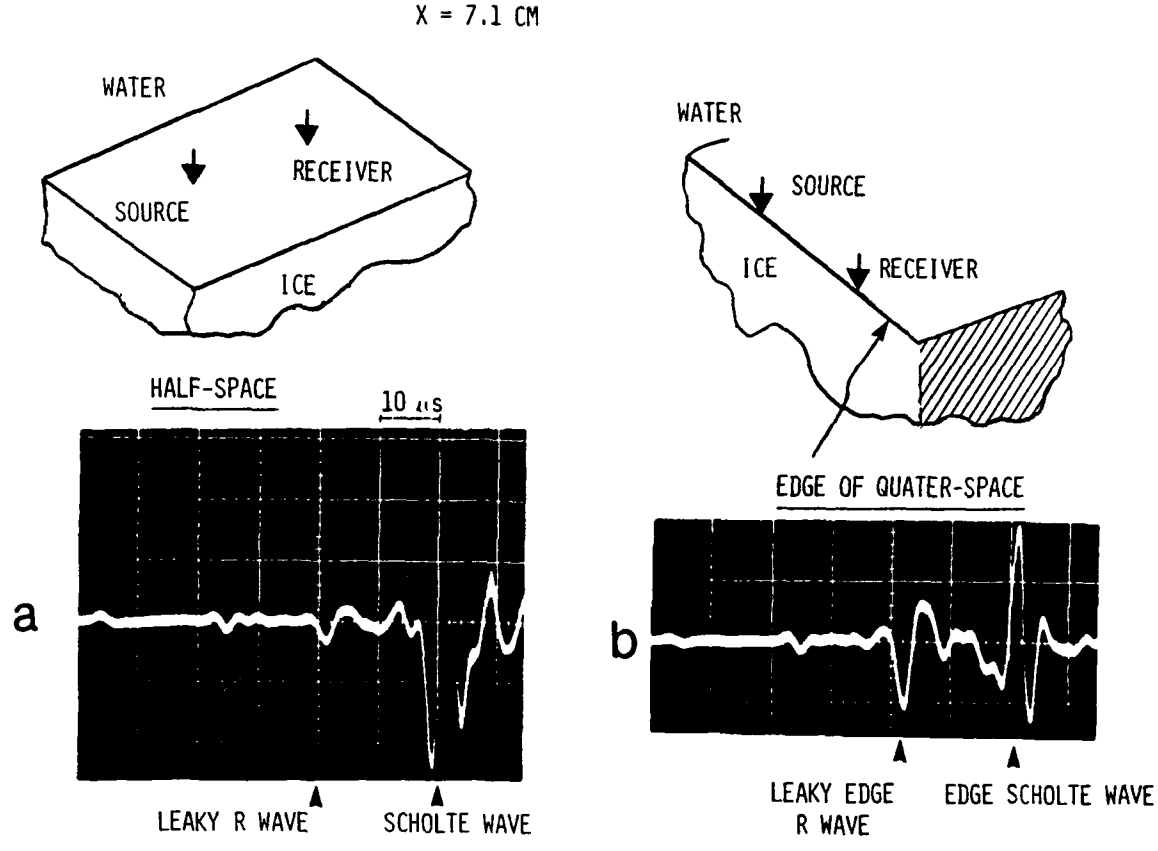

FIG. 9.4. Large amplitude edge leaky Rayleigh wave detected along edge of ice quarter-space immersed in water. A reference leaky Rayleigh wave from the ice/water half-space model (away from edges) is shown in the left trace. The edge leaky Rayleigh wave amplitude decays exponentially within one wavelength from the edge on both the horizontal and vertical surfaces. Its velocity is slightly slower than the leaky Rayleigh wave from the half-space.

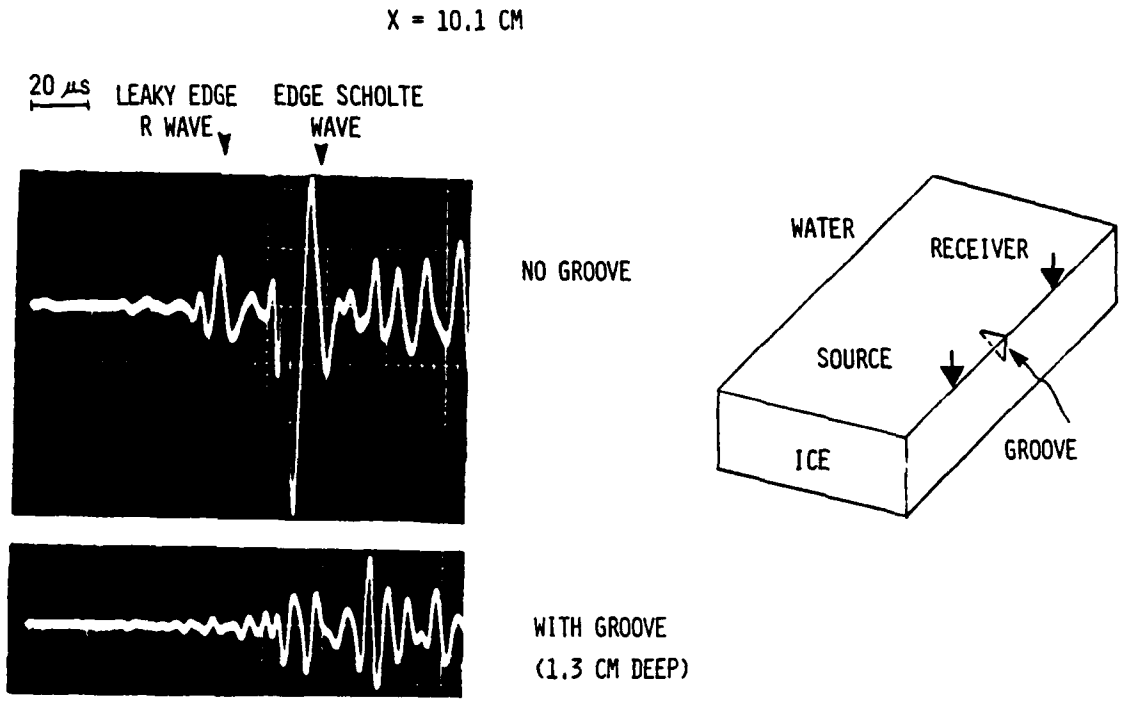

FIG. 9.5. Effect of groove on edge waves in ice/water model.

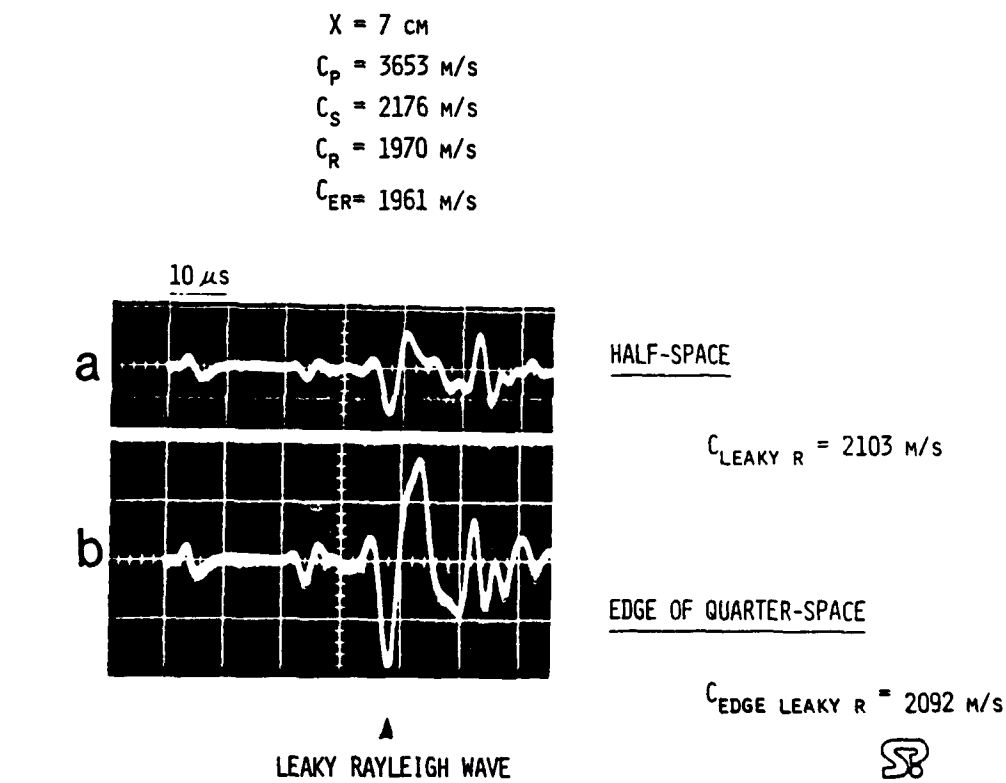

FIG. 9.6. Edge leaky Rayleigh wave propagating along apex of limestone 90 degree wedge in water.

along the edge of the block, and an edge leaky Rayleigh wave was obtained. (FIG. 9.6(b)). The edge leaky Rayleigh wave velocity was 2092 m/s. Notice the large amplitude of the edge leaky Rayleigh wave from the limestone block (FIG. 9.6(b) similar to the water/ice example of figure 9.4(b).

WATER/ALUMINUM MODEL

The experimental results shown in figure 9.7 compare the waveshapes and velocities of: a) the Rayleigh wave, b) the edge Rayleigh wave, c) the leaky Rayleigh wave, and d) the edge leaky Rayleigh wave from aluminum/water models. The source-receiver range was fixed at x = 7.25 cm.

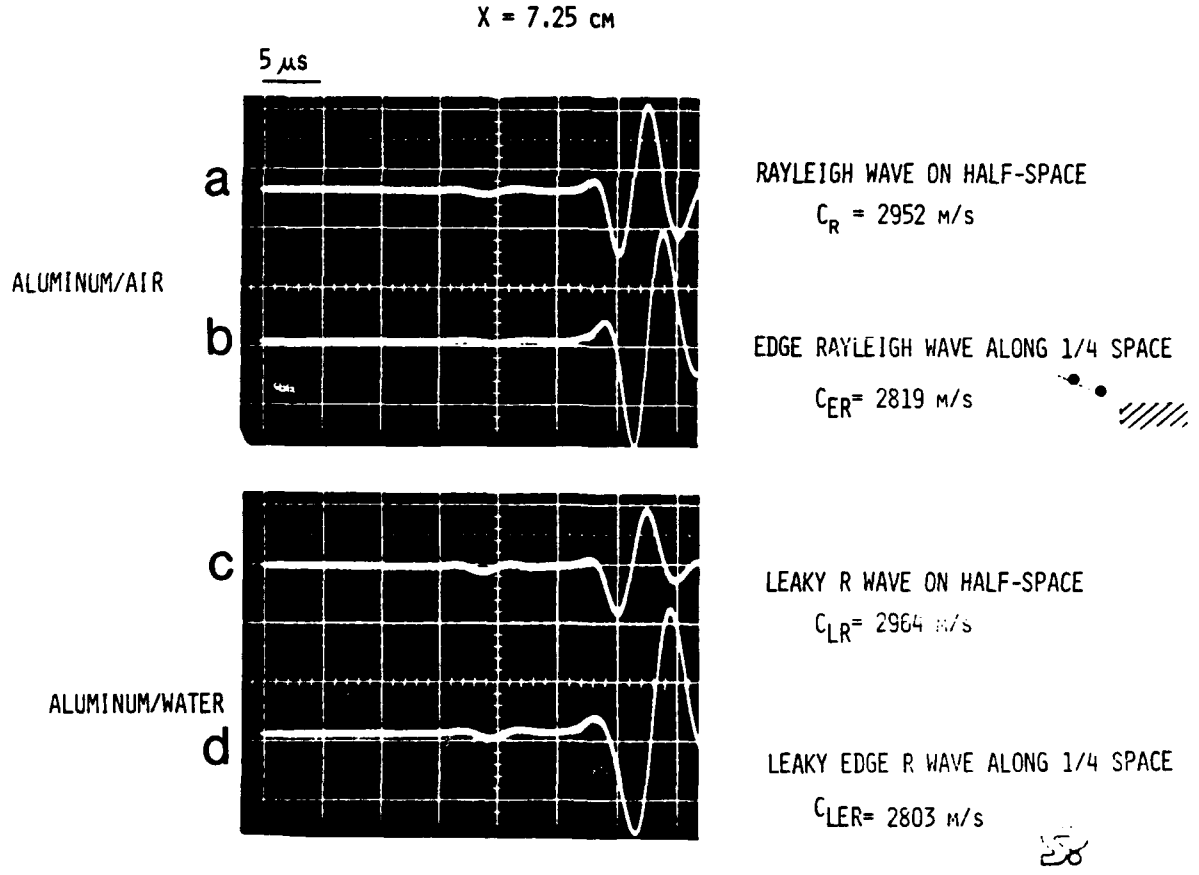

FIG. 9.7. Comparison of waveshape and velocity of Rayleigh wave, edge Rayleigh wave, leaky Rayleigh wave, and edge leaky Rayleigh wave from aluminum/air and aluminum/water models.

The edge Rayleigh wave has opposite polarity on the vertical and the horizontal surfaces. This is demonstrated with the aluminum block quarter-space (fig. 9.8). The attenuation of the edge Rayleigh wave with distance from the edge of the quarter-space along the solid surface is shown in figure 9.9. The amplitude of the edge Rayleigh wave drops exponentially from the edge.

The amplitude of the quarter-space edge Rayleigh wave is not only higher than the Rayleigh wave from the half-space, but it does not have geometrical spreading. The relative amplitudes of both waves are compared as function of source-receiver range (Fig. 9.10).

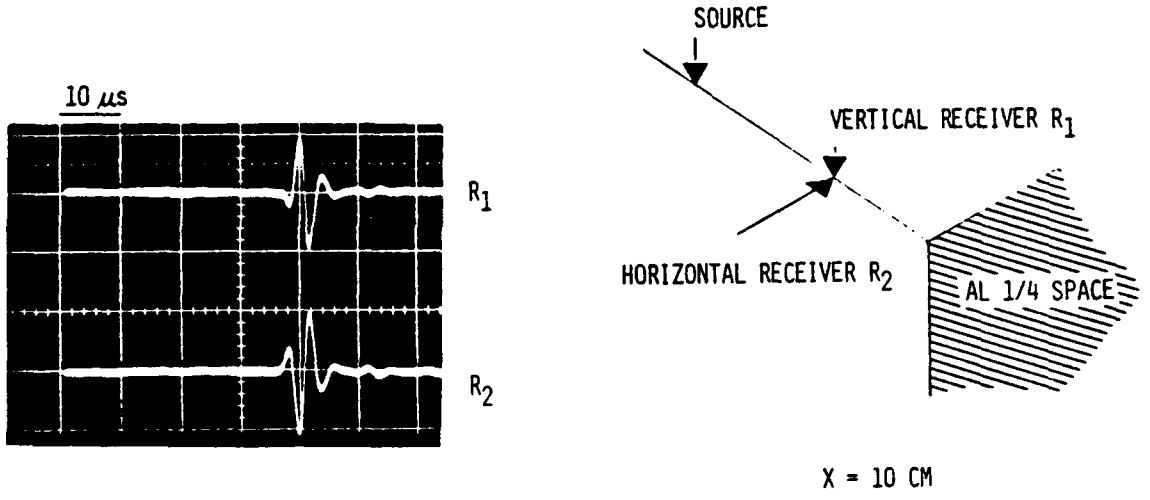

FIG.9.8. Opposite polarity of edge Rayleigh wave along apex of 90 degree wedge surfaces.

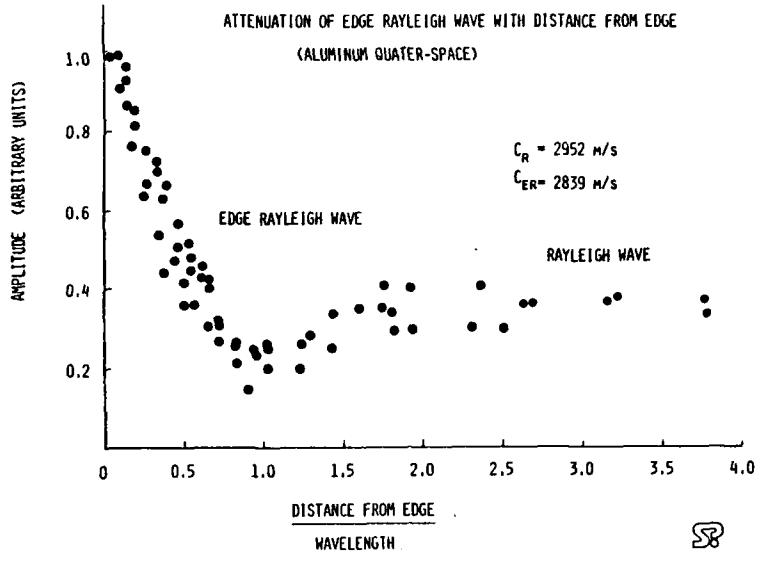

FIG. 9.9. Attenuation of edge Rayleigh wave with distance from edge of quarter-space.

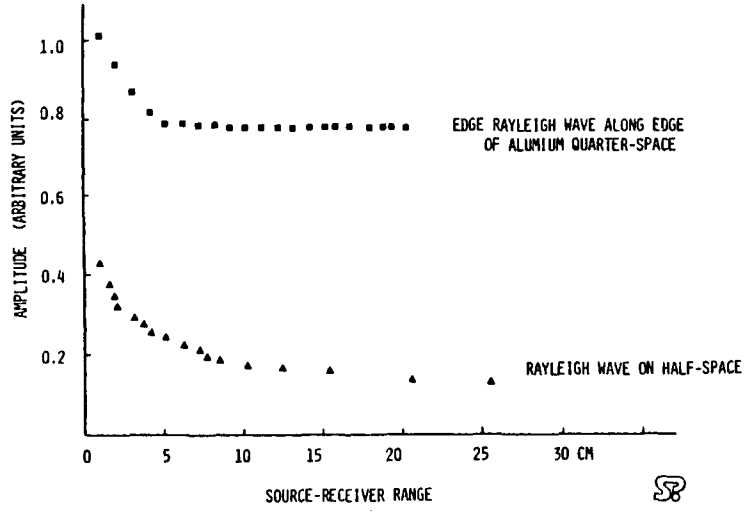

FIG. 9.10. Measured relative amplitudes of edge Rayleigh wave and Rayleigh wave as function of source-receiver range.

WATER/ACRYLIC MODEL

Results from an acrylic model are given in figure 9.11. The Scholte wave velocity was $C_{Scholte} = 1044$ m/s from the half-space acrylic model in contact with a water half-space. The edge Scholte wave was $C_{Edge\ Scholte} = 1033$ m/s.

Table 9.1 summarizes the measured velocities of the different types of waves from the different models.

CONCLUSIONS

In this section, the first experimental results on single-pulse edge waves propagating along the apex of a free solid wedge and along the apex of an immersed solid wedge are reported. A comparison was made between velocities and waveshapes of Rayleigh waves, edge Rayleigh waves, leaky Rayleigh waves, edge leaky Rayleigh waves, Scholte waves and edge Scholte waves. The 90° solid wedge and the small-angle wedge were investigated.

Quantitative results were presented on velocities of various edge waves from hard and soft wedges. Different wave velocities were measured from for the Rayleigh, edge Rayleigh, leaky Rayleigh, leaky Edge Rayleigh, Scholte, and edge Scholte waves. We have also demonstrated the nondispersive edge flexural wave from the small-angle solid wedge, and the dispersive effects of the truncated wedge.

The experimental results revealed the presence of a large edge leaky Rayleigh wave propagating along the edge of an immersed ice quarter-space (90° wedge) in water. Edge waves exist along cracks in floating ice plates and along frozen ridges and keels. Waves in the ice can also convert into edge waves. As an upper limit example, a frozen 50 m deep by 100 m wide ice ridge may support leaky Rayleigh waves at frequencies down to about 18 Hz. Thermal cracking noise as well as bumping noise can contribute to edge waves. In the Marginal ice zone edge waves should be seriously considered. Current ideal models of triangular keels do not include the effect of edge waves. It is important to be able to detect and characterize a source or an object situated in the water close to a keel or a plate edge. Edge waves would play a role in 3-D propagation effects in water waveguide with abrupt changes in solid boundary topography. At Ultra-low frequencies, underwater acoustic waves interact with edges of rock formation in ocean bottom. Interpretation of field data in the Arctic depends on understanding the radiation of edge waves and their contribution to ambient noise.

X = 6.4 CM

C_P = 2711 M/S

C_S = 1367 M/S

C_W = 1480 M/S

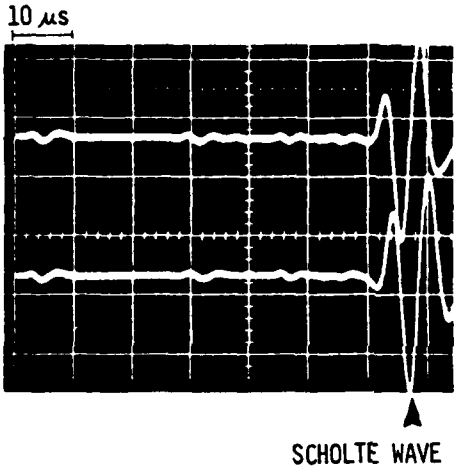

HALF-SPACE

$C_{SCHOLTE}$ = 1044 M/S

EDGE OF QUARTER-SPACE

$C_{EDGE\ SCHOLTE}$ = 1033 M/S

FIG. 9.11. Edge Scholte wave along apex of 90 degree Plexiglas wedge in water.

TABLE. 9.1. Experimental results comparing velocities of body, surface, interface, and edge waves.

	C_P	C_S	C_R	C_{ER}	C_{LR}	C_{ELR}	C_{SCH}	C_{ESCH}	ρ	C_{ER}/C_R	
ALUMINUM 6061	6328	3126	2952	2839	2964	2803			2.7	0.9617	
PLEXIGLASS	2711	1367	1283	1240			1044	1033	1.18	0.9665	
LIMESTONE	3653	2176	1970	1961	2103	2092				0.9954	
ICE * (FRESH)	3825	1952 **	1814	1808	1945		1245	1244		0.9966	***

* Commercial ice stored at -10°C.

** Shear wave velocity varies between 1892-1970 m/s depending on ice temperature and structure.

*** Bonding between ice crystals critical.

10. PULSED LEAKY RAYLEIGH WAVE COMPONENTS IN LIQUID LAYER OVER SOLID HALF-SPACE

Major seismo-acoustic wave phenomena occur when the source and receiver are within a wavelength from a solid boundary such as an ocean bottom. Supersonic seismo-acoustic waves radiate to the water and contribute the characteristics of low-frequency underwater acoustic waves. Ideal models predict total reflection of incident underwater acoustic waves when critical incident angles are exceeded. Realistic range dependent ocean boundaries such as variable-depth rough bottom with abrupt rock/sediment interfaces do not yield total reflection of waves incident beyond the critical angles. This contributes to low-frequency transmission losses not accounted for by the ideal range independent models. Leaky waves cannot be ignored for range-dependent underwater acoustic wave propagation.

At the interface of a liquid half-space in contact with a "hard" solid half-space, a leaky Rayleigh wave exists as was described in Section 4. The leaky Rayleigh wave being faster than the liquid compressional wave velocity, it radiates its energy to the liquid at the Rayleigh angle and decays with range. The leaky Rayleigh wave is represented by a complex pole from the characteristic equation (4.1). In addition to the leaky Rayleigh wave, a true interface wave exists known as the Scholte wave which is trapped along the interface and travels with a velocity slower than the liquid compressional wave velocity.

When the liquid half-space is replaced by a liquid layer, it is known that the lowest propagating mode in a liquid layer in contact with a hard solid half-space is dispersive (FIG. 10.1) and has its phase velocity approaches: a) the Scholte wave velocity at high kH (where k is the wavenumber and H is the liquid layer thickness), and b) the Rayleigh wave velocity at very low kH (see for example reference [89-91]). The coexistence of a leaky Rayleigh wave at large kh is not mentioned. In the geophysics field, the liquid-filled borehole problem is somewhat analogous and there seem to be unresolved issues on the co-existence of the leaky Rayleigh wave and its mathematical representation [15-17].

The classic book by Viktorov [32] presented the dispersion characteristics for the liquid layer over a solid half-space with the wrong sign which he corrected 10 years later [40]. Viktorov's corrected results shows that the second normal mode starts with the shear wave velocity and decreases to the Rayleigh wave velocity with increasing H and then continues to decrease towards the wave velocity in the liquid. The results of Tolstoy, Viktorov, and Phinney show that the velocity dispersion curve of the second mode has a small region with a phase velocity equal to the Rayleigh wave velocity. This however does not indicate the presence of a leaky Rayleigh wave

since the corresponding group velocity is much smaller than the Rayleigh wave velocity. The same argument applies to the findings of Paillet and White on the borehole [15] where they focused on the phase velocity and not the group velocity to demonstrate the existence of a leaky Rayleigh wave. Tsang and Rader [16] utilized a truncated ray expansion to demonstrate the existence of a leaky Rayleigh wave pole at high frequencies.

Our laboratory ultrasonic modeling investigations using broadband pulsed waves have clearly demonstrated the existence of multiple leaky Rayleigh wave components at short range in the liquid layer over solid bottom model in addition to the Scholte mode as described below. The findings are fundamental to low-frequency underwater acoustics and ambient noise where bottom interactions occur.

Preliminary ultrasonic experimental investigations were conducted to assess the potential role of low-frequency leaky Rayleigh waves associated with the ocean bottom. Underwater acoustic waves propagating in a "perfect waveguide" air/water/air were compared with waves in a water layer in contact with a hard solid half-space.

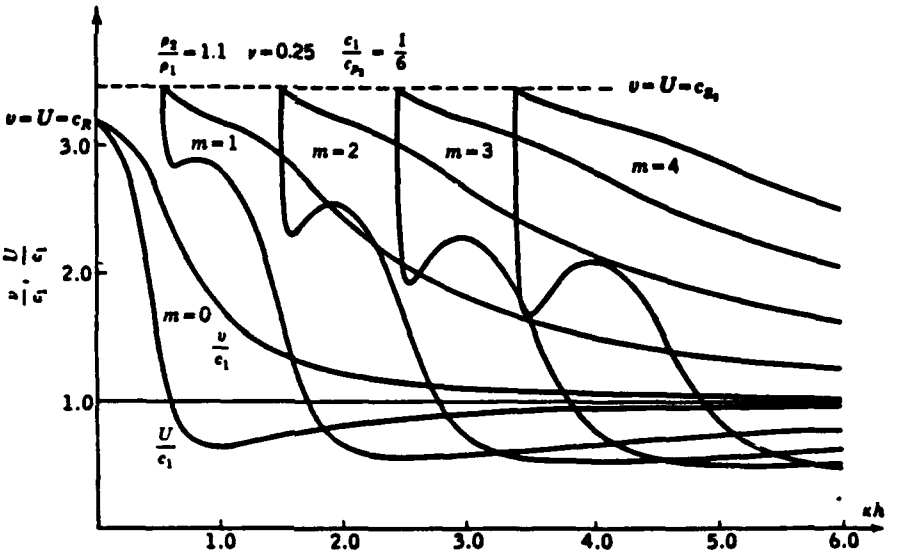

Fig. 4.33 Dispersion curves for a fluid layer overlying a semi-infinite elastic solid, for the first five modes.

FIG. 10.1. Dispersion curves of normal modes do not indicate the presence of a leaky Rayleigh wave component at high frequencies and close range. Above results copied from I. Tolstoy 1954 presented in "Ocean Acoustics" 1987 edition by Tolstoy and Clay, page 136.

The experimental setup was as follows: A large aluminum block was chosen to represent a hard solid half-space. A 0.09 mm thick plastic sheet was placed on the top surface of the aluminum block. The edges of the plastic sheet were taped to the aluminum surface allowing a thin air layer to be trapped between the plastic sheet and the block. The aluminum block was then immersed in water with a water layer of thickness H above it. Source and receiver transducers were located near the top surface of the water layer. The source-receiver range " x " was selected in each experiment. With the plastic sheet in place, "perfect waveguide" data were obtained and recorded from the air/water/air model. Without disturbing the set-up, the plastic sheet was then removed allowing the water to become in contact with the aluminum block. The data from the air/water/aluminum model were obtained, recorded, and compared to the corresponding "perfect waveguide" results. The procedure was repeated for different X and H (FIG. 10.2-10.5). The elastic properties of the aluminum block were C_p = 6328 m/s, C_s = 3126 m/s, and density of 2.7 kg/m^3. The water compressional velocity was C_w = 1480 m/s, and the measured leaky Rayleigh wave velocity C_{RL} = 2964 m/s. From Snell's law, the leaky Rayleigh wave angle θ_{RL} was equal to 29.95°.

Figures 10.2-10.5 are self-explanatory. In the model of figure 10.2, X was 9.5 cm and H = 5 cm. Underwater acoustic waves from the air/water/air model (Fig. 10.2(a)) were compared to the air/water/aluminum waves (Fig. 10.2(b)). The two main pulses 1 and 2 in Fig. 10.2(a) corresponded respectively to one bottom water/air reflection, and to bottom/top/bottom water/air reflections as shown. When the water layer was in contact with the aluminum block (Fig. 10.2(b)), major leaky Rayleigh wave components were generated in addition to the specularly reflected acoustic waves from the interface. Ray number 4 (Fig. 10.2(b)) was incident at the Rayleigh angle, traveled along a portion of the interface with the leaky Rayleigh wave velocity, and radiated into the water with the same angle. At the generating point, the radiated leaky Rayleigh wave 3 was superimposed on the specularly reflected water wave. Ray 3 traveled upward, was reflected by the water/air boundary, and interacted again with the aluminum regenerating a second leaky Rayleigh wave component having its own radiated field in the water. The geometry of figure 10.2 allowed near-overlapping of the specularly reflected acoustic wave with the leaky Rayleigh wave. The calculated times of arrival of rays 1, 2, 3, and 4 were 93.2 us, 149.6 us, 151.2 us, and 90.6 us , respectively. The phase of each component depended on the number of reflections from the air or aluminum interfaces causing constructive or destructive interference.

In figure 10.4, the water depth remained equal to 5 cm, and the range was increased to X = 17.8 cm to clearly separate the first acoustic bottom reflected wave (137.9 us) from the leaky Rayleigh wave (118.6 us). Notice that the leaky Rayleigh wave arrived before the acoustic wave.

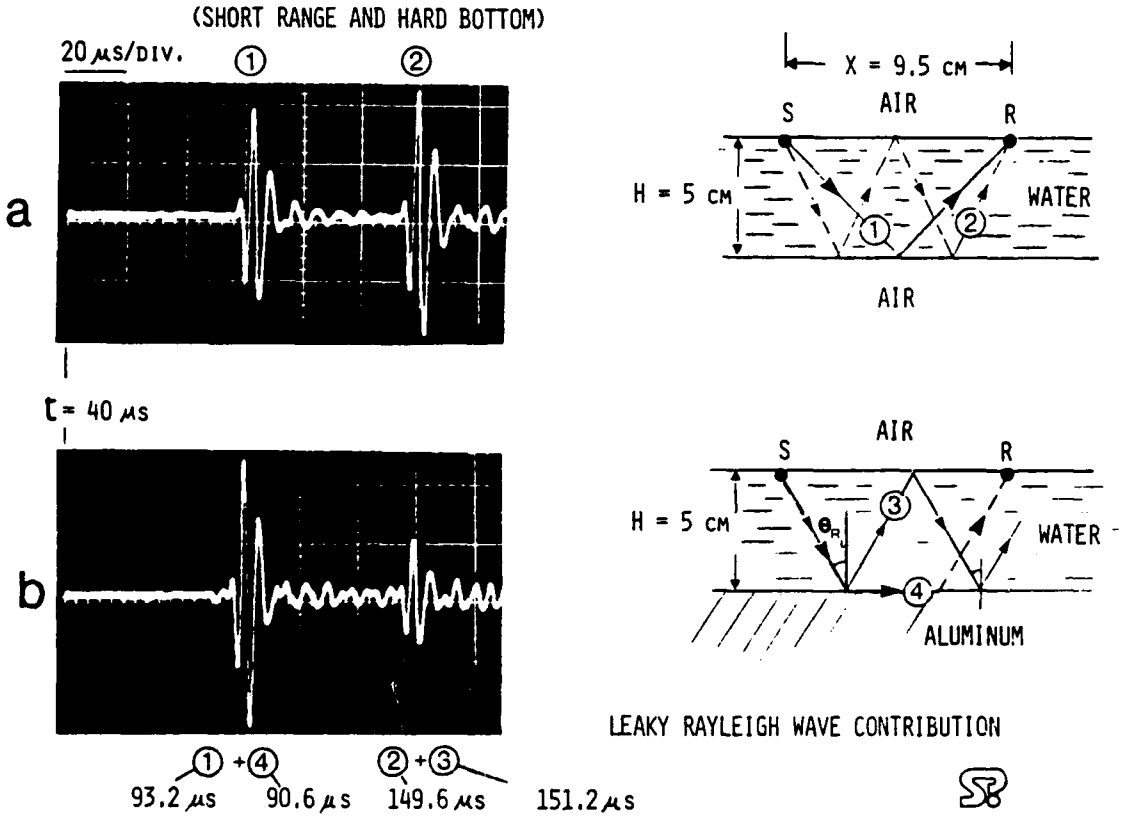

FIG. 10.2 Interference of leaky Rayleigh wave components with specularly reflected acoustic waves in water from a water layer over a "hard" bottom.

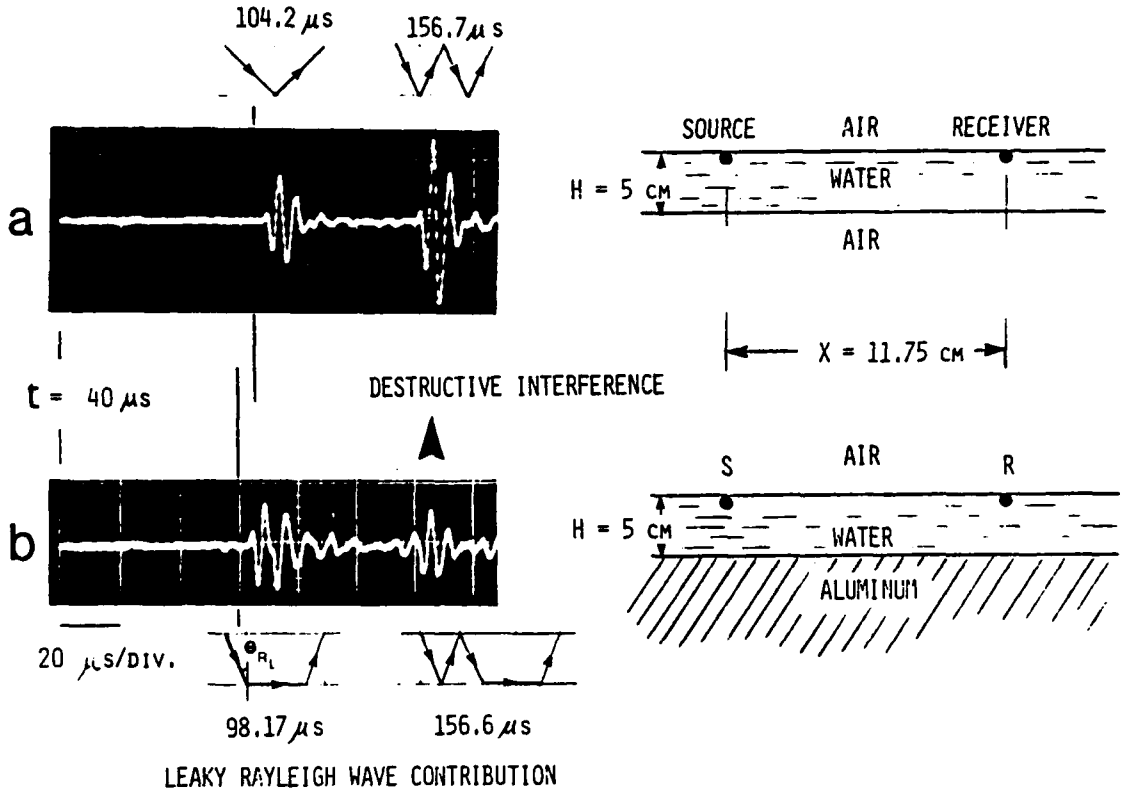

FIG. 10.3. Example showing creation of a second leaky Rayleigh wave component from multiple reflection of underwater acoustic wave originating from the leaky Rayleigh wave.

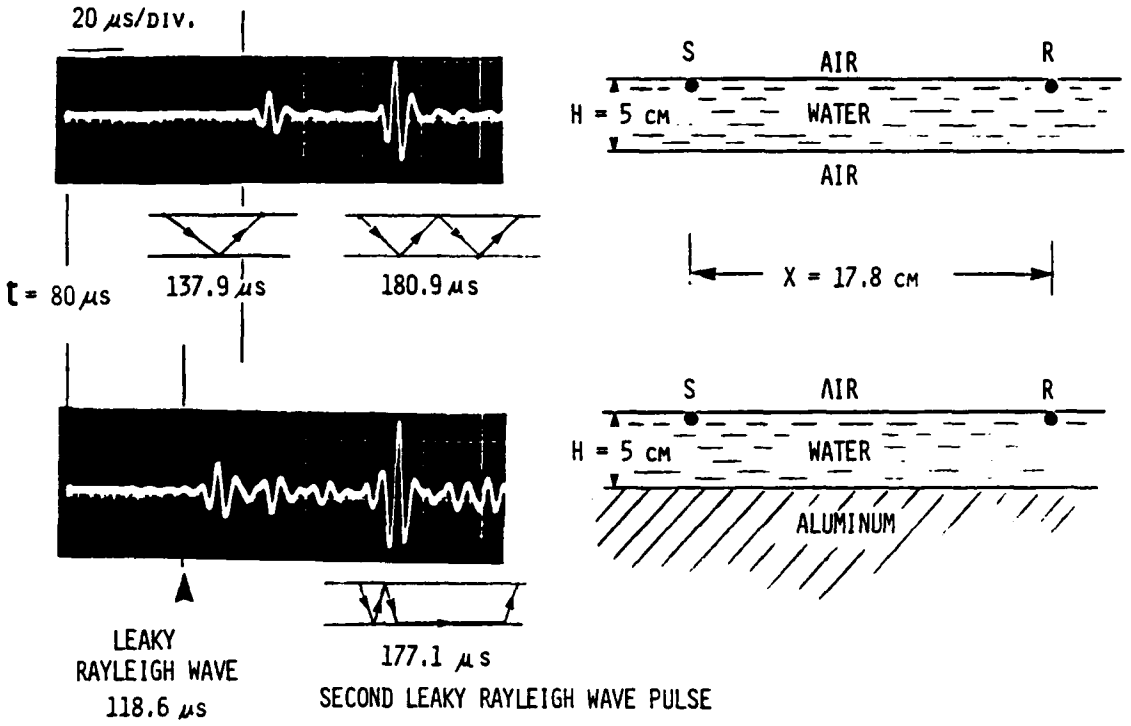

FIG. 10.4. Constructive interference of second leaky Rayleigh wave pulse with underwater acoustic wave as shown.

The waveshapes shown in figure 10.3 were obtained with X = 11.75 cm and H = 5cm. The leaky Rayleigh wave arrived at 98.17 us and the acoustic bottom reflection at 104.2 us. If one is not aware of the existence of the leaky Rayleigh wave, one may interpret the mixture of these two signals as an early arriving acoustic wave originating from a source at a closer range. The second generated leaky Rayleigh wave (156.6 us) destructively interfered with the acoustic wave (156.7 us) in this case.

A shallow-water example is presented in figure 10.5. The water depth was 1.5 cm and the range X = 17.8 cm. The acoustic waves in the "perfect waveguide" consisted of a series of pulses starting at t = X/C_w . The air/water/aluminum model had multiple low-frequency leaky Rayleigh wave components arriving at 77.6 us, 95.1 us, 112.7 us before the "perfect waveguide" acoustic waves. These leaky Rayleigh wave components may explain the early arrival of low-frequency waves observed by G. H. Brooke in 1977 in the Canadian Arctic as indicated by region "A" in figure 10.6 (water depth was 150 m, range X = 13 km, source depth 20 m, and receiver at the bottom). The shear wave velocity of the hard bottom was roughly close to that of aluminum. These leaky Rayleigh wave components described in this section are in addition to the lateral waves described by Brekhovskikh [33] and Brooke [93]. In an ideal lossless model, the energy released by the leaky Rayleigh wave into the solid is returned back to the interface and no apparent "leaky" mode exists. For a continuous wave steady state model, interference occurs between the reflected water waves and the leaky Rayleigh wave along the entire interface, and no leaky Rayleigh wave complex pole exists for the continuous wave case [92].

The author hypothesizes that for the pulsed wave case, a pulsed leaky Rayleigh wave is generated in the solid, travels as a packet with supersonic speed towards the receiver and arrives without the interference of the slow acoustic waves. The underwater acoustic waves did not have the time to travel to the top surface of the water and come back to interfere with the supersonic leaky Rayleigh wave packet. In this model one is not looking for a resonance condition satisfying both the normal modes and the horizontal leaky Rayleigh wave velocity at the interface. This fundamental point has not yet been fully verified mathematically for either the pulsed or bounded beam cases.

It is interesting to point out that the angles of the acoustic rays in the water depend on the source-receiver location, while the leaky Rayleigh wave angle is independent of the water depth and source-receiver location. Therefore in a water waveguide, frequencies of all modes matching the leaky Rayleigh wave angle would be greatly affected. One implication of this observation is

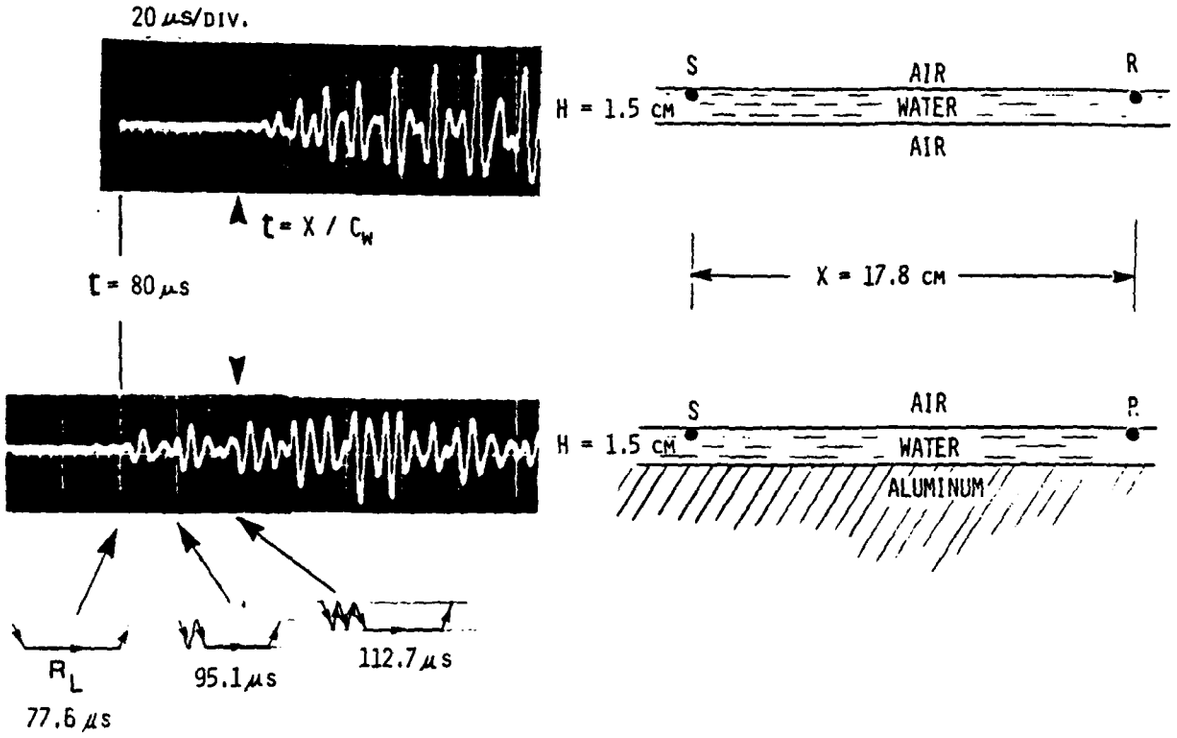

FIG. 10.5.Presence of water layer on solid bottom creates multiple pulsed supersonic leaky Rayleigh wave components as shown.

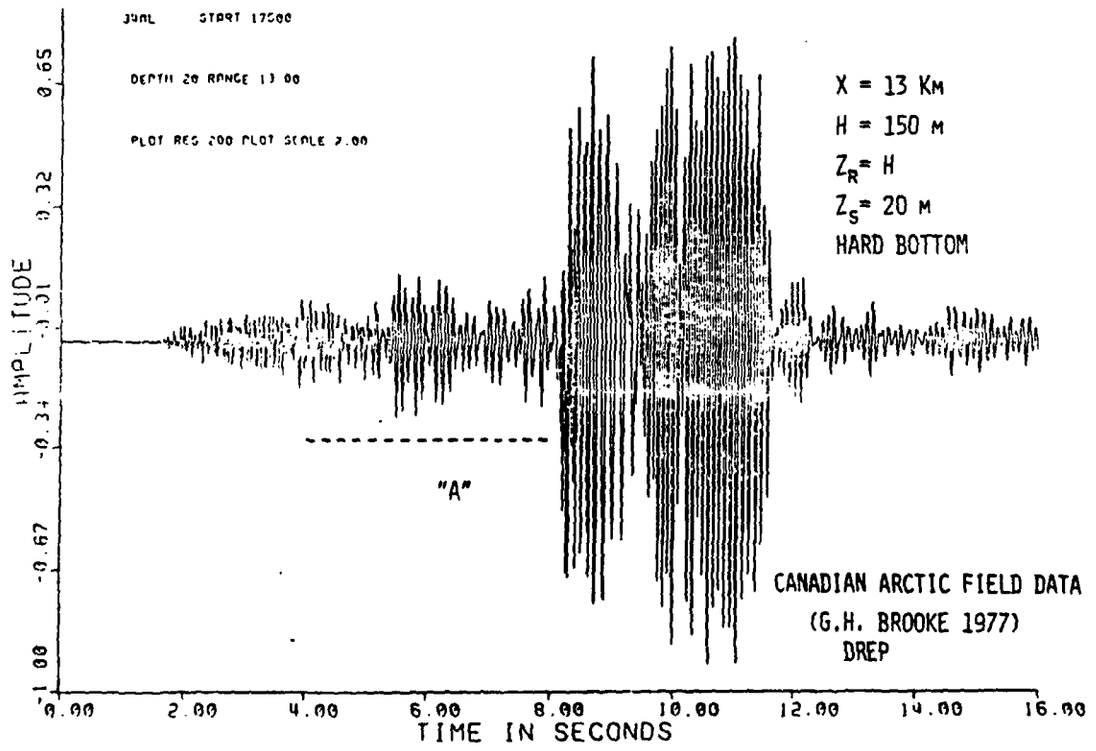

FIG.10.6. Multiple leaky Rayleigh wave components observed in the ultrasonic models may explain the supersonic waves marked by the dotted line "A" above. Canadian Arctic field data Brooke/DREP.

that low-frequency attenuation in the ocean does not depend only on absorption and scattering in the water, but also on the leaky Rayleigh wave components which depend on the bottom properties and the water depth.

The attenuation coefficient of the leaky Rayleigh wave differs from the attenuation coefficient of body waves. The presence of surface cracks, roughness, vertical step discontinuities, or thin sediment layers can drastically affect the losses stemming from the leaky Rayleigh wave.

An significant point regarding leaky Rayleigh waves is best described by examining the reflection coefficient for all angles of incidence for a lossless vs. a dissipative model (Fig. 10.7 copied from G. Mott [93]). Notice that at the critical Rayleigh angle, a strong null occurs in the continuous-wave reflection coefficient for the dissipative case, while no dip is present for the lossless case. Therefore if the attenuation coefficient for the leaky Rayleigh wave is not properly selected, the theoretical models would not predict the great losses attributed to the leaky Rayleigh wave.

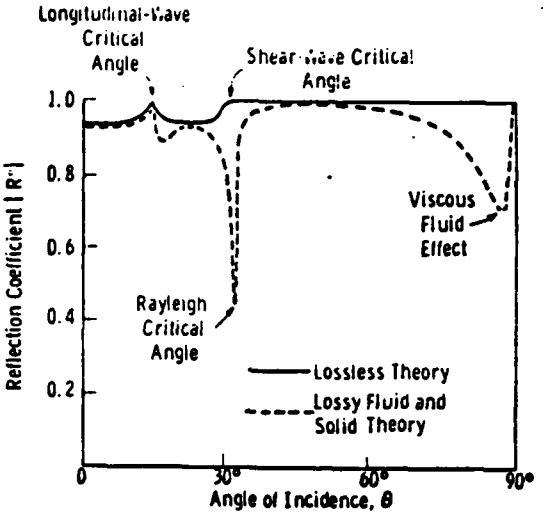

FIG. 1. Reflection coefficient for all angles of incidence for longitudinal waves at a water-stainless steel interface. The curves shown are calculated at 10 MHz for the lossless and dissipative cases.

FIG.10.7. The lossless model does not show the conversion into Rayleigh waves at the Rayleigh angle. The lossy model shows a sharp dip in the reflection coefficient at the Rayleigh angle. Results copied from G. Mott, J. Acoust. Soc. Am. 50(3), part 2, page 821, 1971.

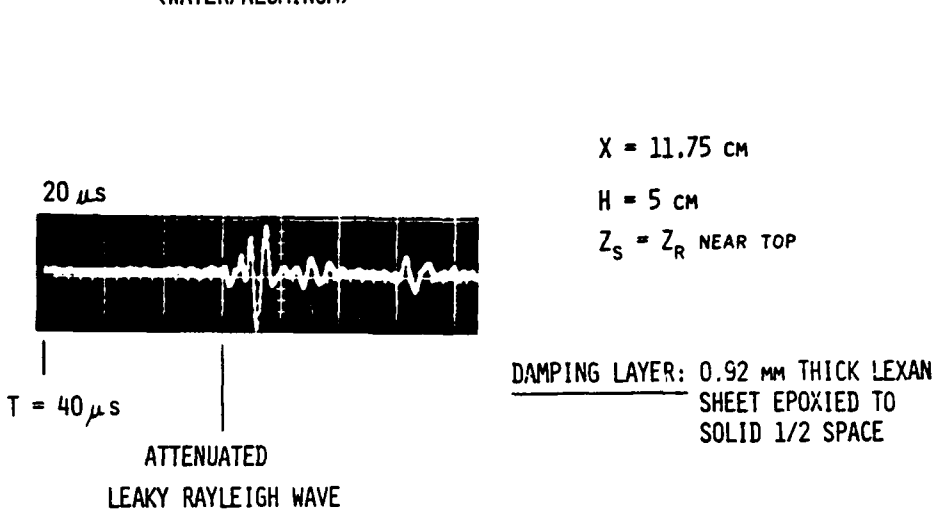

FIG. 10.8. Attenuation of leaky Rayleigh wave components with added thin damping layer on solid half-space bounding the water layer. Water/aluminum model. Compare this waveform with figure 10.3(b). The presence of thin sediment layer on hard ocean floor, small scale roughness, or abrupt surface discontinuities may be represented using an effective attenuation coefficient for the leaky Rayleigh wave that is higher than the attenuation coefficient of body waves. This leads to more accurate modeling of low-frequency transmission loss by conversion into leaky Rayleigh waves.

In figure 10.8, a thin damping layer was added to the surface of the aluminum block to increase the attenuation coefficient of the leaky Rayleigh wave relative to the body waves attenuation coefficients. The water depth and range were the same as in figure 10.3. By comparing trace "B" of figure 10.3 with figure 10.8, one notices the attenuation of the leaky Rayleigh wave arriving at 98.17 us. Therefore leaky Rayleigh wave components associated with a hard ocean bottom can contribute to low-frequency transmission losses if one properly accounts for the leaky Rayleigh wave " effective" high attenuation coefficient resulting from small scale surface roughness, near surface cracks, and sediment layer on the solid bottom. Conventional underwater acoustic models have used the low attenuation coefficient of body waves in the bottom. Propagation in a range dependent environment causes mode conversion and greater coupling to the ocean bottom therefore increasing the importance of leaky Rayleigh wave components.

11. SUMMARY

3-D range dependent Arctic acoustic problems involving liquid/solid boundaries with steep sloped discontinuities were investigated using ultrasonic modeling techniques. The models covered a wide range of relative liquid/solid elastic properties and geometries. The research identified factors affecting the interpretation of field data. Seismo-acoustic wave components contributing to ambient noise have been isolated.

This report presented the first published experimental results and implications on the following:

a) Existence of a leaky flexural wave in a floating ice plate and its effect on apparent group velocity maximum of flexural waves.
b) Existence of a leaky Rayleigh wave at a water/ice interface.
c) Low-frequency plate-edge leaky Rayleigh wave in floating ice plate (horizontal particle motion).
d) Nondispersive edge flexural wave broadband single pulse propagating along sharp apex of small-angle solid wedge.
e) Existence of edge Scholte and edge leaky Rayleigh waves propagating along apex of immersed solid wedge.
f) Conversion of underwater acoustic waves into plate waves by keel under floating plate.
g) low-frequency backscatter from keel-width resonance in floating plate.
h) Existence of water-coupled seismo-acoustic wave components in floating plate that do not exist in the immersed plate.
i) Generation of a precursor to the signature from an underwater acoustic target in the presence of a finite floating plate on the surface of the water waveguide.
j) Reduction of flexural wave velocity in floating plate by multiple shallow cracks.
k) Interference of forward scatter and backscatter from cracks in a waveguide.
l) Upward refraction in the water increases the importance of cracks and ridges.
m) Presence of cracks reduce backscattering from trailing edge of floating plate.
n) Substantial acoustic coupling between floating plates by edge leaky Rayleigh wave.
o) Trapped air pockets underneath the floating plate can decouple wave components from the underwater acoustic waves.
p) The existence of multiple pulsed leaky Rayleigh wave components in a water layer over a solid bottom.
q) Edge flexural wave in floating plate.

A temperature controlled experiment was conducted demonstrating the behavior of leaky Rayleigh wave showing the behavior of the leaky Rayleigh wave at a liquid/solid interface as the relative elastic parameters were controlled to cross the theoretical existence limit.

Two mechanisms have been identified on ice plate thickness determination discrepancies mentioned by Hunkins [4]. The first is due to the decrease in the ice flexural wave velocity by cracks and the second is caused by overestimating the shear wave velocity due to the interference of the leaky flexural wave with the onset of the Scholte flexural wave branch. Both effects result in predicting an ice plate thickness that is smaller than actual. Demonstrated interference of forward and backscattered underwater acoustic waves generated by multiple cracks in floating plate.

Demonstrated that scattering from the edges of a floating plate is dominated by the backscatter from the trailing edge of the plate. The backscatter consists of a seismo-acoustic wave component that is coupled to the water waves.

Demonstrated combined seismo-acoustic phenomena and waveguide effects modifying the spectrum of backscatter from trailing edge of floating plate. Results from cracks and ridges, indicate that the reflection coefficient is function of both angle of incidence and frequency.

The findings also provided possible answers to existing discrepancies between measured and predicted low-frequency backscatter and transmission loss by having identified: a) conversion of underwater acoustic waves into leaky flexural waves in the floating ice, b) backscatter from cracks in floating plate of near-grazing underwater acoustic wave components, c) conversion into plate waves by keel, d) backscatter from keel-width resonances, e) conversion into ocean bottom leaky Rayleigh wave components, and f) conversion into guided waves along ice keels and floe edges.

12. CONCLUSIONS

A collection of ultrasonic modeling findings and experimental techniques have been presented in this report pioneering in a broad range of hidden low-frequency liquid-solid wave phenomena generally beyond the state-of-the-art of theoretical and numerical analysis. The studies have successfully isolated and characterized seismo-acoustic wave phenomena affecting low-frequency underwater acoustic wave transmission loss prediction and ambient noise characteristics. The results provided physical insight and advanced our fundamental understanding of complex Arctic acoustic wave phenomena on leaky, trapped, and coupled modes. The efforts focused on pulsed waves interaction with 3-D range dependent liquid-solid boundaries having steep-sloped discontinuities with dimensions comparable to the wavelength under severe fluid loading conditions. The new findings were reported at a series of meetings of the Acoustical Society of America between 1986 and 1989 and have influenced the course of Arctic theoretical modeling and field experiments. Generic results have been obtained of potential importance to Arctic acoustics, seismology, nondestructive testing, geophysics, microwave surface acoustic wave devices, acoustic microscopy, and noise control of fluid-loaded structures. The ultrasonic modeling studies revealed how little is known about Arctic acoustics. Future efforts will focus on quantifying selected phenomena. It is evident that field experiments, theoretical and numerical methods, and laboratory studies complement each other and are all needed to handle realistic naval operations underwater acoustic problems. The results were presented for the exchange and stimulation of ideas.

12. REFERENCES

1. D. L. Anderson, "Use of long-period surface waves for determination of elastic and petrological properties of ice masses," Chapter 6 figure 1, page 65 of " Ice and Snow / Properties, Processes, and Applications," W. D. Kingery, editor, The MIT Press, Cambridge, MA (1963).

2. D. L. Anderson, "The mathematical theory of elastic wave propagation in floating ice sheets. (Unpublished) (1961).

3. P. J. Stein, "Acoustic Monopole in a Floating Ice Plate," Doctoral Thesis, Dept. of Ocean Eng., MIT, Cambridge, MA and Woods Hole Oceanographic Inst., Woods Hole, MA , page 104, Fig. 2-24, (1986).

4. K. Hunkins, "Seismic Studies of Sea Ice," Journal of Geophysical Research 65(10), 3459-3472 (1960).

5. W. M. Ewing, W. S. Jardetzky, and F. Press, "Elastic Waves in Layered Media," page 298, Fig. 6-7, McGraw-Hill Book Co., New York, 1957.

6. J. R. Chamuel, "On the controversial leaky Rayleigh wave at a water/ice interface," J. Acoust. Soc. Am. 80(S1), paper Y8, S54 (1986).

7. A. J. Langley, "Acoustic emission from the Arctic ice sheet," J. Acoust. Soc. Am. 85(2), 692-701 (1989).

8. J. H. M. T. van der Hijden, "Quantitative analysis of the pseudo-Rayleigh phenomenon," J. Acoust. Soc. Am. 75(4), 1041-1047 (1984).

9. N. G. Brower, D. E. Himberger, W. G. Mayer, "Restrictions on the Existence of leaky Rayleigh waves," IEEE Trans. Sonics and Ultrasonics, SU 26, NO.4, 306-308 (1979).

10. D. F. Gordon, Naval Ocean Systems Center Technical Report No. 1099, 1 April 1986.

11. R. H. Mellen, "Early history of Arctic research," in Proceedings of the 12th International Congress on Acoustics, Toronto July 1986, Vl. III, paper H2-1.

12. F. DiNapoli and R. H. Mellen, "Low-frequency attenuation in the Arctic Ocean," in Ocean Seismo-Acoustics low-frequency underwater acoustics, edited by T. Akal and J. M. Berkson, 387-395, Plenum Press, New York (1986).

13. W. A. Kuperman and H. Schmidt, "Rough surface elastic wave scattering in a horizontally stratified ocean," J. Acoust. Soc. Am. 79, 1767-1777 (1986).

14.E. Livingston and O. Diachok, "Estimation of average under-ice reflection amplitudes and phases using matched-field processing," J. Acoust. Soc. Am. 86(5),1909-1919 (1989).

15.F. L. Paillet and J. E. White, "Acoustic modes of propagation in the borehole and their relationship to rock properties," Figure 2, Geophysics 47(8), 1215-1228 (1982).

16.L. Tsang and D. Rader, "Numerical evaluation of the transient acoustic waveform due to a point source in a fluid-filled borehole," Geophysics 44(10), 1706-1720 (1979).

17.C. H. Cheng and M. N. Toksoz, "Elastic wave propagation in a fluid-filled borehole and synthetic acoustic logs," Geophysics 46, 1042-1053 (1981).

18.J. R. Chamuel and G. H. Brooke, "Low-frequency transmissiom losses and effective flexural rigidity of cracked ice cover," J. Acoust. Soc. Am. S1 79, S57, paper Z14 (1986).

19.J. R. Chamuel and G. H. Brooke, "Arctic low-frequency propagation loss from shallow cracks in ice plates," J. Acoust. Soc. Am. 80(S1), S115 (A) (1986).

20.J. R. Chamuel and G. H. Brooke, "New findings on scattering from floating with lateral heterogeneities," 83(S1), S47 (1988).

21.J. R. Chamuel, G. H. Brooke, "Relative scattering from dry cracks, ice ridges, and leads," J. Acoust. Soc. Am. 82(S1), S31-2(1987).

22.J. R. Chamuel, "Low-frequency underwater acoustic waves from ice plate-edge leaky Rayleigh wave," J. Acoust. Soc. Am. 81(S1), S10 (1987).

23.J. R. Chamuel and G. H. Brooke, "Propagation of Rayleigh and Scholte Waves Along Edge of Quarter-Space," J. Acoust. Soc. Am. Suppl. 1, vol. 85, paper JJ7, S88 (1989).

24.R. Obrochta, editor " Arctic Acoustics Workshop Proceedings, at MIT 14-15 February 1989," Office of Naval Research , Report No. OCNR 112589-19, pp. 10-26, "Fundamental Arctic Acoustics Ultrasonic Modeling Studies," by J.R. Chamuel, June 1989.

25.J. R. Chamuel and G. H. Brooke, "Shallow-water acoustic studies using an air-suspended water waveguide model," J. Acoust. Soc. Am. 84(5), 1777-1786 (1988).

26.J. R. Chamuel and G. H. Brooke, "Nearfield scattered acoustic waves in shallow-water waveguides with boundary topography," J. Acoust. Soc. Am. S1, 78, S58 (1985).

27.G. Kurtze and R. H. Bolt, "On the interaction between plate bending waves and their radiation load," Acustica 9, 238-243 (1959).

28.H. Schmidt, "Modeling of pulse propagation in layered media using a new Fast-Field program, in "Hybrid Formulation of Wave Propagation and Scattering," edited by L. B. Felsen, NATO ASI Series, Nijhoff, Dordecht (1984).

29.J. W. S. Rayleigh, "On waves propagated along the plane surface of an elastic solid," Proc. London Math. Soc. 17, 4-11 (1887).

30.W. L. Roever and T. F. Vining, "Propagation of elastic wave motion from an impulsive source along a fluid/solid interface, Part I: Experimental pressure response," Phil. Trans. Roy. Soc. London A 251, 456-465 (1959).

31.E. Strick, "Propagation of elastic wave motion from an impulse source along a fluid/solid interface, Part II: Theoretical and pressure response, and Part III: The pseudo-Rayleigh wave," Phil. Trans. Roy. Soc. London A 251, 465-523 (1959).

32.I. A. Viktorov, Rayleigh and Lamb Waves Physical Theory and Applications, Plenum Press, New York, 1967.

33.L. M. Brekhovskikh, Waves in Layered Media , Academic Press, New York, 1960.

34.R. A. Phinney, "Propagation of leaking interface waves," Bull. Seism. Soc. Am. 51(4), 527-555 (1961).

35.J. R. Chamuel, "Experimental observations on liquid/solid interface waves," J. Acoust. Soc. Am. 72,S1, S99, AAA4 (1982).

36.T. J. Plona, M. Behravesh, and W. G. Mayer, "Rayleigh and Lamb waves at liquid-solid boundaries," Ultrasonics, 171-174 (1975).

37.D. E. Chimenti, A. H. Nayfeh, and D. L. Butler, "Leaky Rayleigh wave on a layered halfspace," J. Appl. Phys. 53(1), 170-176 (1982).

38.M. F. M. Osborne and S. D. Hart, "Transmission, reflection and guiding of an exponential pulse by a steel plate in water: I," J. Acoust. Soc. Am. 17, 1-18 (1945).

39.V. M. Papadopoulos, "A line source on an interface between a fluid and an elastic solid," Proc. Royal Society London A 257, 515-533 (1960).

40.I. A. Viktorov, "Calculations of the phase velocities of surface waves on the boundary of a solid half-space with a liquid layer," Soviet Physics Acoustics 23(6), 541-542 (1977).

41.H. L. Bertoni and T. Tamir, "Unified theory of Rayleigh-angle phenomena for acoustic beams at liquid-solid interfaces," J. Appl. Phys. 2, 157-172 (1973).

42.O. Diachock and W. G. Mayer, "Conical Reflection of ultrasound from a liquid-solid interface," J. Acoust. Soc. Am. 47(1), 155-157 (1970).

43.M. de Billy, L. Adler, G. Quentin, "Parameters affecting backscattered ultrasonic leaky-Rayleigh waves from liquid-solid interfaces," J. Acoust. Soc. Am. 72(3), 1018-1020 (1982).

44.F. Press and M. Ewing, "Propagation of elastic waves in a floating ice sheet," Transactions American Geophys. Union 32(5), 673-678 (1951).

45.H. Lamb, "On the propagation of tremors over the surface of an elastic solid," Phil. Trans. Roy. Soc. (London) A203, 1-42 (1904).

46.W. D. Kingery and R. L. Coble, "Cracks in sea-ice and their effect on operations," in Ice and Snow edited by W. D. Kingery, The M.I.T. Press, 322-334 (1962).

47.A. Assur, "Breakup of pack-ice floes," in Ice and Snow edited by W. D. Kingery, The M.I. T. Press 335-347 (1962).

48.J. M. Berkson, C. S. Clay and T. K. Kan, "Mapping of the underside of Arctic sea-ice by scattered sound," J. Acoust. Soc. Am. 53, 777-781 (1973).

49.F. Press and M. Ewing, "Propagation of elastic waves in a floating ice sheet," Transactions, American Geophysical Union 32(5), 673-678 (1951).

50.I. Tolstoy, "Effect of roughness on subsonic flexural waves in a thin plate overlying a compressible fluid," J. Acoust. Soc. Am. 79(3), 666-672 (1986).

51.L. Cremer, "Calculation of sound propagation in structure," Acustica 3(5), 317-335 (1953).

52.G. H. Brooke, "Time series plots for selected field seismic runs, Defence Research Establishment Pacific, Letter to J. R. Chamuel 16 May 1986.

53.D. F. McCammon and S. T. McDaniel, "The influence of the physical properties of ice on reflectivity," J. Acoust. Soc. Am. 77(2), 499-507 (1985).

54.F. Press and M. Ewing, "Theory of air-coupled flexural waves," Journal of Applied Physics 22, 892-899 (1951).

55.A. R. Milne, "Thermal tension cracking in sea-ice: A source of underice noise," J. Geophys. Res. 77(12), 2177-2192 (1972).

56.R. J. Evans, "Thermal cracks in floating ice sheets," Journal of Geophysical Res. 76(3), 694-703 (1971).

57.A. P. Crary, "Seismic studies on Fletcher's Ice Island,T-3," Trans. Am. Geophys. Union, 35(2), 293-300 (1954).

58.J. R. Chamuel and G. H. Brooke, "Transient Scholte wave transmission along rough liquid-solid interfaces," J. Acoust. Soc. Am. 83(4), 1336-1344 (1988).

59.J. R. Chamuel and G. H. Brooke, "Transient Rayleigh wave transmission along periodic and random grooved surfaces," J. Acoust. Soc. Am. 84(4), 1363-1372 (1988).

60.A. C. Kibblewhite and L. D. Hampton, "A review of deep ocean sound attenuation data at very low frequencies," J. Acoust. Soc. Am. 67, 147-157 (1980).

61.R. R. Greene and A. P. Stokes, "A model of acoustic backscatter from Arctic sea-ice," J. Acoust. Soc. Am. 78, 1699-1701 (1985).

62.T. C. Yang and C. W. Votaw, "Underice reflectivities at frequencies below 1 kHz," J. Acoust. Soc. Am. 70(3), 841-851 (1981).

63.Y. K. Konenkov, "A Rayleigh-type flexural wave," Soviet Physics Acoust. 6,122 (1960).

64.R. N. Thurston, "Flexural acoustic waves along the edge of a plate," IEEE Trans. Sonics Ultrasonics SU-21(4), 296-297 (1974).

65.D. P. Kouzov and V. D. Luk'yanov, "Waves propagating along edges of plates," Sov. Physics Acoustics 18(4), 456-459 (1973).

66.D. G. Gazis and R. D. Mindlin, "Extensional vibrations and waves in a circular disk and semi-infinite plate," J. Appl. Phys. Mech. 27, 541-547 (1960).

67.P. J. Torvik, "Reflection of wave trains in semi-infinite plates," J. Acoust. Soc. Am. 41, 346-353 (1967).

68.B. A. Auld, and E. M. Tsao, "A variational analysis of edge resonance in semi-infinite plate," IEEE Transactions on Sonics and Ultrasonics, SU-24(5), 317-326 (1977).

69.P. Diodati and G. Tassi, "Lamb wave reflection at plate edges," Appl. Phys. Lett 47(6), 573-575 (1985).

70.S. Y. Zhang, J. Z. Shen, and C. F. Ying, "The reflection of the Lamb wave by a free plate edge: Visualization and theory," Materials Evaluation 46, 638-641 (1988).

71.H. Medwin, M. J. Browne, K. R. Johnson, and P. L. Denny, "Low-frequency backscatter from Arctic leads," J. Acoust. Soc. Am. 83(5), 1794-1803 (1988).

72.M. Pierucci and T. S. Graham, "A study of bending waves in fluid-loaded thick plates," J. Acoust. Soc. Am. 65(5), 1190-1197 (1979).

73.J. R. Fricke, R. A. Stephen, and A. B. Baggeroer, "Numerical modeling of the scattered acoustic field from elastic ice," J. Acoust. Soc. Am. Suppl. 1, 83, S37 (1988). Also in the ONR "Arctic Acoustic Workshop Proceedings, 14-15 February 1989, held at MIT, 106-118, edited by R. Obrochta.

74.P. E. Lagasse, "Analysis of a Dispersionfree Guide for Elastic Waves," Electronics Letters, 8(15), 372-373 (1972).

75.P. E. Lagasse, I. M. Mason, and E. A. Ash, "Acoustic Surface Waveguides - Analysis and Assessment," IEEE Trans. on Microwave Theory and Tech., MTT-21, No. 4, 225-236 (1973).

76.A. A. Maradudin, R. F. Wallis, D. L. Mills, and R. L. Ballard, "Vibrational Edge Modes in Finite Crystals," Physical Review B, 6(4), 1106-1111 (1972).

77.E. A. Ash, R. M. De La Rue,and R. F. Humphryes, "Microsound Surface Waveguides," IEEE Trans. Microwave Theory and Tech., MTT-17, No.11, 882-892 (1969).

78.N. P. Bestuzheva and V. N. Durova, "Propagation of Edge Waves in Elastic Media," Sov. Phys. Acoust. 27(4), 272-274 (1981).

79.V. V. Bozhenko, K. M. Ivanov-Shits, M. I. Sluch, and I. Yu. Solodov, "Experimental Study of Wedge Acoustic Waves," Sov. Phys. Acoust. 31(2), 151-152 (1985).

80.W. Pajewski, M. Szalewski and P. Kielczynski, "Ondes Acoustiques sur L'Arête d'un Solide," Revue Phys. Appl. 22, 113-118 (1987).

81.J. McKenna, Gary D. Boyd, and R. N. Thurston, "Plate Theory Solution for Guided Flexural Acoustic Waves Along the Tip of a Wedge," IEEE Trans. Sonics and Ultrasonics, SU-21(3), 178-186 (1974).

82.S. Datta and B. J. Hunsinger, "Analysis of Line Acoustical Waves in General Piezoelectric Crystals," Physical Review B, 16(10), 4224-4229 (1977).

83.V. S. Bondarenko and V. F. Dubovitskii, "Acoustic Edge Waves in Isotropic Solids," Sov. Phys. Acoust. 22(2), 159-160 (1976).

84.P. E. Lagasse, M. Cabus, and M. Verplanken, "The Influence of Truncation on Dispersion of Wedge Guides," Proc. IEEE Ultrasonic Symp. 121-124 (1974).

85.S. L. Moss, A. A. Maradudin, and S. L. Cunningham, "Vibrational Edge Modes for Wedges with Arbitrary Interior Angles," Physical Review B, 8(6), 2999-3008 (1973).

86.T. M. Sharon, A. A. Maradudin, S. L. Cunningham, "Vibrational Edge Modes for Small-Angle Wedges," Physical Review B, 8(12), 6024-6026 (1973).

87.H. F. Tiersten and D. Rubin, "On the Fundamental Antisymmetric Mode of the

Wedge Guide," Proc. IEEE Ultrasonics Symp., 117-120 (1974).

88.M. A. Biot, "The interaction of Rayleigh and Stoneley waves in the ocean bottom," Bull. Seism. Soc. Am. 42, 81-93 (1952).

89.I. Tolstoy, "Dispersive properties of a fluid layer overlying a semi-infinite elastic solid," Bull. Seismological Soc. Am. 44, 493-512 (1954).

90.I. A. Tolstoy, and C. S. Clay, "Ocean Acoustics / Theory and Experiment in Underwater Sound, 1987 edition, Fig. 4.33, page 136, American Institute of Physics, New York, 1987.

91.R. A. Phinney, "Leaking modes in the crustal waveguide Part 1. The oceanic PL Wave," J. Geophys. Res. 66(5), 1445-1469 (1961).

92.G. H. Brooke/DREP private communication, March 1990.

93.G. H. Brooke, D. J. Thomson, and R. F. MacKinnon, "Some characteristics of virtual modes in shallow water with high speed bottom," in Ocean Seismo-Acoustics low-frequency acoustics, edited by T. Akal and J. M. Berkson, NATO Conference Series IV:16, 233-242 (1986).

94.G. Mott, "Reflection and refraction coefficients at a fluid-solid interface," J. Acoust. Soc. Am. 50(3), 819-829 (1971).

95.T. J. Plona, M. Behravesh, aand W. G. Mayer, "Rayleigh and Lamb waves at liquid-solid boundaries," Ultrasonics 171-174 (1975).

96.R. D. Woods, "Screening of surface waves in soils," J. Soil Mech. 94, 951-979 (1968).

97.O. I. Diachok, "Effects of Sea-ice ridges on sound propagation in the Arctic Ocean," J. Acoust. Soc. Am. 59(5), 1110-1120 (1976).

98.O. I. Diachok, "Acoustics of Sea ice ridges," Proceedings of the 12th International Congress on Acoustics, Toronto, Canada, paper H2-4 (1986).